CNWRA 96-004

THERMAL STABILITY AND MECHANICAL PROPERTIES OF HIGH-LEVEL RADIOACTIVE WASTE CONTAINER MATERIALS: ASSESSMENT OF CARBON AND LOW-ALLOY STEELS

Prepared for

Nuclear Regulatory Commission
Contract NRC-02-93-005

Prepared by

Center for Nuclear Waste Regulatory Analyses
San Antonio, Texas

May 1996

CNWRA 96-004

THERMAL STABILITY AND MECHANICAL PROPERTIES OF HIGH-LEVEL RADIOACTIVE WASTE CONTAINER MATERIALS: ASSESSMENT OF CARBON AND LOW-ALLOY STEELS

Prepared for

Nuclear Regulatory Commission
Contract NRC-02-93-005

Prepared by

Gustavo A. Cragnolino
Hersh K. Manaktala
Yi-Ming Pan

Center for Nuclear Waste Regulatory Analyses
San Antonio, Texas

May 1996

PREVIOUS REPORTS IN SERIES

Number	Name	Date Issued
CNWRA 91-004	A Review of Localized Corrosion of High-Level Nuclear Waste Container Materials—I	April 1991
CNWRA 91-008	Hydrogen Embrittlement of Candidate Container Materials	June 1991
CNWRA 92-021	A Review of Stress Corrosion Cracking of High-Level Nuclear Waste Container Materials—I	August 1992
CNWRA 93-003	Long-Term Stability of High-Level Nuclear Waste Container Materials: I—Thermal Stability of Alloy 825	February 1993
CNWRA 93-004	Experimental Investigations of Localized Corrosion of High-Level Nuclear Waste Container Materials	February 1993
CNWRA 93-014	A Review of the Potential for Microbially Influenced Corrosion of High-Level Nuclear Waste Containers	June 1993
CNWRA 94-010	Review of Degradation Modes of Alternate Container Designs and Materials	April 1994
CNWRA 94-028	Environmental Effects on Stress Corrosion Cracking of Type 316L Stainless Steel and Alloy 825 as High-Level Nuclear Waste Container Materials	October 1994
CNWRA 95-010	Experimental Investigations of Failure Processes of High-Level Radioactive Waste Container Materials	May 1995

ABSTRACT

The potential for embrittlement of the outer disposal overpack in the current U.S. Department of Energy (DOE) design of the waste packages for the proposed repository at the Yucca Mountain site is reviewed. Two materials: (i) a wrought carbon-manganese steel, A516 Grade 55, and (ii) a low-alloy steel, A387 Grade 22 (2.25Cr-1Mo), have been selected by the DOE for further evaluation. On the basis of an extensive review of the literature, it is concluded that A387 Grade 22, and to a lesser degree A516 Grade 55, may be prone to substantial degradation in toughness as a consequence of long-term thermal aging. Thermal embrittlement due to phosphorus segregation to grain boundaries can be promoted by exposures to temperatures ranging from 250 to 100 °C, for thousands of years, conditions which are expected in the repository if a high thermal loading strategy is adopted. Important metallurgical variables, such as steel composition, microstructure, grain size and effects of welds are reviewed, in connection to the closely related phenomenon of temper embrittlement that affects tempered low-alloy steels as a result of isothermal heating or slow cooling within the temperature range of 325 to 575 °C. Expressions, based on models of the thermodynamics and kinetics of segregation, are suggested for predicting the long-term behavior at lower temperatures. Empirical equations relating embrittlement to chemical composition of steels and correlations used to estimate fracture toughness, K_{Ic}, by using values of impact energy obtained with Charpy V-notched specimens, were compiled. A procedure is suggested for assessing thermal stability and the critical size of a crack or flaw that can be tolerated without brittle failure under a certain level of stress. Recommendations for further investigation of this thermal stability problem that may affect the performance of waste packages are included.

CONTENTS

CONTENTS (cont'd)

FIGURES

FIGURES (cont'd)

TABLES

ACKNOWLEDGMENTS

This report was prepared to document work performed by the Center for Nuclear Waste Regulatory Analyses (CNWRA) for the Nuclear Regulatory Commission (NRC) under Contract No. NRC-02-93-005. The activities reported here were performed on behalf of the NRC Office of Nuclear Material Safety and Safeguards (NMSS), Division of Waste Management (DWM). The report is an independent product of the CNWRA and does not necessarily reflect the views or regulatory position of the NRC. Sources of data are referenced in each chapter. The respective sources of these data should be consulted for determining their levels of quality assurance.

The authors gratefully acknowledge the suggestions and comments of Narasi Sridhar, the contribution of Randy Manteufel in the thermal calculations, the technical review of Fred F. Lyle, Jr., and the programmatic review of Wesley C. Patrick. Appreciation is due to Bonnie L. Garcia for her assistance in the preparation of this report.

EXECUTIVE SUMMARY

The waste package is the primary engineered barrier in the mined geological disposal system (MGDS) envisioned by the U.S. Department of Energy (DOE) for the proposed high-level radioactive waste repository at Yucca Mountain. The performance of the waste packages during the initial several thousand years after waste emplacement is extremely important in the current DOE strategy for waste containment and isolation. It is assumed that the flow of groundwater into the repository will be low. By using the heat from the radioactive decay of the waste and adopting a high thermal loading strategy, the DOE intends that water will be vaporized and driven away from the vicinity of the waste packages, resulting in almost dry conditions for extended periods of time. Although the establishment and preservation of these conditions may prevent or delay the occurrence of accelerated and localized forms of aqueous corrosion, the waste package materials can be exposed to temperatures well above 100 °C for thousands of years. No consideration has been given in the DOE Total System Performance Assessment (TRW Environmental Systems, 1995b), however, to the effect of prolonged exposures at these temperatures on material stability and specific mechanical properties.

In the current DOE repository concept, the waste package will be composed of at least two concentric containers (overpacks) surrounding the multi-purpose canister (MPC) containing spent fuel or the "uncanistered" spent fuel. The primary candidate material for the inner container of the disposal overpack is alloy 825, which is a Ni-base, corrosion-resistant alloy. The outer disposal overpack will be fabricated from a corrosion-allowance material. The two candidate materials currently proposed by the DOE for the outer steel overpack are: (i) a wrought C-Mn steel, A516 Grade 55, which is primarily used in the form of plates for welded pressure vessels, and (ii) a low-alloy steel, A387 Grade 22 (2.25Cr-1Mo), which is utilized primarily for welded boilers and pressure vessels designed for elevated temperature service. The purpose of this report is to examine the long-term thermal stability of the steels currently considered as main candidates for disposal overpacks on the basis of a critical review of the available literature. This report is a follow-up of the preliminary and limited evaluation conducted previously (Sridhar et al., 1994), in which the issue of thermal stability and possible embrittlement of the steels following prolonged exposure at the temperatures prevailing in the repository was suggested.

On the basis of an extensive review of the literature, it is concluded that low-alloy steels, such as A387 Grade 22, and eventually C-Mn steels, such as A516 Grade 55, may be susceptible to a substantial degradation in toughness as a consequence of long-term thermal aging. This phenomenon, named thermal embrittlement, is related to the well known phenomenon of temper embrittlement that affects tempered low-alloy steels as a result of isothermal heating or slow cooling within the temperature range of 325 to 575 °C. Temper embrittlement is of major concern to the integrity of engineering components that operate within that critical temperature range and also to heavy section components which are slowly cooled through the critical temperature range after heat treatment or welding operations. Examples of such components are pressure vessels and turbine rotors. However, the potential for embrittlement of C and low-alloy steels at temperatures lower than 300 °C as a result of the very extended exposures (hundreds to thousands of years) expected under repository conditions, has never been investigated. The lack of information is undoubtedly related to the extended times that could be required to induce the occurrence of this phenomenon, if it occurs, at such relatively low temperatures.

Temper embrittlement occurs when impurities originally present in the steel, such as Sb, P, Sn, and As, segregate along prior austenite grain boundaries during exposure to temperatures ranging from 300 to 600 °C. The segregation of P, which in the case of commercial steels is the predominant impurity,

promotes fracture of notched specimens upon impact and leads to a change in the low-temperature fracture mode from transgranular cleavage to intergranular fracture. By reviewing the available literature on temper embrittlement of low-alloy steels, useful expressions were found to predict the long-term behavior at lower temperatures. These expressions are based on the thermodynamics and kinetics of segregation model originally developed by McLean (1957). They have been successfully applied to the diffusion and segregation of P following long-term aging (20,000 hr) at temperatures above 300 °C in steels such as A508 and A533B which are used as pressure vessel materials in nuclear power plants. The amount of P segregation was found to be linearly related to the susceptibility to embrittlement as measured through the shift in the ductile brittle transition temperature (DBTT).

It was found that an important metallurgical factor controlling the degree of embrittlement is the grain size. The degree of embrittlement has been evaluated in various studies by comparing base materials, welds, and their associated heat affected zones (HAZs) using weldments or simulated microstructures. It appears that welds are less susceptible than the base metal, but coarse grain microstructures developed in the HAZ could be significantly more embrittled than the base metal.

Empirical equations relating embrittlement with chemical composition of steels were compiled, in which the effect of alloying elements and detrimental impurities is included. Nevertheless, it should be noted that significant variability has been reported for components made from the same nominal grade of pressure vessel steel. Correlations used to estimate fracture toughness, K_{Ic}, by using values of impact energy obtained with Charpy V-notched specimens, were compiled. A procedure is suggested for assessing thermal stability and the critical size of a crack or flaw that can be tolerated without brittle failure under a certain level of stress.

From the review of the available information, the following recommendations are made for future work:

- Develop a complete assessment of the potential for thermal embrittlement of an outer disposal overpack made of A387 Grade 22 steel using the data available in the literature and following the approach described in Section 3.6.

- On the basis of such assessment, identify the critical aspects that require further study. The aspect that should be better defined is the use of fracture mechanics concepts to establish the failure criterion. Analysis of alternative approaches based on fracture stress concepts should be explored.

- Apply the Guttmann theory to the case of C-Mn steels such as A516 Grade 55 to explore the potential for P segregation to grain boundaries on a thermodynamic basis. Use McLean's model to calculate the concentration at grain boundaries after a detailed review of certain critical modeling parameters, such as the diffusion coefficient of P in steels.

- Define an experimental program, if it appears justified, on microstructural and mechanical factors that may contribute to the risk of thermal embrittlement of the overpack.

The results of these activities would provide Nuclear Regulatory Commission (NRC) with a better understanding of the potential for thermal embrittlement of overpack materials due to long-term aging. These studies are needed to support sensitivity analyses, and to address uncertainties in models (i.e., applicability of Guttmann and McLean theory to C-Mn steels), parameters (i.e., coefficient diffusion of P in steels), and data (i.e., correlations between ΔDBTT and K_{Ic}). A more complete evaluation of the

embrittlement of steel overpacks under repository conditions will provide staff with the knowledge base needed to assess the adequacy of the DOE treatment of this potential failure mode.

1 INTRODUCTION

The objectives of the Container Life and Source Term Key Technical Issue (KTI) implementation plan are to: (i) examine and understand the scope and quality of the U.S. Department of Energy (DOE) waste package (WP) program for the mined geological disposal system (MGDS) planned at the Yucca Mountain (YM) repository site and (ii) conduct sensitivity analyses on the performance of the Engineered Barrier System (EBS) due to uncertainties in models and data. One of the technical assessment needs of this KTI is to evaluate the effect of long-term thermal exposure and various repository mechanical loads on the metallurgical and mechanical stability of WP materials.

The WP is the primary engineered barrier in the MGDS, and the performance of the WPs for the initial several thousand years after radioactive waste emplacement is extremely important in the current DOE strategy for waste containment and isolation for the proposed YM repository (TRW Environmental Safety Systems, 1995a). Several hypotheses have been formulated that, if correct, would demonstrate that radioactive waste can be isolated for long periods of time. The hypotheses pertaining to the performance of the WPs include: (i) the flow of groundwater into the repository will be low; (ii) corrosion of waste containers will be negligible for thousands of years because the heat from the radioactive decay of the waste will cause low relative humidity and thus prevent an aqueous film from forming on the WP surface; (iii) the outer overpack will cathodically protect the inner overpack and thus limit the corrosion rate; (iv) once WPs are breached, the mobilization of radionuclides will be slow; and (v) the engineered barriers, possibly including backfill, will limit the migration of radionuclides into the host rock and the groundwater.

In the current DOE repository concept, there are two types of spent fuel WP designs (TRW Environmental Safety Systems, 1994). The primary type is the multi-purpose canister (MPC) based design which will be utilized by most of the commercial nuclear power plants, whereas an "uncanistered" spent fuel package will be used in the remaining reactors.* For disposal, the WP will be composed of at least two concentric containers (overpacks) surrounding the MPC or the "uncanistered" spent fuel. The primary candidate material for the inner container of the disposal overpack is alloy 825, which is a Ni-base, corrosion-resistant alloy. The outer disposal overpack will be fabricated from a corrosion-allowance material. Using a sufficiently thick wall and assuming that uniform corrosion will prevail under the assumed environmental conditions of the repository when a liquid water film forms on the outer surface, it is estimated that the outer overpack could last for thousands of years (Doering, 1993). On the basis of predictable uniform corrosion rates, good shielding characteristics for γ-radiation, relatively low cost, and material availability, C and low-alloy steels have been selected as candidate materials for the outer overpack. An additional containment barrier of a moderately corrosion-resistant alloy, such as alloy 400 (Ni-35Cu) or CDA 715 (Cu-30Ni), is included in the low thermal-load repository design (TRW Environmental Safety Systems, 1994).

The three candidate materials currently selected by the DOE (TRW Environmental Safety Systems, 1994; McCright, 1995) for the outer steel overpack are: (i) a wrought C-Mn steel, A516 Grade 55, which is primarily used in the form of plates for welded pressure vessels; (ii) a centrifugally cast C steel, similar in chemical composition to A516 Grade 55 steel; and (iii) a low-alloy steel, A387 Grade 22, which is utilized primarily for welded boilers and pressure vessels designed for elevated temperature service. Since A516 Grade 55 is the primary material recommended for further testing (TRW Environmental Safety

* According to the most recent DOE plans for the advanced conceptual design of the waste package. The development of the MPC may be subject to changes based on available funding.

Systems, 1994) and the alternate one is A387 Grade 22, the cast material designated either as A27 Grade 70-40 (McCright, 1995) or A426 steel (TRW Environmental Safety Systems, 1994) is not considered in this report. The nominal chemical compositions of these steels and their mechanical properties, as specified by the American Society for Testing and Materials (ASTM), are listed in Tables 1-1 and 1-2.

Recently, an extensive survey of the degradation modes of iron-base, corrosion-allowance materials for high-level radioactive waste (HLRW) disposal containers to be used in the MGDS planned at the YM site was published (Vinson et al., 1995). Although many forms of corrosion, such as air oxidation; atmospheric, aqueous and soil corrosion; microbially influenced corrosion; galvanic corrosion; and stress corrosion cracking (SCC) were reviewed, no consideration was given to the long-term effect of thermal exposures at temperatures ranging from 150 to 300 °C on metallurgical stability and specific mechanical properties of C and low-alloy steels. Therefore, the purpose of this report is to examine the long-term thermal stability of the steels currently considered as main candidates for disposal overpacks on the basis of a critical review of the available literature. This report is a follow-up of the preliminary and limited evaluation conducted earlier (Sridhar et al., 1994), in which the issue of thermal stability and possible embrittlement of the steels following prolonged exposure at the temperatures prevailing in the repository was suggested.

1.1 THERMAL CONDITIONS OF WASTE PACKAGES

Consistent with the hypotheses postulated by the DOE to assure waste containment and isolation noted above, a high thermal loading option has been considered (TRW Environmental Systems, 1995b). Thermal loading is determined by the spatial density of the WPs and the amount of waste in each WP emplaced in the repository. It is currently characterized by the areal mass loading (AML), which relates the amount of waste given in metric tons of uranium (MTU) to the emplacement area, and it is usually expressed in MTU/acre. Using a constant emplacement drift spacing and spacing the WPs within the drift according to the AML approach, it is assumed that relatively uniform thermal conditions can be maintained over the long term because the WP heat output will be nearly the same after several hundred years for packages containing approximately the same amount of waste.

By adopting a high thermal loading strategy, with AML values ranging from 80 to 100 MTU/acre (TRW Environmental Systems, 1995b), the DOE intends that water will be vaporized and driven away from the vicinity of the WPs, resulting in dry conditions for extended periods of time and, hence, improved waste containment and isolation. As noted above, however, no consideration has been given to the effect of prolonged exposures at temperatures above 100 to 150 °C on materials stability and mechanical properties of WP materials.

Figure 1-1 shows the evolution with time of the temperature at the WP surface in the MGDS corresponding to two values of AML for typical WPs, containing 8.8 MTU/package of 26 yr-old fuel, emplaced horizontally in a drift with 25 m drift spacing[1]. A three-dimensional transient model has been used for these calculations (Manteufel, 1996) assuming: (i) no ventilation of the drift during the first 100 yr and (ii) emplacement of backfill (a low conductivity medium as a result of the insulating effect of crushed tuff) after 100 yr. It is seen in Figure 1-1 that the temperature reaches a peak following backfilling of the drift and then decreases slowly with time. In the case of an AML of 80 MTU/acre

[1] Manteufel, R.D. 1996. *Personal Communication.*

Table 1-1. Chemical composition of A515 Grade 55 and A387 Grade 22 steels (extracted from American Society for Testing and Materials, 1995a, b)

Steel	Element, wt. %						
	C	Mn	Si	Cr	Mo	S	P
A516 Grade 55 (UNS K01800)	<0.24[a]	0.55–1.30[b]	0.13–0.45	—	—	0.035 max	0.035 max
A387 Grade 22 (UNS K21590)	<0.17[a]	0.25–0.66[b]	0.50 max	1.88–2.62[b]	0.85–1.15[b]	0.035 max	0.035 max

[a] — 100 to 200-mm-thick plate
[b] — Product analysis

Table 1-2. Mechanical properties of A516 Grade 55 and A387 Grade 22 steels (extracted from American Society for Testing and Materials, 1995a, b)

Steel		Tensile Strength (MPa)	Yield Strength, min (0.2% Offset) (MPa)	Elongation in 50 mm, min (%)	Reduction in Area, min (%)
A516 Grade 55 (UNS K01800)		380–515	205	27	—
A387 Grade 22 (UNS K21590)	Class 1	415–585	208	18	40
	Class 2	515–690	310	18	40

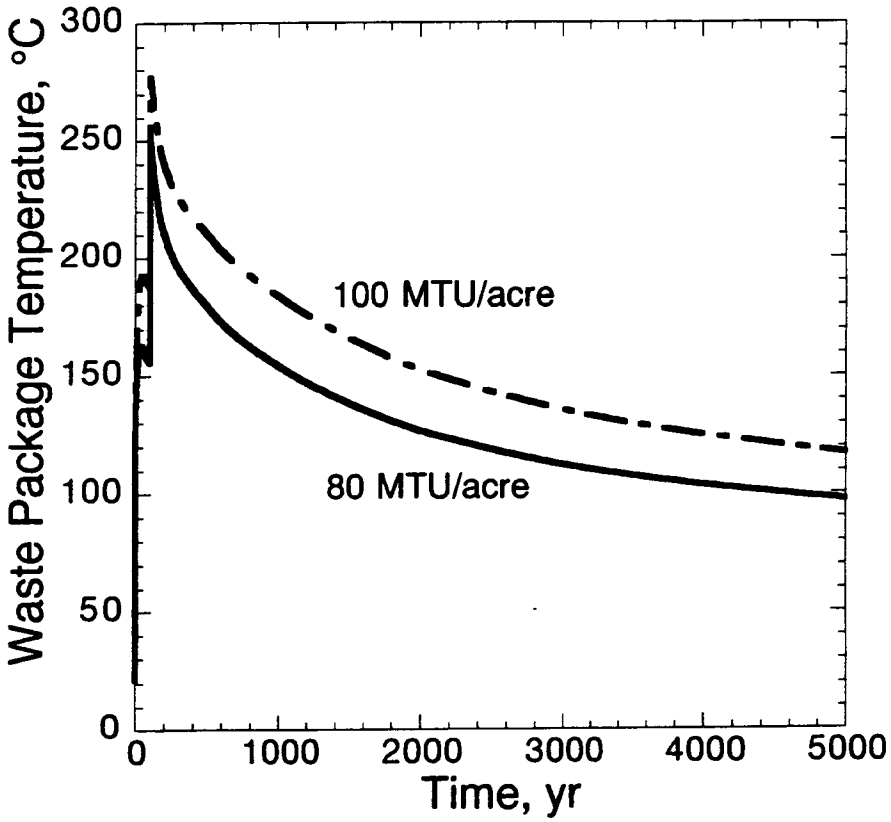

Figure 1-1. Effect of thermal loading on the waste package temperature as a function of time[2]

(18 m spacing between WPs), the WP surface temperature is still higher than 120 °C at 2,000 yr after emplacement, whereas for 100 MTU/acre (14 m spacing between WPs), the temperature remains above 150 °C for the same period.

1.2 THERMAL STABILITY OF STEELS

As discussed previously (Sridhar et al., 1994), in addition to various forms of corrosion, C and low-alloy steels may become susceptible to failure, resulting from degradation of specific mechanical properties, as a consequence of prolonged exposure at elevated temperatures. One of the important mechanical properties required for a material to be used as a component of the WP is toughness, which is the ability to absorb energy in the form of plastic deformation without fracturing. Carbon steels are alloyed singly or in combination with Cr, Ni, Cu, Mo, and V, among other elements, in the range of a few percent or less to produce low-alloy steels. Alloying additions are made for better mechanical properties and hardenability. Strengths, which are achieved with minor additions of carbide-forming elements such as Ti, Nb, and V, are appreciably higher than those of plain C steels having a ferrite-pearlite microstructure and are usually required for pressure boundary components. These additions enhance mechanical properties, but toughness can be reduced. Other additions that improve mechanical properties are Ni and Mo, both having a beneficial effect on toughness.

[2] Manteufel. 1996. *Personal Communication.*

However, toughness is significantly affected by a phenomenon termed temper embrittlement. Temper embrittlement, also known as temper brittleness, two-step temper embrittlement, or reversible temper embrittlement, occurs in low-alloy, medium-strength steels used in stationary steam turbines as rotor materials, in boilers, in steam generator shells, or in reactor pressure vessels that have been quenched and subsequently tempered (heat treated at about 600 to 700 °C) to attain a desired strength. This is a phenomenon characterized by an upward shift in the ductile-brittle transition temperature (DBTT), as a result of exposure to the temperature range of 350 to 575 °C through isothermal heating or slow cooling, as shown schematically in Figure 1-2, where the variation of the impact fracture energy for notched specimens is represented as a function of test temperature. Usually, DBTT is determined at some fixed value of the impact energy. For example, the 20 J (15 ft·lb) transition temperature can be used and denoted as DBTT (20 J).

This form of embrittlement is of major concern to the integrity of engineering components that operate within that critical temperature range and also to heavy section components such as pressure vessels or turbine rotors which are slowly cooled through the critical temperature range after heat treatment or welding operations. However, the potential for embrittlement of C and low-alloy steels at temperatures lower than 300 °C as a result of the very extended exposures (hundreds to thousands of years) expected under repository conditions has never been investigated. The lack of information is undoubtedly related to the extended times that could be required to induce the occurrence of this phenomenon, if it occurs, at such relatively low temperatures.

For this reason, the available literature on low-alloy steels, in particular pressure vessel steels such as A302, A508, and A533B among others, has been reviewed in an attempt to establish correlations useful for predicting the long-term behavior at lower temperatures, extending these correlations from low-alloy steels with different compositions to C steels when possible. All the various constituents of the component, including base materials, welds, and their associated heat affected zones (HAZs), would be assessed on the basis of the available information.

It is now recognized that segregation of impurities, such as Sb, P, Sn, and As, along prior austenite grain boundaries, is the main cause of temper embrittlement (Briant and Banerji, 1983), leading to a change in the low-temperature fracture mode from transgranular cleavage to intergranular fracture. Although a body of evidence was built in the late 1960s regarding the key elements in steels contributing to temper embrittlement, it was the introduction of Auger electron spectroscopy (AES) that led to the direct identification of elements segregated at fractured grain boundaries (Joshi and Stein, 1972; Seah, 1983; Briant, 1988).

In addition to interfacial segregation of mobile species, thermal aging may lead to microstructural changes as a result of long-term precipitation reactions arising from metastable phases. However, these types of processes generally occur in steels at higher temperatures. Predictive models can be constructed based on accelerated test data and mechanistic studies. Although higher thermal aging temperatures undoubtedly accelerate thermally activated processes, attention should be given to potential changes in both the mechanism and the degree of embrittlement attained. For example, increasing temperature will decrease the equilibrium grain boundary segregation level but accelerate the kinetics of achieving the equilibrium condition. However, substantial increases in temperatures may promote additional microstructural changes affecting the thermodynamic conditions controlling segregation which might not occur at lower temperatures.

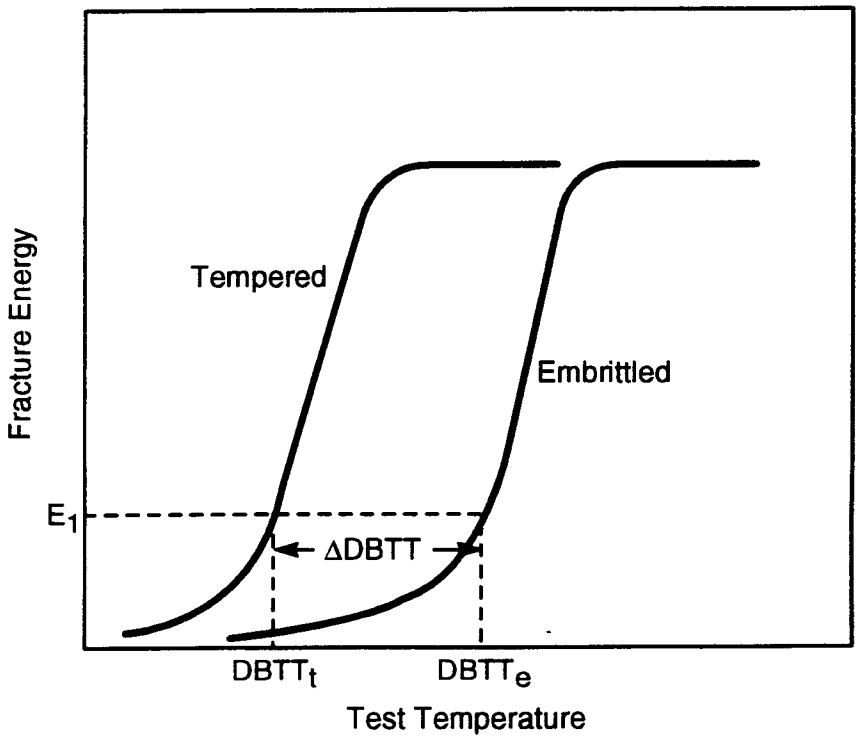

Figure 1-2. Schematic diagram of the effect of embrittlement on the ductile brittle transition temperature (DBTT) as a function of test temperature

Steels are also susceptible to other forms of embrittlement after heat treatments at temperatures below 500 °C. One of them is "blue brittleness" which occurs in plain C steels. This phenomenon is briefly discussed in Section 2.1. Another embrittlement phenomenon occurs in low-alloy steels with very high yield strengths in which the martensite has been tempered for short times at temperatures ranging from 200 to 500 °C. Because this state of embrittlement occurs after a single tempering treatment of the martensite, it is known as "one-step temper embrittlement" or "350 °C embrittlement." However, this phenomenon is not reviewed in this report because it is confined to low-alloy steels with very high yield strengths (1,300 MPa) which are not considered appropriate materials for the outer disposal overpacks.

2 THERMAL AGING AND EMBRITTLEMENT OF STEELS

As noted in Section 1.2, temper embrittlement is a problem associated with tempered alloy steels that are heated within or slowly cooled through a critical temperature range of about 350 to 575 °C. The thermal exposure in this temperature range causes a decrease in notch toughness as determined by using Charpy V-notch (CVN) impact specimens (Vander Voort, 1990).

As shown in Figure 1-2, temper embrittled steels exhibit an increase in the DBTT, accompanied by a change in the fracture mode in the impact test from transgranular cleavage to intergranular fracture over the low temperature range designated as the lower shelf region. The region of the curve in Figure 1-2 in which the fracture is entirely ductile is referred to as the upper shelf region. In addition to the definition given in Section 1.2, the DBTT can be assessed in several other ways. One of the most common is the fracture appearance transition temperature (FATT), defined as the temperature at which 50 percent of the fracture is ductile and the remaining 50 percent brittle. Another definition is based on the lowest temperature at which the fracture is 100 percent ductile (100 percent fibrous criterion) (Vander Voort, 1990). Other commonly adopted definitions to characterize the transition temperature have been briefly reviewed by Viswanathan (1989).

McMahon (1968) and Viswanathan (1989) have reported that many investigators observed that temper embrittlement exhibits a C-shaped curve in a temperature-time plot, similar to the plots used to represent temperature-time-precipitation (TTP) processes or other solid-state phase transformations, as shown in Figure 2-1 for a 2.25Cr-1Mo steel. It is apparent from this plot, in which the contours indicate increasing values of ΔFATT, that the nose of the C-curve corresponds to a maximum in embrittlement as a result of at least two competing processes. At high temperatures, the kinetics of impurity diffusion to grain boundaries is rapid, but the tendency to segregate is low because the matrix solubility for the impurity elements increases with temperature. Hence, embrittlement occurs rapidly but to a small degree. At low temperatures, the tendency to segregate is high, but the diffusion kinetics are not rapid enough to reach maximum embrittlement. The favorable combination of kinetics and thermodynamic factors promoting maximum embrittlement occurs at an intermediate temperature defined by the nose of the C-curve.

An isothermal aging treatment at a particular temperature within the temper embrittlement range generally requires well in excess of 1,000 hr to promote embrittlement of commercial rotor steels. For this reason, a two-step heat treatment or a step-cooling treatment is often employed to accelerate the temper embrittlement of steels in laboratory studies. One such treatment consists of the following steps: (i) 1 hr at 593 °C, (ii) 15 hr at 538 °C, (iii) 24 hr at 524 °C, (iv) 48 hr at 496 °C, (v) 72 hr at 468 °C, followed by furnace cooling to 315 °C, and then air cooling to room temperature (Khadkikar and Wieser, 1986). Most of the studies discussed in this report have used this step sequence or a similar one to attain accelerated embrittlement. In certain specific studies, isothermal aging for relatively long times on a laboratory time scale (10,000 hr or more), has been used.

One important observation is that temper embrittlement is reversible. The toughness of embrittled steels can be restored by tempering them above the critical region (at about 600 °C) followed by rapid cooling (e.g., water quenching). This retempering decreases the DBTT to the original value, and, accordingly, it restores the appearance of the low-temperature brittle fracture from intergranular in the embrittled condition to the cleavage mode characteristic of the tempered condition. As noted by McMahon (1968), steels that are embrittled by a step-cooling treatment of about 2 weeks, can be de-embrittled by a 5 min treatment at 593 °C and in 1 min at 677 °C.

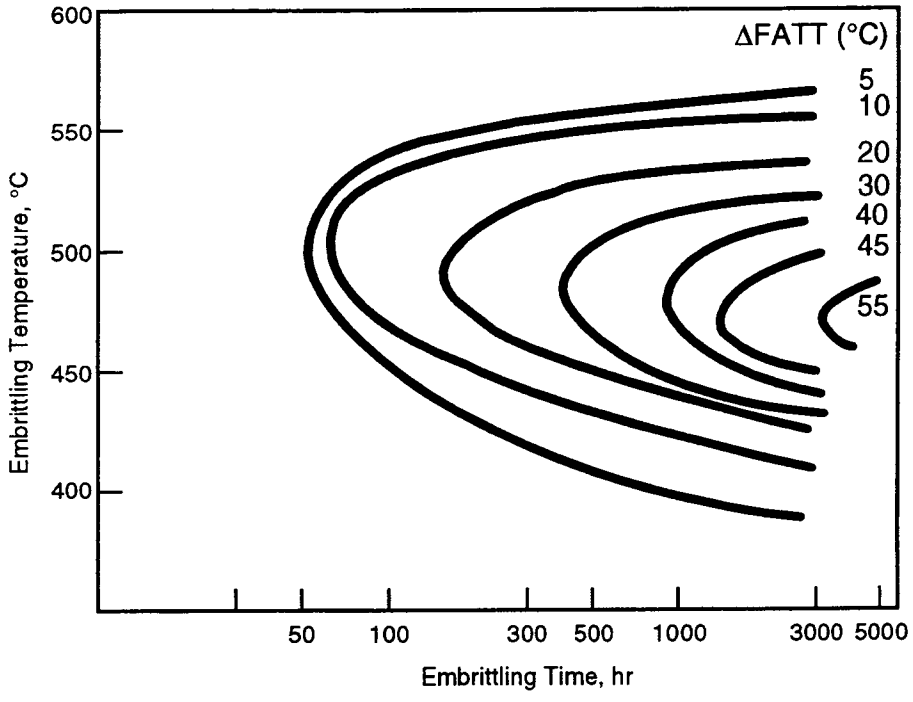

Figure 2-1. Temperature-time plot for the temper embrittlement of 2.25Cr-1Mo steel showing contours for various ΔFATT (adapted from Viswanathan, 1989)

2.1 TEMPER EMBRITTLEMENT IN PLAIN CARBON STEELS

Although it is almost universally accepted that plain C steels are not susceptible to temper embrittlement, Jaffe and Buffum (1949) reported in an early investigation temper embrittlement in SAE 1045 steel. The chemical composition of the steel investigated was: 0.47% C, 0.81% Mn, 0.21% Si, 0.037% S, 0.013% P, 0.01% Ni, 0.07% Cr, 0.01% Mo, balance Fe. The authors compared the behavior of plain SAE 1045 and SAE 3140 (0.39% C, 0.79% Mn, 0.30% Si, 0.028% S, 0.015% P, 1.26% Ni, 0.77% Cr, 0.02% Mo, balance Fe) steels after specimens of these steels were austenitized and tempered. The specimens were impact tested in that condition and also after being aged for 50 hr at 455 °C. Since the plain C steel exhibited a higher transition temperature than the alloy steel without being aged, Jaffe and Buffum (1949) concluded that plain C steels are also susceptible to temper embrittlement, and it occurs so rapidly in plain C steels that it cannot be prevented by quenching from the austenitizing temperature. However, their observations have not been confirmed in more than four decades since the cited investigation was published.

McMahon (1968) has concluded in his review that plain C steels containing less than 0.5 percent Mn are not susceptible to temper embrittlement. However, McMahon also noted the strong effect of Mn as an enhancer of the P effect on temper embrittlement. For example, a 0.1 percent C steel with 1.5 percent Mn and 0.04 percent P exhibited an increase in the DBTT of more than 100 °C after an

embrittlement treatment of 670 hr at 500 °C. Currently, it is believed that plain C steels do not exhibit temper embrittlement (Vander Voort, 1990). However, it is apparent that not enough data exists on the long-term aging of plain C-Mn steels, particularly those containing relatively high Mn contents, to disregard the possibility of embrittlement.

In addition, C steels generally exhibit an increase in strength and a marked decrease in ductility and toughness when heated between 230 and 370 °C (Vander Voort, 1990). Because heating at such temperatures produces a bluish temper color on the surface of the steel, this phenomenon has been named blue brittleness. It is believed that blue brittleness is an accelerated form of strain-age embrittlement. Deformation while the steel is heated in the blue heat range results in even higher hardness and tensile strength after cooling to room temperature. If the strain rate is increased, the blue brittle temperature range is increased (Low, 1978). Blue brittleness can be eliminated if elements that tie up N, such as Al or Ti, are added to the steel (Vander Voort, 1990).

2.2 TEMPER EMBRITTLEMENT IN LOW-ALLOY STEELS

2.2.1 Effect of Chemical Composition

The degree of embrittlement varies with the chemical composition of the steel. Therefore, the alloying elements present, and their combinations and levels, are important factors. Only a few systems are sufficiently well characterized. However, alloying elements can be classified into three broad categories based on how they affect the embrittlement process: (i) promoters of segregation which act by cosegregating with impurities, (ii) promoters which do not themselves segregate, and (iii) scavengers which bind impurities in the matrix inhibiting segregation. The elements now thought to belong to these three categories are indicated in the Periodic Table shown in Figure 2-2 (Briant and Banerji, 1978). In addition, all the potential embrittling elements, many of which are found as impurities in steels, are indicated in Figure 2-2.

The embrittling elements, aside from the specific case of hydrogen, belong to the Groups IVA, VA and VIA of the Periodic Table. Although S is a potent embrittler for iron, it is tied to Mn as MnS inclusions in steels precluding any deleterious segregation to grain boundaries. The most potent embrittling elements, in order of decreasing potency, are Sb, Sn, P, and As. Si, which is an alloying element added for deoxidation in steels, is a weaker embrittling element, whereas the effect of Bi is not well established. Nevertheless, Bi is not usually found as an impurity in steels. Of these elements, P is the most common embrittling element found in commercial low-alloy steels. According to Briant and Banerji (1983), this detrimental role is a consequence of the following facts: (i) P segregates during austenitization and tempering, as well as during aging; (ii) it segregates rapidly even at low temperatures; and (iii) its concentration in commercial steels is usually greater than that of other embrittling elements. In importance, P is followed by Sn and Si, since Sb and As are not generally present in sufficiently large quantities in commercial steels.

Although steels containing Cr or Ni are susceptible, steels containing Cr and Ni in combination are more susceptible than those that contain Cr or Ni separately. Low et al. (1968) demonstrated that removing Cr or Ni from a Cr-Ni steel decreased the embrittlement caused by Sb, Sn, P, or As. Mn also increases the susceptibility to embrittlement and, according to McMahon (1968), is roughly twice as strong as Cr as an enhancer of the P effect, suggesting that the embrittlement-enhancing power decreases in the order: Mn > Cr > Ni. On the contrary, Mo additions are effective in retarding or eliminating temper

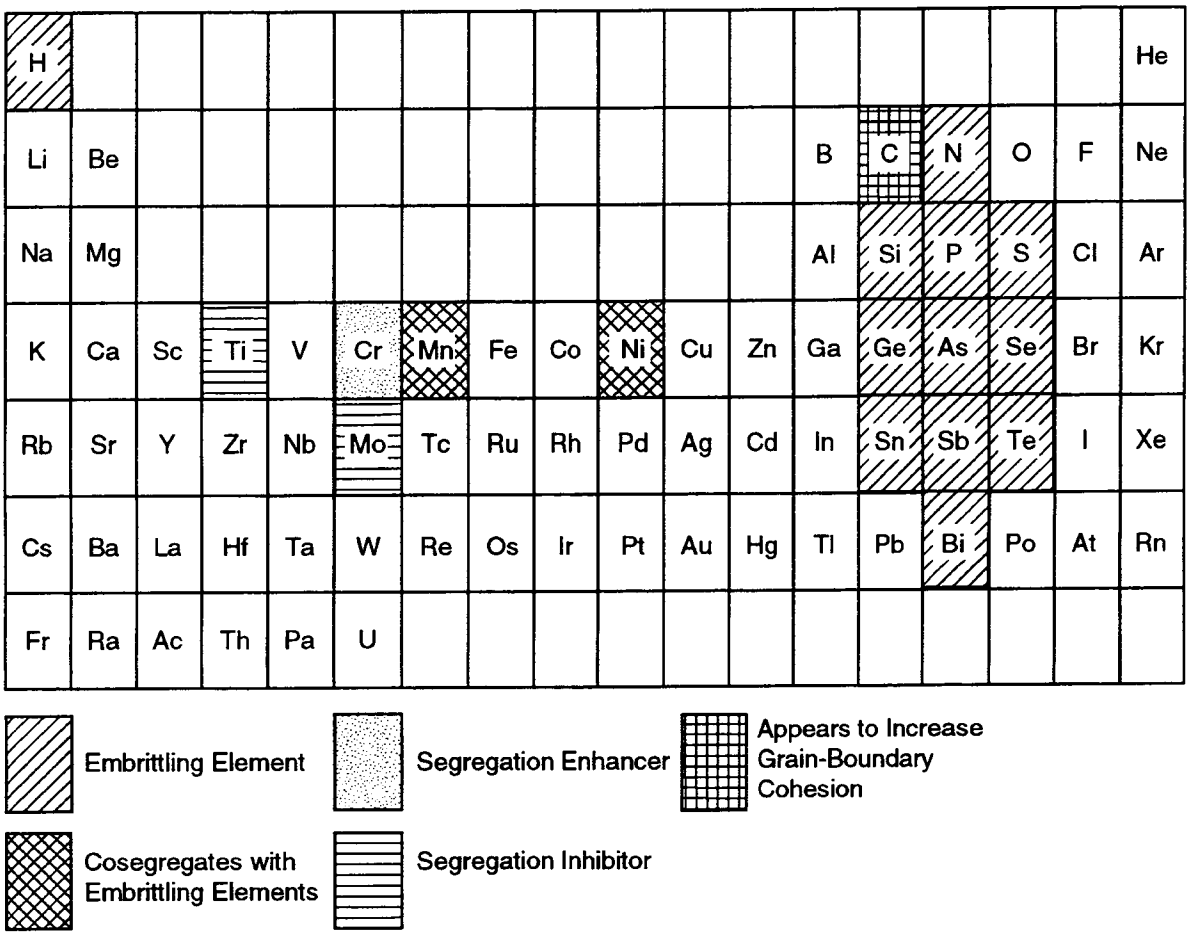

Figure 2-2. Various elements considered to play a role in temper embrittlement of steels (Briant and Banerji, 1978)

embrittlement when impurities are present. However, in order to be effective, Mo must be dissolved in the ferritic matrix and not tied up as carbides, and, therefore, its effect is a function of the Cr/Mo ratio. If the ratio is high, Cr carbides will tend to precipitate preferentially, leaving a higher concentration of Mo in solution.

2.2.2 Temper Embrittlement of Specific Low-Alloy Steel Systems

2.2.2.1 C-Mn and C-Mn-Mo Steels

Lei et al. (1983) reported the results of an investigation on the role of Mo by comparing two C-Mn steels (viz., 0.4C-2Mn and 0.4C-2Mn-0.5Mo) in both water cooled (WC) and furnace cooled (FC) conditions followed by an aging treatment to induce temper embrittlement. The chemical compositions of these steels are shown in Table 2-1 (Lei et al., 1983). Figure 2-3 shows that after tempering at various temperatures, steel A (0.4C-2Mn) is susceptible to temper embrittlement whereas steel B (0.4C-2Mn-0.5Mo), with a 0.5 percent Mo addition, is practically immune. The impact toughness at various testing temperatures for the tempered and tempered plus aged (aged 12 hr at 500 °C) conditions

Table 2-1. Chemical composition of C-Mn and C-Mn-Mo steels (Lei et al., 1983)

Steel	Element, wt. %					
	C	Mn	Si	Mo	S	P
A (0.4C–2Mn)	0.42	1.80	0.21	—	0.020	0.013
B (0.4C–2Mn–0.5Mo)	0.40	1.89	0.014	0.54	0.030	0.015

of both steels are shown in Figure 2-4. Steel A exhibits a severe degree of temper embrittlement with a considerable decrease in upper shelf impact toughness and a higher transition temperature for the initial 830 and 1,200 °C quenching conditions. The addition of Mo provides nearly the same toughness curves for the tempered and the tempered plus aged conditions, although the upper shelf impact toughness is lowered to some extent. It can be concluded that the susceptibility of C-Mn steels to temper embrittlement can be reduced substantially by the addition of Mo.

2.2.2.2 Cr-Mo and Cr-Mo-V Steels

Table 2-2 provides the composition of Cr-Mo and Cr-Mo-V steels and the results of an investigation reported by Khadkikar and Wieser (1986) on the temper embrittlement behavior in which both wrought and cast alloys were studied. The impurities in these steels were controlled to a level equal to or less than that present in commercially available steels. Table 2-2 shows that vacuum melted 2.25Cr-1Mo cast steels at a P level of 0.006 percent did not exhibit temper embrittlement regardless of the Si, Mn, and S contents. At higher P and Si levels of 0.012 and 0.28 percent, respectively, a small increase (15 °C) in the FATT was noted. With a further increase in the P, Si, and Mn levels (0.021, 0.59, and 0.68 percent, respectively), the increase in the FATT was relatively larger (47 °C). The fracture mode also changed from pure cleavage to partially intergranular fracture (Khadkikar and Wieser, 1986). Air-melted Cr-Mo-V cast steels at two Si levels, with P and S contents of 0.01 percent each, and at a low Si content (0.08 percent) showed no temper embrittlement, as shown in Table 2-2. At a higher Si level (0.35 percent), however, an increase in the FATT was observed as indicated in the same table. The Mn content of this steel was also higher. The higher Si steel exhibited an intergranular fracture mode.

Forged commercial purity (vacuum melted) Cr-Mo-V, Ni-Cr-Mo-V, and Cr-Mo steels were also studied by Khadkikar and Wieser (1986) using 10,000 hr isothermal aging treatments at 399, 454, and 482 °C. The results are shown in Table 2-2, where it is seen that Cr-Mo-V steels did not exhibit practically any temper embrittlement, regardless of the Si or Mn contents, probably due to the low P content. Ni-Cr-Mo-V steels exhibited temper embrittlement at 0.17 and 0.37 percent Mn, but the isothermal aging temperature did not affect the degree of temper embrittlement. On the other hand, the temper embrittlement of 2.25Cr-1Mo steels varied with the aging temperature and the Si and Mn levels. At 399 °C, no temper embrittlement was noted irrespective of the Si and Mn contents. After aging at 454 °C, moderate temper embrittlement was observed at 0.47 percent Mn, and 0.012 and 0.22 percent Si as shown in Table 2-2. A higher degree of temper embrittlement at the 0.47 percent Mn and 0.22 percent Si level was noted with the 482 °C treatment that decreased when the Si level was lowered to 0.012 percent.

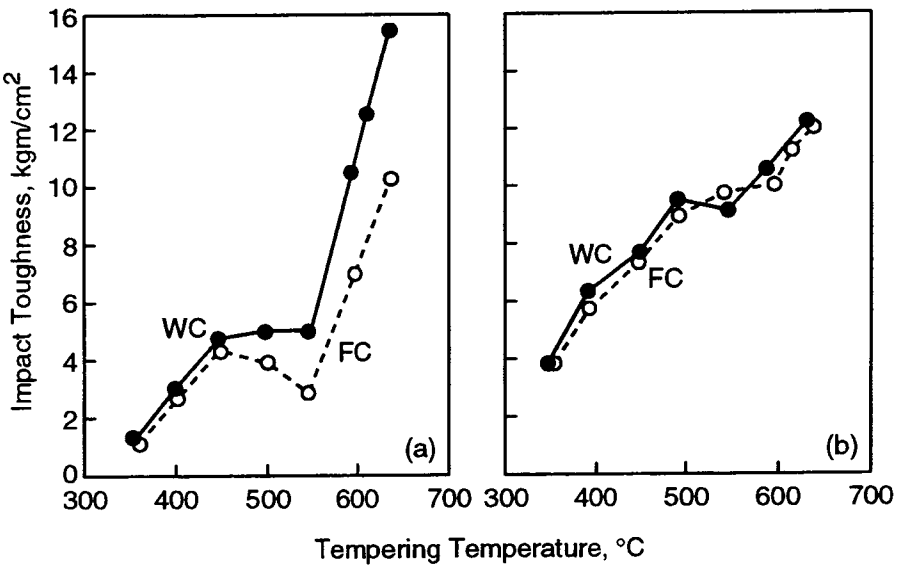

Figure 2-3. Room temperature impact toughness values of quenched (a) Steel A (830 °C) and (b) Steel B (890 °C) after 2 hr tempering at various temperatures. WC = water-cooled condition; FC = furnace-cooled condition (Lei et al., 1983).

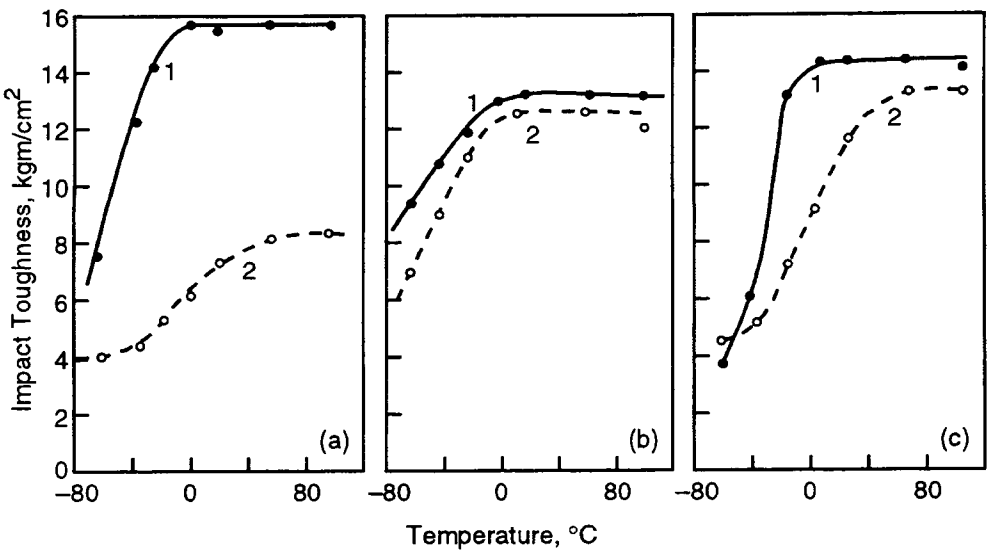

Figure 2-4. Impact toughness values of (a) steel A: quenched from 830 °C; (b) steel B: quenched from 890 °C; and (c) steel A: quenched from 1,200 °C, at various testing temperatures: curve 1 = tempered (650 °C for 2 hr); curve 2 = tempered+aged (500 °C for 12 hr (Lei et al., 1983)

Table 2-2. Chemical composition and temper embrittlement data for Cr-Mo, Cr-Mo-V, and Ni-Cr-Mo-V steels (Khadkikar and Wieser, 1986)

Steel	Chemical Composition, wt. %											As Tempered 50% FATT	Aging Temp.	ΔFAT T
	C	Cr	Mo	Ni	V	Si	Mn	P	S	Sb	Sn	(°C)	(°C)	(°C)
Cast Cr-Mo	0.14	2.40	1.01	—	—	0.32	0.03	0.006	0.004	—	—	−59	S.C.	0
	0.14	2.35	1.00	—	—	0.28	0.64	0.006	0.004	—	—	−79	S.C.	0
	0.15	2.29	1.00	—	—	0.35	0.24	0.006	0.012	—	—	−61	S.C.	0
	0.15	2.35	1.00	—	—	0.28	0.01	0.012	0.007	—	—	−59	S.C.	15
	0.12	2.36	1.03	—	—	0.59	0.68	0.021	0.004	—	—	−13	S.C.	47
Cast Cr-Mo-V	0.15	1.19	0.94	0.16	0.24	0.08	0.08	0.010	0.010	—	—	74	S.C.	−5
	0.16	1.21	0.96	0.15	0.25	0.35	0.87	0.011	0.009	—	—	80	S.C.	−43
Forged Cr-Mo-V	0.29	1.14	1.18	0.36	0.24	0.012	0.21	0.006	0.006	0.0014	0.008	113	399 454 482	4 −10 11
	0.28	1.13	1.19	0.36	0.24	0.013	0.77	0.005	0.006	0.0014	0.008	85	399 454 482	8 12 14
	0.29	1.14	1.18	0.36	0.24	0.20	0.74	0.006	0.005	0.0013	0.008	85	399 454 482	−6 16 12
Forged Ni-Cr-Mo-V	0.24	1.68	0.44	3.57	0.10	0.012	0.17	0.010	0.008	0.0016	0.010	−22	399 454 482	56 54 65
	0.24	1.67	0.44	3.52	0.10	0.014	0.37	0.010	0.008	0.0014	0.010	0	399 454 482	51 51 53

* step cooled

Table 2-2. Chemical composition and temper embrittlement data for Cr-Mo, Cr-Mo-V, and Ni-Cr-Mo-V steels (Khadkikar and Wieser, 1986) (cont'd)

Steel	Chemical Composition, wt. %											As Tempered 50% FATT	Aging Temp.	ΔFATT
	C	Cr	Mo	Ni	V	Si	Mn	P	S	Sb	Sn	(°C)	(°C)	(°C)
Forged Cr-Mo	0.14	2.31	0.99	0.21	0.002	0.013	0.21	0.010	0.011	0.0018	0.009	−29	399 454 482	7 −4 −4
	0.14	2.33	0.98	0.21	0.002	0.012	0.47	0.009	0.010	0.002	0.010	−34	399 454 482	4 19 15
	0.15	2.20	0.98	0.21	0.002	0.22	0.47	0.010	0.009	0.0015	0.009	−1	399 454 482	−1 20 31

* step cooled

Hudson et al. (1988) have compared the behavior of samples from 255-mm-thick tube plate forgings of 2.25Cr-1Mo steel aged up to 2×10^4 hr at two temperatures, 450 and 525 °C, as shown in Figures 2-5 and 2-6, respectively. At 450 °C, the DBTT and the percentage of intergranular fracture increased with aging time, but both parameters reached a constant value after 5,000 hr, whereas no change in hardness was detected. The constant value of the DBTT was attained when the degree of P segregation to the grain boundaries reached saturation (Figure 2-5). On the other hand, a significant increase in DBTT accompanied by a decrease in hardness occurred at 525 °C after the P level at the grain boundary reached saturation, even in a shorter time (1,000 hr).

Microstructural studies showed a ferrite-carbide microstructure with little evidence of the original bainitic structure (Hudson et al., 1988). Three distinct types of carbides (viz., M_2C, M_7C, and M_6C) were observed. They were all globular in morphology and increased in size in the order shown. The M_6C was present only in a very low concentration in the initial aging conditions. The variation of carbide type as a function of aging time shows the progressive formation of M_6C at the expense of M_2C (Hudson et al., 1988). As the matrix softens with the transformation to more Cr- and Mo-rich carbides, the degree of P segregation to grain boundaries rises to reach a maximum on the precipitation of M_6C from M_2C. This level of P is comparable to the level predicted for the equivalent Fe-P binary system, indicating the absence of significant interactions between elements Mo-P, Cr-P, etc. The embrittlement due to microstructural changes and the volume fraction of M_6C precipitates are correlated. Below 550 °C, a linear variation in the rise in DBTT was observed, but at long aging times at higher temperatures, significant matrix softening occurred to destroy the relationship. In addition to the rise in DBTT, M_6C precipitation also resulted in a small decrease in the upper shelf energy (USE) measured in Charpy impact tests. This result suggests that M_6C acts in combination with P segregation in causing temper embrittlement.

2.2.2.3 A533B and A508 Steels

In a series of publications, Druce and coworkers (Druce et al., 1986; Hudson et al., 1988; Vatter et al., 1993) reported an extensive investigation on the effects of thermal aging in the temperature range of 300 to 550 °C for up to 2×10^4 hr of A533B and A508 steels including samples of the quenched and tempered base metal and simulated HAZ material. All specimens were given a simulated post-weld heat treatment (PWHT) prior to testing. The typical grain sizes of the materials studied were 100–150 μm for simulated coarse-grained HAZ, 10 μm for fine-grained HAZ, and 17 μm for base material. A combination of tensile, hardness, and CVN impact tests was used to assess changes in the mechanical properties and, in particular, toughness as measured by the DBTT.

Aging in the temperature range of 300 to 550 °C produced no significant change in tensile strength or USE of A533B for all material conditions (Druce et al., 1986; Hudson et al., 1988). However, aging increased the DBTT by an amount dependent on material condition and temperature. By far the largest effect was observed in the material heat treated to simulate the coarse-grained component of an HAZ microstructure, as summarized in Figure 2-7, which shows changes in four parameters as a function of aging time at various temperatures. At 300 °C, there were no measured changes in DBTT, hardness, or fracture mode. Aging at 400 and 450 °C resulted in a relatively large increase in DBTT, and although similar changes had occurred at both temperatures in 2×10^4 hr, saturation was only achieved at 450 °C. Embrittlement was accompanied by an increase in the percentage of the intergranular mode of brittle fracture, but it should be noted that even prior to aging, the fracture was predominantly intergranular. Embrittlement at 500 and 550 °C was very rapid, occurring within 10^3 and 10^2 hr, respectively, with softening due to microstructural changes at longer aging times.

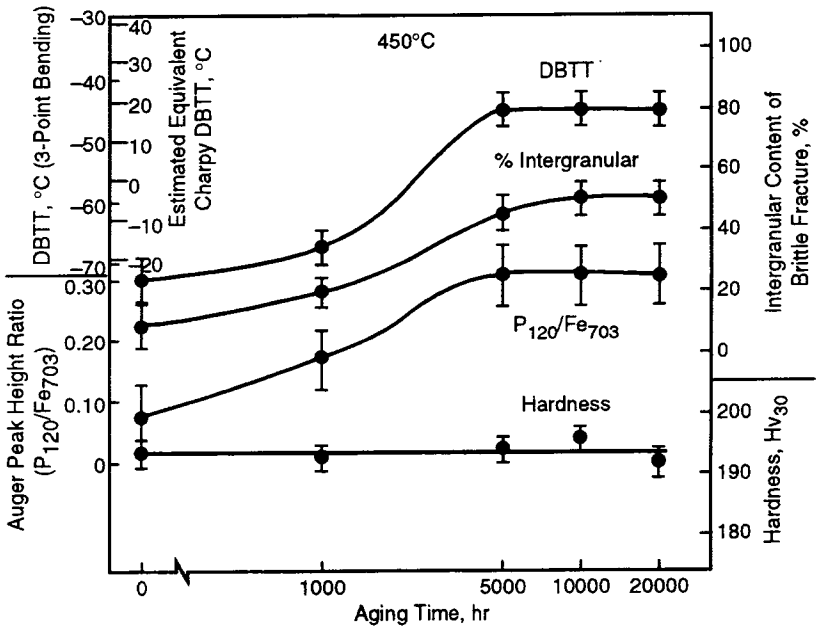

Figure 2-5. The influence of isothermal aging at 450 °C on the DBTT, hardness, amount of intergranular fracture and the degree of phosphorus segregation in 2.25Cr-1Mo steel (Hudson et al., 1988)

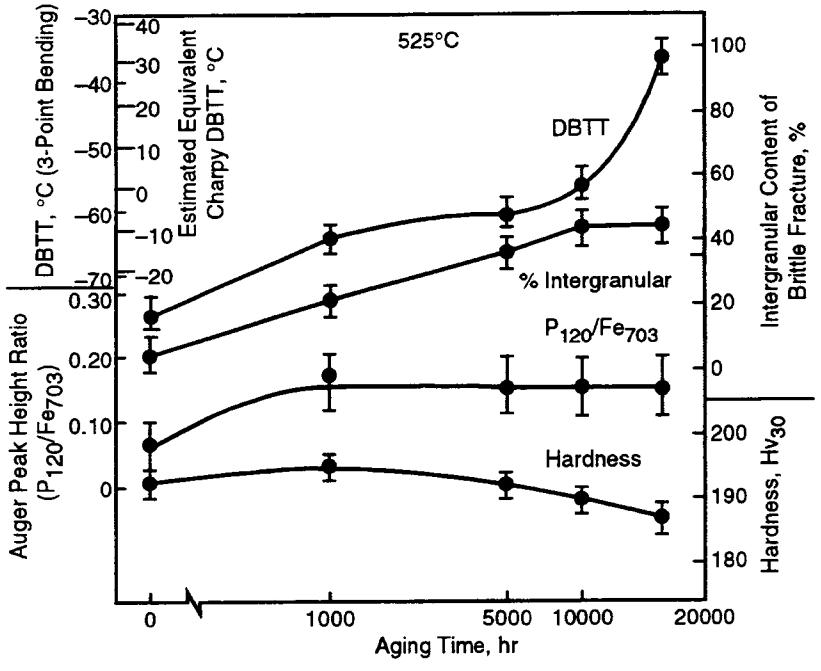

Figure 2-6. The influence of isothermal aging at 525 °C on the DBTT, hardness, amount of intergranular fracture and the degree of phosphorus segregation in 2.25Cr-1Mo steel (Hudson et al., 1988)

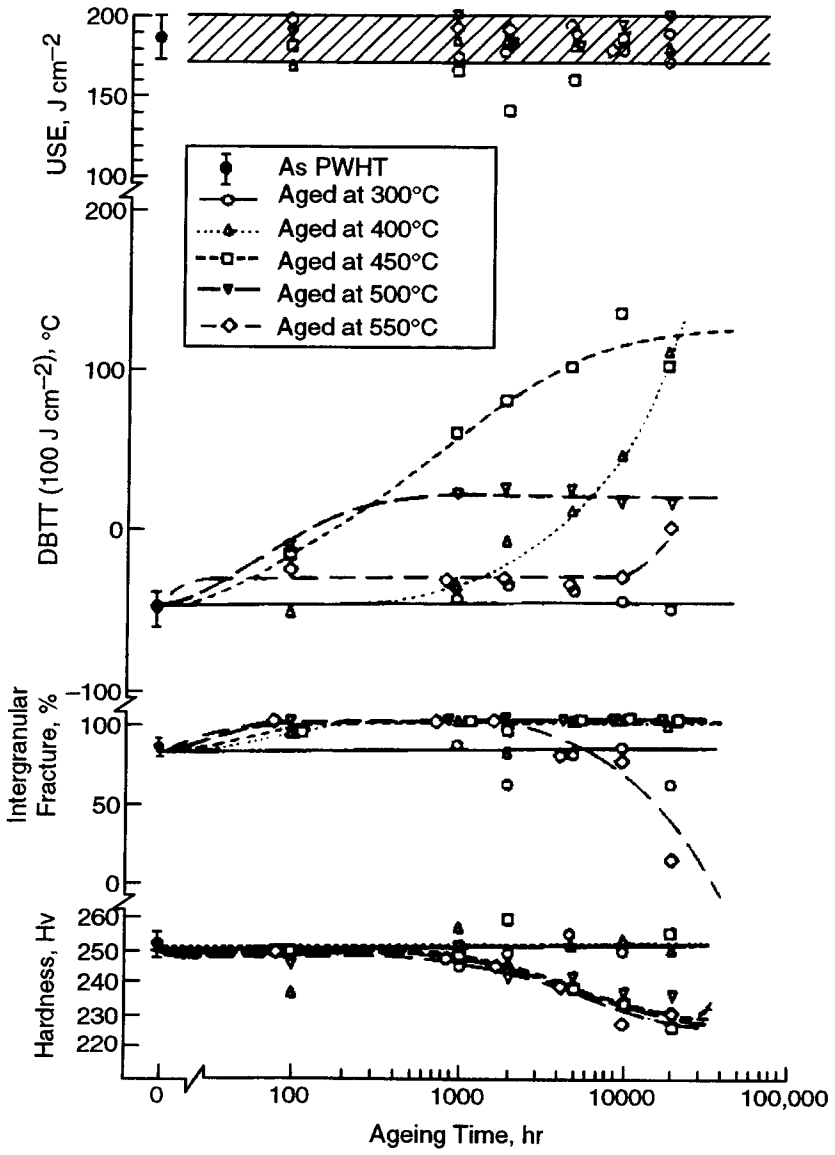

Figure 2-7. The effect of aging on the mechanical properties and fracture appearance of A533B-1 simulated coarse-grained heat affected zone (Druce et al., 1986)

Comparison between the coarse-grained HAZ conditions of A533B and A508 steels indicated that prior to aging the DBTT and USE properties of A508 were superior (Druce et al., 1986). Also, the hardness and percentage of intergranular fracture were lower. Following aging, there was a clear correlation between DBTT and the percentage of intergranular fracture, with no effect in either parameter at 300 °C but increases in both upon aging at 400 and 500 °C. Saturation was achieved after 10^3 hr at 500 °C, but at 400 °C the degree of embrittlement was still increasing after 10^3 hr. The changes in DBTT were found to be similar for both A533B and A508 materials, but, at 400 °C, the embrittlement

susceptibility of A508 is lower. No changes in USE or hardness were observed following aging of the coarse-grained HAZ simulation of the A508 steel.

The A533B fine-grained HAZ material exhibited a smaller degree of susceptibility to embrittlement compared to the data plotted in Figure 2-7 (Druce et al., 1986; Hudson et al., 1988). Prior to aging, the DBTT was similar to that of the coarse-grained material, but the USE was higher, the hardness was lower, and no low temperature intergranular fracture was observed. No changes in these parameters were observed by aging at 300 °C for up to 10^4 hr. Aging at 400 and 500 °C resulted in some increases in DBTT and percentage of intergranular fracture. However, the degree of embrittlement was less than that of the coarse-grained HAZ material. The A533B material was also examined in the PWHT quenched and tempered condition as summarized in Figure 2-8. The low temperature fracture mode was almost completely cleavage and the hardness was the lowest of all the conditions investigated. Subsequent aging had little or no effect on USE or the fracture mode. Some changes in DBTT were observed, although these were considerably smaller than for the simulated HAZ conditions. Following 2×10^4 hr aging, it was observed that there was no change at 300 °C, some increase at 400 and 450 °C, and a smaller increase at 500 °C. Saturation was reported to occur at 500 and 450 °C. At 550 °C, an initial saturation occurred very rapidly, and then DBTT increased at aging times after 10^4 hr, accompanied by a significant drop in tensile strength. Changes in tensile properties that occurred at both 500 and 550 °C after 10^3 hr aging were reproduced by hardness measurements supporting, in this case, the use of hardness as a useful parameter to assess any possible variation in tensile strength.

The inducement of fracture along the prior austenite grain boundaries enabled the composition to be evaluated at this location by AES. Changes in the P/Fe peak height ratio (PHR) as a function of aging time and temperature for the coarse-grained material are shown in Figure 2-9 (Hudson et al., 1988). The equilibrium nature of the segregation is evident, with saturation reached at 550, 500, and 450 °C and the degree of coverage increasing with decreasing temperature. A progressive increase in the P level was observed at 400 °C, which had not saturated even after 2×10^4 hr. In contrast, aging at 300 °C had very little effect at all.

The grain boundary P segregation and the embrittlement data for this material condition are clearly correlated. Figure 2-10 (Hudson et al., 1988) shows the change in DBTT as a function of average P/Fe PHR obtained on aging for various times over the temperature range 300–500 °C. This figure indicates a linear dependence between embrittlement and the degree of P segregation over the P/Fe PHR range from 0.065 to 0.2 and strongly suggests that embrittlement is controlled by P segregation. Based on the data, it was predicted, as an example, that anticipated increases in DBTT at 325 °C for the design life of a pressurized water reactor (32 yr of effective full power) are: base materials, $\leq$10 °C; simulated fine-grained HAZ, approximately 30 °C; simulated refined grained HAZ $\leq$10 °C; actual HAZ, approximately 30 °C; actual weld metal $\leq$10 °C (Hudson et al., 1988).

Based on a review of data contained in the Power Reactor Embrittlement Data Base (PR-EDB) and other studies, Nanstad et al. (1995) concluded that no substantial embrittlement has been observed for typical reactor pressure vessels (i.e., A302B, A533B, and A508) at about 300 °C for up to 100,000 hr (11.4 yr). However, they also indicated that there was no fundamental basis to dismiss the possible occurrence of thermal embrittlement over the reactor life because it occurs rapidly at slightly higher temperatures (>350 °C). Synergistic effects between Cu and Ni, as well as Ni and P, may lead to significant uncertainties in predictions based on short-term data.

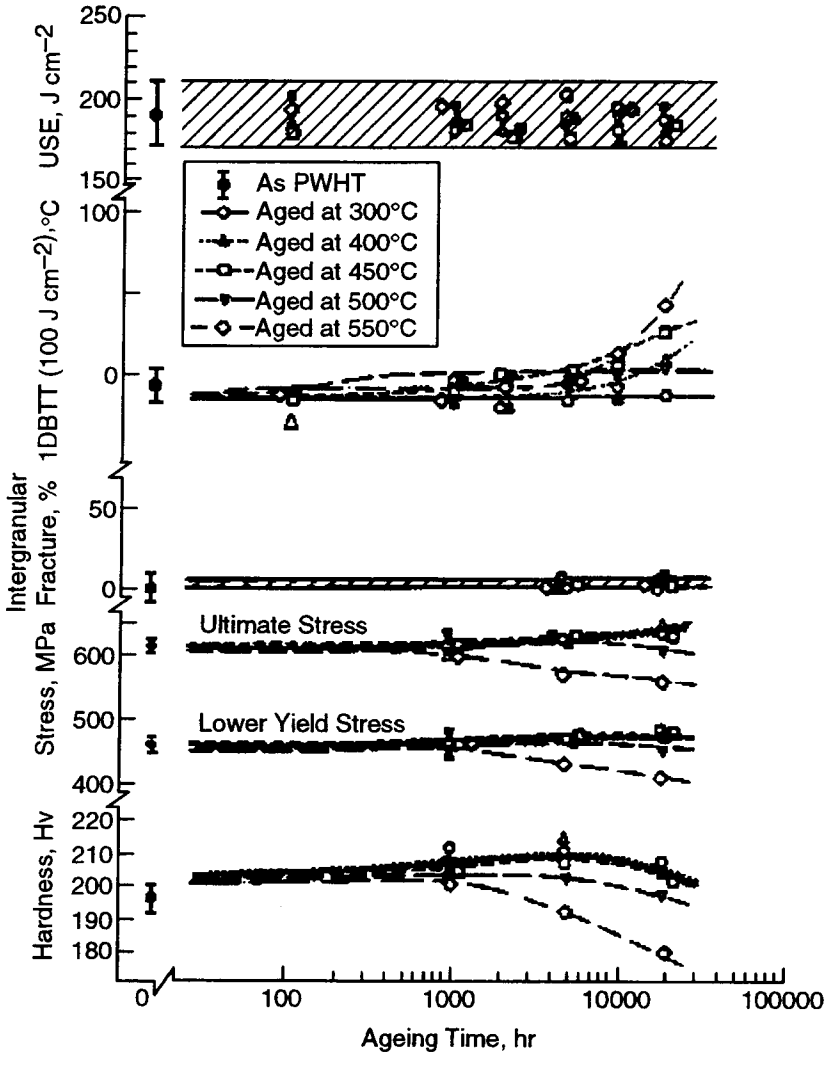

Figure 2-8. The effect of aging on the mechanical properties and fracture appearance of quenched and tempered A533B Class 1 steel in the post-weld heat treatment condition (Druce et al., 1986)

2.2.3 Effect of Carbide Precipitation

The precipitation of carbides affects the alloy content in the matrix and, therefore, influences the kinetics of temper embrittlement. Figure 2-11 shows pertinent data for a P-doped 2.25Cr-1Mo steel which had been tempered to two different hardness levels (HRC 30 and HRC 13) prior to the aging treatment to produce temper embrittlement (Yu and McMahon, 1980a). Rapid embrittlement can be observed for the low hardness steel aged at 520 °C. The high hardness steel embrittled gradually and required about 3,000 hr to reach the same degree of embrittlement exhibited by the softer material after a relatively short period (approximately 100 hr) (Yu and McMahon, 1980a). Prior tempering had produced a higher fraction of Mo-rich carbides of the M_2C type in the low hardness steel. This

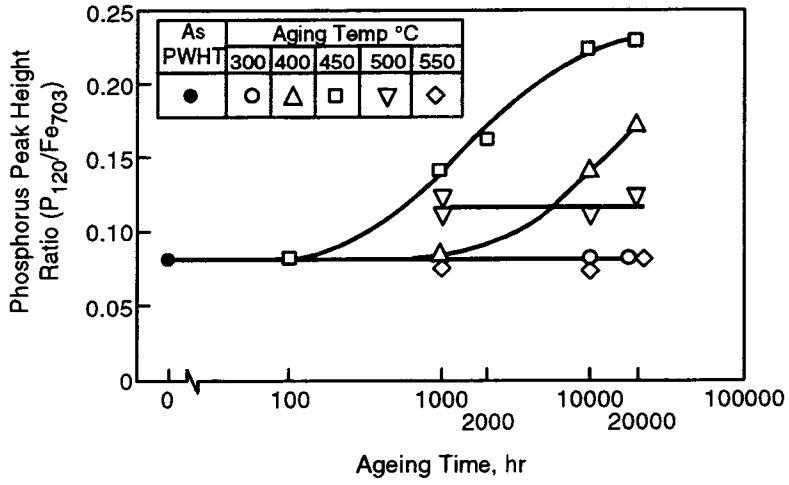

Figure 2-9. The effect of aging time and temperature on the grain boundary segregation of phosphorus in A533B-1 simulated coarse-grained heat affected zone (Druce et al., 1986)

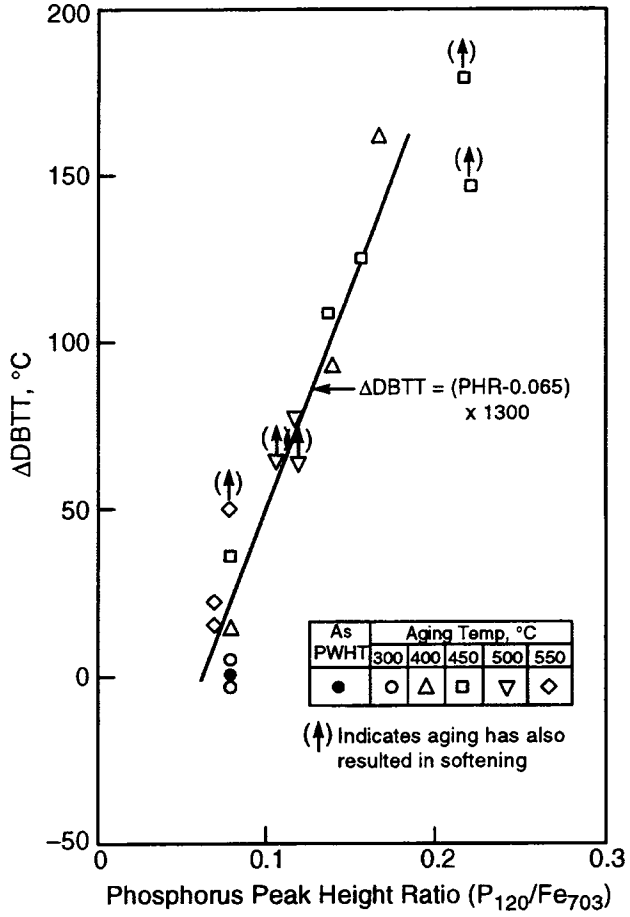

Figure 2-10. Embrittlement as a function of phosphorus segregation in A533B-1 simulated coarse-grained heat affected zone (Druce et al., 1986)

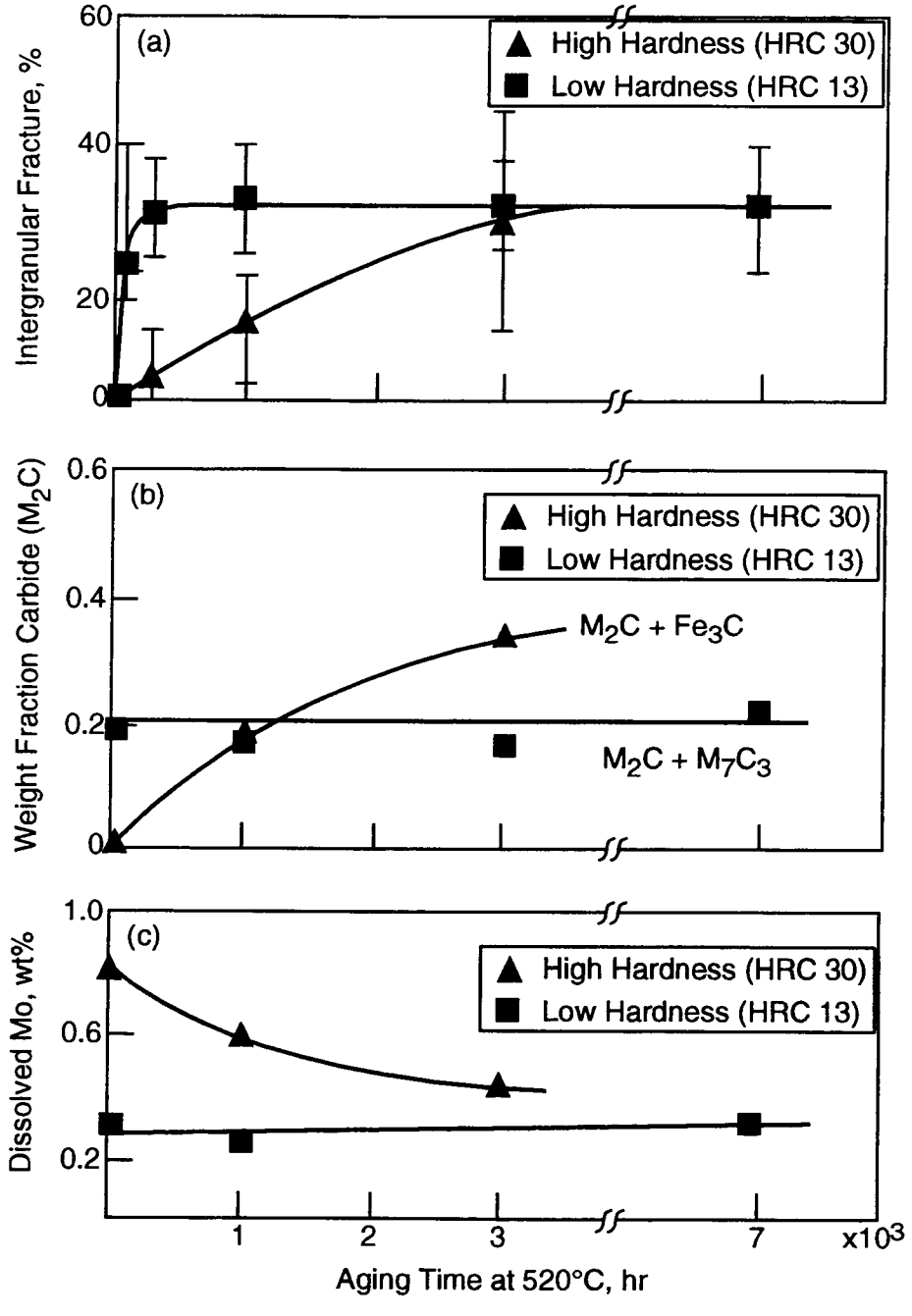

Figure 2-11. Effect of carbide precipitation on the concentration of Mo dissolved in ferrite (0.04% P, 2.25Cr-1Mo steel) (adapted from Yu and McMahon, 1980a; Khadkikar and Wieser, 1986)

precipitation of Mo-rich carbides depleted the concentration of Mo dissolved in the ferrite phase allowing P to segregate freely to the grain boundaries. In the high hardness steel, no Mo-rich carbides were initially present. These carbides formed gradually during the aging treatment intended to produce temper embrittlement. The accompanying Mo depletion of the ferrite phase then permitted P segregation and, therefore, temper embrittlement (Yu and McMahon, 1980).

The kinetics of temper embrittlement are illustrated in Figure 2-12 for P-doped 2.25Cr-1Mo steels (Murza and McMahon, 1980). Several steels with and without P addition are shown: with Mn only, Si only, and Mn-Si. These authors explained temper embrittlement response to the aging treatment on the basis of the formation of Mo-rich, M_2C carbides. The rate of temper embrittlement was slowest for the Mn-P-doped steel, intermediate for the Si-P-doped steel and fastest for the Mn-Si-P-doped steel. The temper resistance was also reported to increase in the same order [i.e., longer tempering times and/or higher tempering temperatures were necessary for the Mn-Si-P-doped steel (72 hr at 720 °C) compared to the Si-P-doped steel (40 hr at 690 °C) to obtain the same hardness level (R_c 15)]. Mn-P-doped steel (16 hr at 690 °C) required the least tempering time. Longer tempering times and higher tempering temperatures result in the Mo depletion of the matrix due to the precipitation of Mo-rich carbides. Therefore, the amount of P that is free to segregate and produce temper embrittlement is largest in the Mn-Si-P-doped steel. The amount is lowest in the Mn-P-doped steel and intermediate in the Si-P-doped steel. This effect of Mo-rich carbide precipitation, however, is transient in nature because M_2C will eventually precipitate in all the steels.

In a study of carbide precipitation, grain boundary segregation, and temper embrittlement in Ni-Cr-Mo-V rotor steels, Bandyopadhyay et al. (1985) found that after 1 hr of tempering at 600 °C, only Fe-rich M_3C carbides were precipitated. With increasing tempering time, the Cr content of these carbides increased. With a further increase in the tempering time, the Cr-rich M_7C_3 and the Mo-rich M_2C carbides were observed to precipitate. Lower levels of impurity segregation were observed after step- cooling treatment in P- and Sn-doped steels that were tempered for a shorter period of time (1 hr at 600 °C). The difference in the segregation levels with tempering time was attributed to the activity of C because of changes in the carbide composition (Bandyopadhyay et al., 1985). Similar observations by other investigators (Yu and McMahon, 1980; Ph. Dumoulin et al., 1980) have attributed these effects of the tempering time to the variations in the matrix composition, particularly Mo, due to changes in the carbide types. It has been suggested that C competes with P for grain boundary sites and thus reduces the P segregation.

Carbide formation in steel may also affect temper embrittlement due to the rejection of impurity elements from a growing carbide (Rellick and McMahon, 1974). This rejection occurs because the impurity elements are less soluble in the carbide than in the matrix. The resulting build-up of impurities at the carbide-matrix interface is transient in nature as impurities diffuse away with time. This enrichment of the carbide-ferrite interface has been shown to cause transient embrittlement in Sb, Sn, As, and P-doped Fe-0.004 percent C alloys (Rellick and McMahon, 1974). Studies have also indicated a correlation between the concentration of P in the ferrite phase and the formation of alloy carbides (Wada et al., 1982a,b).

2.2.4 Effect of Grain Size

The DBTT is related to the prior austenite grain size (Wada and Hagel, 1976; Londsdale and Flewitt, 1978; Ucisik et al., 1978). The grain size of the wrought product may be controlled by time and

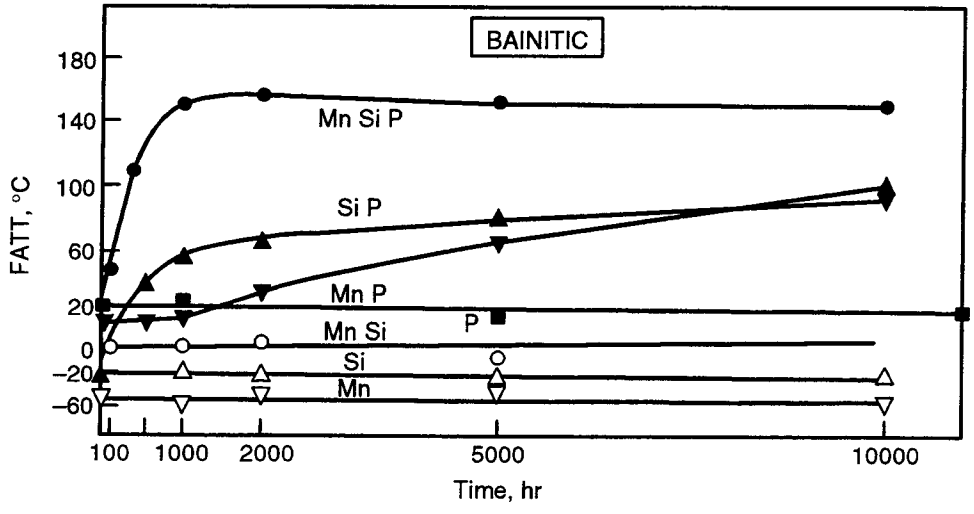

Figure 2-12. Kinetics of temper embrittlement as a function of composition in 2.25Cr-1Mo steels aged at 480 °C (Murza and McMahon, 1980a)

temperature in the austenitic region (Lonsdale and Flewitt, 1978) or by intercritical heat treatment (Wada and Hagel, 1976; Londsdale and Flewitt, 1978). The prior austenite grain size effect is larger for higher impurity levels and in the embrittled condition. In the high-purity steels, which show transgranular cleavage fracture, DBTT is virtually independent of the prior austenite grain size. However, in the presence of embrittling impurities, it can be expected that a higher concentration of impurities will be attained at grain boundaries when fewer boundaries exist due to the larger grain size.

The morphology of the grain boundary also influences the fracture mode in the temper embrittled condition (Ohtani and McMahon, 1975). However, the low temperature intergranular fracture is not necessarily limited to the prior austenite grain boundary network. It has been shown in Sb or P-doped 3.5Ni-1.7Cr temper embrittled steels that fracture may occur along the boundaries of blocky ferrite and upper bainite formed during austenite decomposition (Ohtani and McMahon, 1975).

2.2.5 Effect of Microstructure

A systematic study of the effects of microstructure on the FATT in Cr-Mo-V steel at intermediate hardness (HRC 10–20) has shown that ΔFATT is larger in a tempered martensite structure compared to that in a bainitic structure (Vander Voort, 1990). The same trend is reported for bainitic 2.25Cr-1Mo steel (Yu and McMahon, 1980). A bainitic structure in Cr-Mo-V and 2.25Cr-1Mo steel, however, has a higher FATT in the unembrittled condition (Viswanathan and Joshi, 1975; Wada and Hagel, 1976; Yu and McMahon, 1980a). In general, steels with a large FATT in the unembrittled condition have a small ΔFATT due to temper embrittlement (Viswanathan and Joshi, 1975).

Since bainitic structure, compared to martensitic structure, has a lower susceptibility to temper embrittlement, it is preferred in alloy steels which require service in the embrittling temperature range. Cooling rates as high as 3,318 °C/min and as low as 48 °C/min are reported to lead to a bainitic

structure in 2.25Cr-1Mo steel containing 0.11 percent C, 0.58 percent Mn, and 0.22 percent Si (Wada and Eldis, 1982). This has an important implication in practice as heavy sections up to 400 mm thick can be cooled to a uniform bainitic structure (Sato et al., 1982; Wada and Eldis, 1982).

A convenient parameter to measure the bainitic hardenability of a steel is the critical cooling rate, K_f, which is defined as the slowest cooling rate from the austenitizing temperature that gives a microstructure free of ferrite. K_f is influenced markedly by alloying elements. Except for Si, all elements increase the bainitic hardenability (i.e., decrease K_f) (Wada and Eldis, 1982; Bodnar and Cappellini, 1982). An empirical equation for the minimum time required to reach the ferrite formation is given below (Bodnar and Cappellini, 1982):

$$\log Cf(s) = 3.288\ C - 0.168\ Si + 1.068\ Mn + 1.266\ Cr + 2.087\ Mo + 0.300\ Ni + 0.626\ Cu - 1.931 \quad (2\text{-}1)$$

where the concentration of the alloying elements is expressed in weight percent.

The degree of embrittlement for low-alloy steels is greater for martensite than bainite and least for ferrite-pearlite. However, embrittled martensite is still tougher than nonembrittled bainite, while embrittled bainite is tougher than nonembrittled ferrite-pearlite (Vander Voort, 1990).

2.2.6 Effect of Welding

2.2.6.1 A508 Class 3 Steels

The temper embrittlement susceptibility of A508 Class 3 steel, taken from two commercially produced pressurized water reactor cutouts containing 0.007 and 0.011 percent P, has been reported by Tavassoli et al. (1984). For each heat, two types of microstructures were investigated: (i) base metal, M, and (ii) HAZ of a single-pass weld, X, combined with three heat treatments for each type of microstructure: (i) stress relief treatment, D, representative of that of the final use, (ii) de-embrittling treatment, A, and (iii) embrittling treatment, B. The temperature-time sequence of these treatments is schematically shown in Figure 2-13.

The microstructure of the base metal specimens was tempered bainite with fine grains, whereas that of the HAZ was tempered martensite with coarse grains. The precipitates found at the grain boundaries, lath interfaces, or inside the matrix were mainly cementite (Fe_3C) enriched in Mn. The concentration of Mn in the precipitates was about 3 percent compared with about 1.3 percent in solid solution. The variation in CVN impact toughness with temperature is shown in Figure 2-14. Figures 2-14a and 2-14b show that the temper embrittlement susceptibility of the base metal for the two different heats is not large for any of the three heat treatment conditions. The transition temperature shift (ΔFATT) between de-embrittled and embrittled conditions with respect to the final treatment is in the -30 ± 15 °C range. Figures 2-14c and 2-14d show that the temper embrittlement susceptibility of the HAZ is quite different from that of the base metal. Its FATT after an embrittling treatment is raised to about 80 °C for the low P heat and to 100 °C for the high P heat. The data also show that de-embrittling treatment lowers the FATT of the HAZ microstructure to about -90 °C (i.e., which is well below that of the base metal after the same heat treatment). Tavassoli et al. (1984) attributed the difference in behavior between the HAZ and the base metal to the prior austenite grain size, which is greater in the HAZ material.

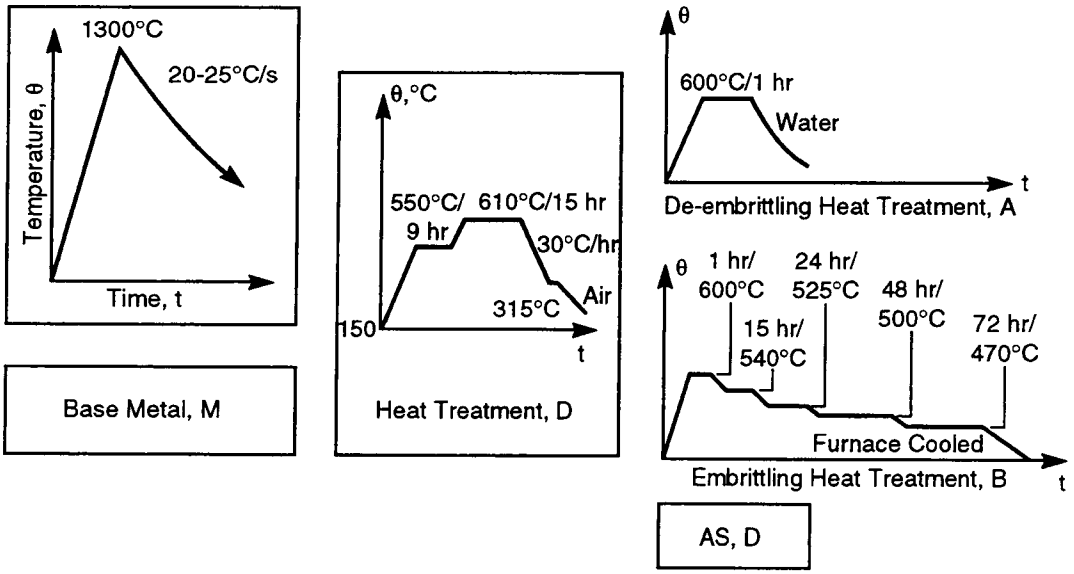

Figure 2-13. Heat treatments scheme investigated for A508 Class 3 steel (Tavassoli et al., 1984)

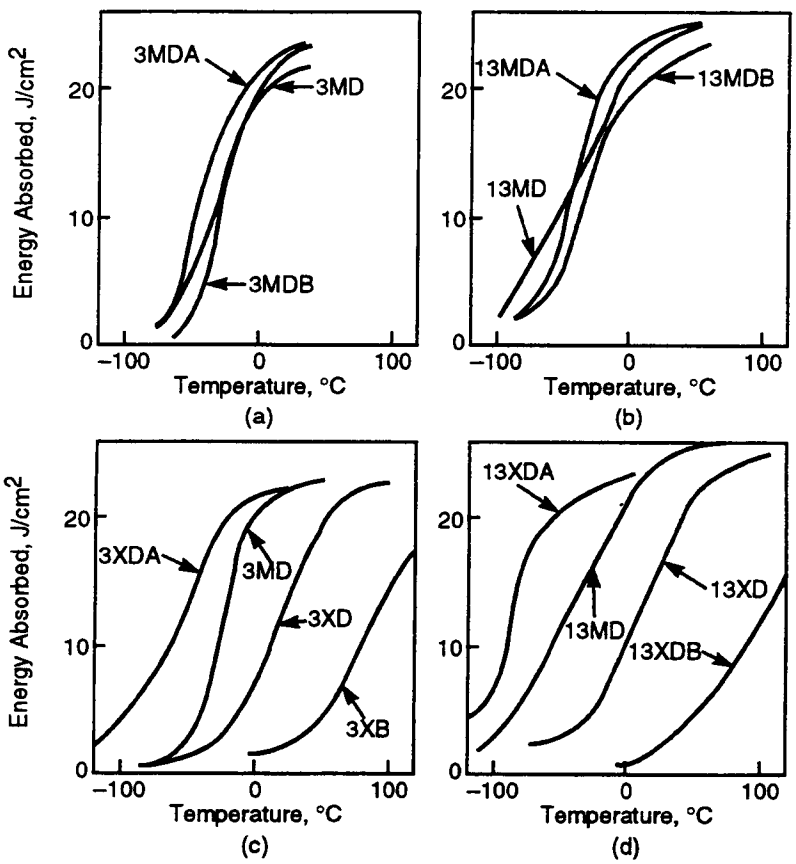

Figure 2-14. Variation in Charpy V-notch impact toughness as a function of test condition (M = base metal; X = welded metal) (Tavassoli et al., 1984)

The fractured impact specimens exhibited ductile fracture at test temperatures in the upper shelf region, whereas two modes of brittle fracture, transgranular cleavage or intergranular, were noted in the low temperature region. The former was dominant in the specimens with tempered bainitic structure (base metal) regardless of the applied heat treatment. The specimens with tempered martensitic structure (HAZ) exhibited a gradual change in the brittle fracture mode with increasing transition temperature from a completely transgranular (13XDA and 3XDA specimens) to almost entirely intergranular along the prior austenite grain boundaries (13XDB and 3XDB specimens).

The previous results can be compared with those obtained by Fukakura et al. (1993). Submerged arc welded plates of A508 Class 3 steel were isothermally aged at 350, 400, and 450 °C for up to 10,000 hr followed by tensile, Charpy impact, and fracture toughness (using compact tension specimens) tests on the base metal and the weld HAZ material. The welded plates were subjected to a PWHT at 595–615 °C for 45.5 hr before testing. Prior austenitic grain size was typically 13 μm for the base metal and 7 μm for the weld HAZ.

The tensile properties after aging at 450 °C are shown in Table 2-3. The data show that tensile properties, measured at room temperature and at 288 °C, are not affected by thermal aging of up to 10,000 hr at three aging temperatures. The DBTT, measured at an absorbed energy of 100 J, which corresponds approximately to half of the USE, slightly increased by thermal aging for both the base metal and the weld HAZ, resulting in a maximum increase of 20 °C in the base metal aged for 10,000 hr at 450 °C, as illustrated in Figure 2-15. The effect of thermal aging on the shift of the DBTT was less in the weld HAZ than in the base metal.

Influence of thermal aging on the fracture toughness properties was examined by measuring J_{IC}, the critical value of the J integral as defined by elastic-plastic fracture mechanics concepts (Ewalds and Wanhill, 1985), in room temperature air. No major difference in the effect of thermal aging on J_{IC} between the base metal and weld HAZ was found. A maximum decrease of 66.6 kN/m for the base metal and 58.8 kN/m for the weld HAZ was observed by aging for 10,000 hr at 450 °C, representing a decrease of about 30 percent with respect to the nonaged materials.

In the case of the base metal, AES showed increased segregation of P to grain boundaries with increasing aging time at 450 °C. However, the relatively low values of the P/Fe PHR explain why only 7 percent of the impact fracture surface exhibited intergranular features. No intergranular fracture was observed in the HAZ material. The lower degree of embrittlement noted in this material with respect to the base metal was attributed by Fukakura et al. (1993) to the smaller grain size of the former.

2.2.6.2 2.25Cr-1Mo Welds

The yield strength and notch toughness properties of a series of 2.25Cr-1Mo welds in the PWHT condition produced by the submerged-arc welding narrow-gap (SAW-NG) process are listed in Table 2-4 (McGrath et al., 1989). All narrow-gap welds were made using a two-pass per layer technique. The welding energy input and the weld composition in terms of C, S, and oxygen contents were the principal variables. All welds for which data were available, exceeded the required minimum yield strength of 420 MPa. The low temperature notch toughness properties expressed by the DBTT (54 J) can be assessed by comparing welds 1 or 3 with weld 6 which have essentially the same chemical composition. All these welds exhibited the required value for DBTT (54 J) of −40 °C even with an increase in the energy input from 2 to 4.3 kJ/mm. The effect of C content on low temperature toughness

Table 2-3. Mechanical properties (mean value of three specimens) of A508 Class 3 steel base metal aged at 450 °C (Fukakura et al., 1993)

Mechanical Properties	Test Temperature	Aging Time, hr					
		0	100	1000	3700	7000	10000
Yield Strength (MPa)	RT	449	458	452	450	431	450
	288 °C	400	399	394	383	385	401
Ultimate Tensile Strength (MPa)	RT	587	591	594	596	587	603
	288 °C	566	552	545	528	533	543
Elongation (%)	RT	26.2	26.9	25.3	26.4	25.7	25.6
	288 °C	21.2	21.0	20.5	20.9	20.3	19.7
Reduction in Area (%)	RT	70.8	71.0	70.3	72.0	70.5	70.3
	288 °C	66.3	68.5	65.8	67.2	69.4	68.1

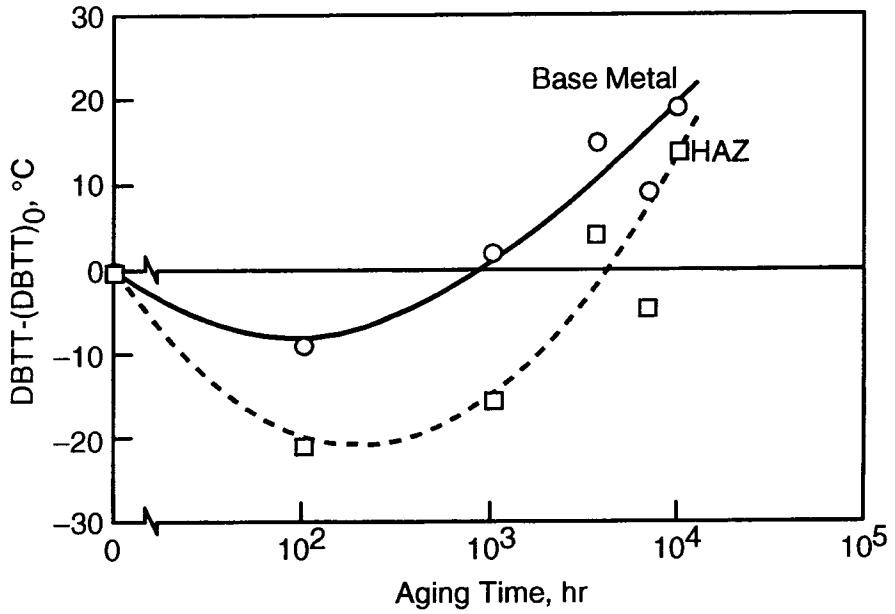

Figure 2-15. Variation of DBTT with aging time at 450 °C (Fukakura et al., 1993)

can be examined by comparing the properties of Welds 1, 3, 4, 7 and 10 in Table 2-4. Despite some dispersion in the data, it is seen that the DBTT (54 J) increased as the C content decreased.

The influence of energy input and weld C content on low temperature toughness can also be related to their effects on the microstructure of the 2.25Cr-1Mo weld metal (McGrath et al., 1989). The continuous cooling transformation diagram for 2.25Cr-1Mo steel, Figure 2-16, indicates that as weld metal cools from the austenitic region, a totally bainitic microstructure will result. A C level of 0.1 percent resulted in a fine bainitic structure. As the C content was lowered and the bainitic microstructure became coarse, Scanning Electron Microscopy (SEM) of fractured surfaces revealed a cleavage facet size which corresponded to the dimensions of the individual bainite packet size. Thus, the finer the bainite packet size the greater the resistance to cleavage fracture at low temperature and the higher the notch toughness properties of the weld.

The resistance to ductile fracture as indicated by the Charpy impact energy at 25 °C (Table 2-4) was influenced principally by the volume fraction of weld metal inclusions. A relationship between oxygen and S weight percent and volume fraction of inclusions was developed. The volume fraction of inclusions is represented by the O+S content in Table 2-4. The impact energy at 25 °C decreased as the O+S content increased. The spherical oxysulfide inclusions particles act as sites for microvoid coalescence when the fracture mode is by ductile tearing. The control of oxygen in SAW welds is mainly through the selection of flux basicity. Those welds listed in Table 2-4 with oxygen contents $\leq$0.035 percent were deposited using highly basic fluxes. The effect of inclusions is not only to lower the USE but to also to shift the Charpy curve to higher temperatures. Thus weld 2, listed in Table 2-4 as having the highest O+S content, had the lowest impact energy at 25 °C and the highest DBTT (54 J).

Table 2-4. Notch toughness of 2.25Cr-1Mo weld metal (adapted from McGrath et al., 1989)

Weld	C (wt %)	S (wt %)	O (wt %)	Tempering Parameter*	Energy Input (kJ/mm)	Yield Strength (MPa)	DBTT (54J) (°C)	Impact Energy at 25 °C (J)
1	0.10	0.009	0.026	20.2	2.0	492	−48	213
2	0.06	0.011	0.085	20.2	2.0	469	−10	98
3	0.10	0.007	0.022	20.2	2.0	456	−60	258
4	0.075	0.005	0.029	20.2	2.0	435	−30	240
5	0.06	0.006	0.054	20.6	4.3	—	−23	—
6	0.11	0.004	0.025	20.6	4.3	—	−50	—
7	0.08	0.005	0.035	20.6	4.3	—	−37	176
8	0.08	0.004	0.047	20.6	4.3	—	−33	152
9	0.055	0.021	0.069	20.4	1.8	456	−37	122
10	0.076	0.007	~0.025	20.4	1.9	468	−28	167

* TP = T (20+log t) × 10^{-3}, where T = tempering temperature in °K; and t = tempering time in hr

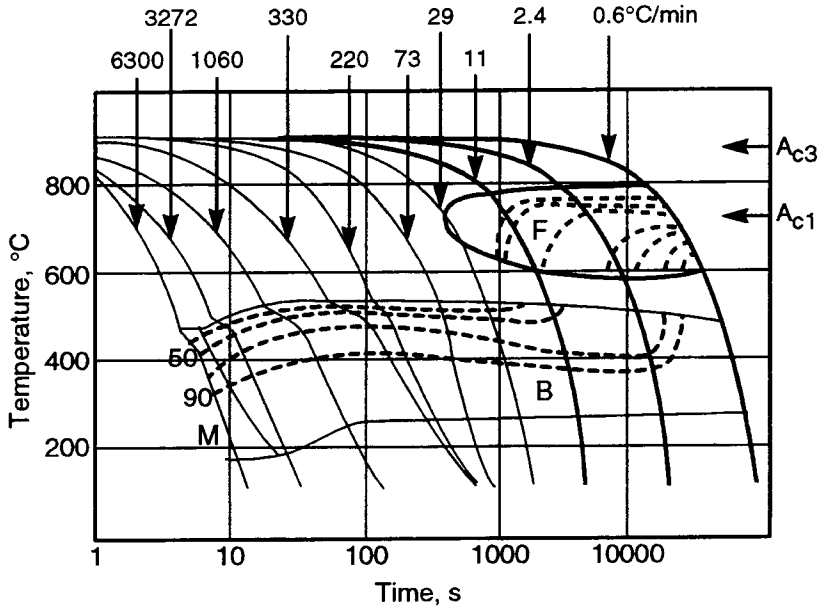

Figure 2-16. Continuous cooling transformation diagram for 2.25Cr-1Mo steel (McGrath et al., 1993)

The notch toughness properties of 2.25Cr-1Mo weld metal can be reduced by long-term exposure in the temperature range of 325–575 °C due to temper embrittlement. By simulating this long exposure with a step-cooling treatment, the notch toughness requirement can be assessed. For 2.25Cr-1Mo weld metal for petrochemical reactor vessels, the requirement is to sustain an impact energy of 54 J at −29 °C. The data in Table 2-5, as summarized by McGrath et al. (1989), show that only two of the welds met the notch toughness requirements of 54 J at −29 °C after step cooling. This observation indicates that in order to minimize temper embrittlement, it is essential to improve the weld notch toughness in the PWHT condition. Table 2-5 also shows values of ΔDBTT (54 J), which ranged from 0 to 35 °C for the different welds. No correlation was found between ΔDBTT and the Bruscato factor (Bruscato, 1970) and the J factor (Watanabe et al., 1974) which are used to quantify the role of impurity and alloying elements on the degree of temper embrittlement, as discussed in Section 3.4. It was concluded that superior resistance to cleavage and ductile fracture in heavy section 2.25Cr-1Mo submerged-arc weld metals can be achieved by the presence of a fine bainitic microstructure with a low inclusion content. Resistance to temper embrittlement after long-term service exposure at elevated temperatures could be assured by having a high toughness in the PWHT condition and a low level of residual elements such as P, Sn, Sb, and As. These toughness properties can be obtained by selecting a welding wire with low residual elements and sufficient C (0.1 percent in the weld metal) combined with a basic flux.

2.2.6.3 A516 Grade 70 Steel Welds

The application of A516 Grade 70 steel for pressure vessels operating in the petrochemical industry at lower temperatures and in less harsh environments than 2.25Cr-1 Mo steel requires less stringent notch toughness properties with a typical requirement of 27 J at −40 °C for base metal and

Table 2-5. Results of temper embrittlement of 2.25Cr-1Mo weld metals (adapted from Grosse-Woerdemann and Dittrich, 1982; Chandel et al., 1985)

Impact Energy, J, at −29 °C	ΔDBTT at 54 J (°C)	Bruscato Factor	J Factor
60	15	18.9	175
12	30	12.8	162
125	8	10.9	86
4	35	12.3	277
13	0	16.3	140
10	10	13.3	118
41	27	10.4	116
28	17	28.7	193

weld metal. The microstructure which controls the notch toughness properties of A516 Grade 70 weld metal is more complex than that of 2.25Cr-1Mo weld metal.

Evaluation of weld metals prepared by the SAW-NG process has been reported in the literature (McGrath et al., 1989). As seen in Table 2-6, welds A and B differ mainly in the levels of the elements contributing to hardenability (i.e., C, Mn, and Mo and in the S and O contents). These differences resulted from the choice of welding wire and flux basicity. The results of tensile tests on specimens A and B, shown in Table 2-7, indicate that both welds exceeded the target yield (275 MPa) and ultimate tensile (482 MPa) strength levels with weld B having slightly higher strength. In terms of notch toughness, McGrath et al. (1989) reported that weld A had superior resistance to low temperature brittle fracture (impact energy at −40 °C) and ductile fracture (impact energy at 20° C) than weld B. The high volume fraction of inclusions in weld B is considered responsible for the low impact energy exhibited at 20 °C.

Table 2-6. Chemical composition of C-Mn and C-Mn-Mo steel welds (adapted from McGrath et al., 1989)

Weld	Element, wt. %							
	C	Mn	Si	Mo	Al	O	S	P
A	0.11	1.37	0.35	<0.005	0.013	0.013	0.008	0.013
B	0.07	0.91	0.52	0.49	0.006	0.080	0.017	0.012

Table 2-7. Mechanical properties of A516 Grade 70 welds (McGrath et al., 1989)

Weld	Yield Strength (MPa)	Ultimate Strength (MPa)	Elongation (%)	Reduction in Area (%)
A	393	510	30	72
B	407	535	27	64

The microstructure of weld A, which consisted mainly of acicular ferrite in the as-deposited columnar region and polygonal ferrite in the reheated region, provided high resistance to brittle fracture at low temperatures. The presence of Mn (1.37 percent) promotes the formation of acicular ferrite in the columnar region and refines the polygonal ferrite in the reheat region. A level of 1.40 percent Mn (C=0.05 percent) resulted in approximately 65 percent acicular ferrite and a fine polygonal ferrite which provided optimum notch toughness properties. In addition to the grain refining effects of Mn in weld A, the low volume fraction of fine oxysulfide inclusions (O+S=0.021 percent) contribute as nucleation sites to the formation of acicular ferrite (McGrath et al., 1989). On the other hand, weld B featured a microstructure of coarse grain boundary ferrite and ferrite with second phase which had poor resistance to brittle fracture. The reheated region also contained a coarser polygonal ferrite than that found in weld A. The coarse ferrite structure in weld B was promoted by the high volume fraction of inclusion particles (O+S=0.097 percent) and the high level of Mo (0.5 percent). Acceptable notch toughness properties in A516 Grade 70 narrow-gap welds are achieved by having a relatively high proportion of acicular ferrite and fine polygonal ferrite combined with a low inclusion content. The presence of sufficient Mn (approximately 1.4 percent) in the weld metal promotes the formation of acicular ferrite and the use of highly basic fluxes lowers the inclusion content.

2.3 APPROACHES FOR REDUCING SUSCEPTIBILITY TO TEMPER EMBRITTLEMENT

The susceptibility to temper embrittlement of some candidate materials for the WP outer disposal overpack can be reduced through modification of the chemical composition or through processing techniques. As an example, two potentially promising methods are briefly described. The first method is based on reducing the amount of P in the steel through a two-step process combining the basic oxygen furnace (BOF) and the ladle refining furnace (LRF) processes, and the second one is accomplished by small but controlled additions of Al and B, accompanied by reductions in the Si content.

2.3.1 2.25Cr-1Mo Steels

Reduction in the Si and Mn contents, as well as in the amount of impurity elements such as P and Sn, decreases the susceptibility to temper embrittlement. However, reduction of Si and Mn without the addition of other strengtheners typically results in lowering the strength both at room and elevated temperature. The reduction of Si and Mn decreases the hardenability for normalizing so that the microstructure transforms with poor strength and toughness (Nakanishi et al., 1984). Use of ultra low-P steel refined through the BOF and the LRF process appears to solve the problem. The BOF-LRF refined

2.25Cr-1Mo steel contains a normal or higher Si content and an extremely low P content (<0.005 weight percent).

A study of the temper embrittlement susceptibility and tensile properties at elevated temperatures of a BOF-LRF ultra low-P 2.25Cr-1Mo steel plates and weldments has been reported (Kusuhara et al., 1980). The steel showed low susceptibility to temper embrittlement despite its higher Si content and impurities. The results of tensile tests at 454 °C following a simulated PWHT are plotted in Figure 2-17 against a tempering parameter (TP) given by $T(20+\log t)\times 10^{-3}$, where T is the tempering temperature in °K and t is the tempering time in hr. No differences in the yield strength are observed between the two types of steel. The results of temper embrittlement tests are shown in Figure 2-18. The highest toughness, corresponding to a minimum in the FATT, was observed at a tempering parameter value ranging from 20.0 to 20.5 in all cases. Both before and after the step cooling, the toughness of 75-mm-thick normalized and tempered plate was inferior to that of the 180-mm-thick quenched and tempered plate. The difference was attributed to the formation of pro-eutectoid ferrites formed during the air cooling after the normalizing treatment. The embrittlement caused by the step cooling was negligible in both 75 mm and 180-mm-thick plate. The ΔFATT was 10 °C or less, and a high toughness corresponding to a FATT of −40 °C, even after the embrittlement treatment, is evident. Figure 2-19 shows the results of Charpy impact tests on specimens of weld metal, bond, and HAZ before and after the step-cooling treatment. The data reveals very little embrittlement as a result of the embrittling treatment in all three types of specimens. Based on this study it appears that the ultra low-P type 2.25Cr-1Mo steel manufactured by the BOF-LRF method has a much lower susceptibility to temper embrittlement than the normal steel despite its higher Si content. Similar conclusions have been reported in a later publication (Kikutake et al., 1983).

Another method to reduce the susceptibility of 2.25Cr-1Mo steels to temper embrittlement while retaining strength is based on the addition of Al and B (Nakanishi et al., 1984). This method is discussed in more detail in the following section. Although Al-B treated low-Si steel contains a small amount of ferrite, the mechanical properties of the Al-B treated steel do not show the degradation in strength typically observed in low-Si 2.25Cr-1Mo steels.

2.3.2 A515 Grade 70 and A516 Grade 70 Steels

The effective combination of soluble Al and B is shown in Figure 2-20 as reported by Nakanishi et al. (1984). The necessary soluble Al content is higher for C steel than for 2.25Cr-1Mo steel as shown in Figure 2-20. The microstructures of A515 Grade 70 and A516 Grade 70 consist of ferrite and lamellar pearlite. With the addition of Al and B to these steels, the microstructure changed from ferrite+lamellar pearlite to ferrite+bainite+pearlite, leading to an increase in the tensile strength of the processed steels. Figure 2-21 shows that it is possible to decrease the C content by 0.06 percent or more while retaining the tensile strength by the addition of Al and B treatment. Toughness is also improved by lowering the C content. Table 2-8 shows the chemical compositions of Al- and B-treated low C A515 Grade 70 and A516 Grade 70 with 0.066 percent Al compared with the ordinary steels. A Mo content of 0.15 percent or more reportedly has to coexist with B to obtain the desired effect of B (Nakanishi et al., 1984). In modern steel making practice, total B can easily be controlled from 3 to 9 ppm. Therefore, large scale production of such a steel is possible.

The investigation by Nakanishi et al. (1984) also showed that the weldability of Al-B treated low-C A516 Grade 70 also improved as exhibited by the increased toughness for the same C content

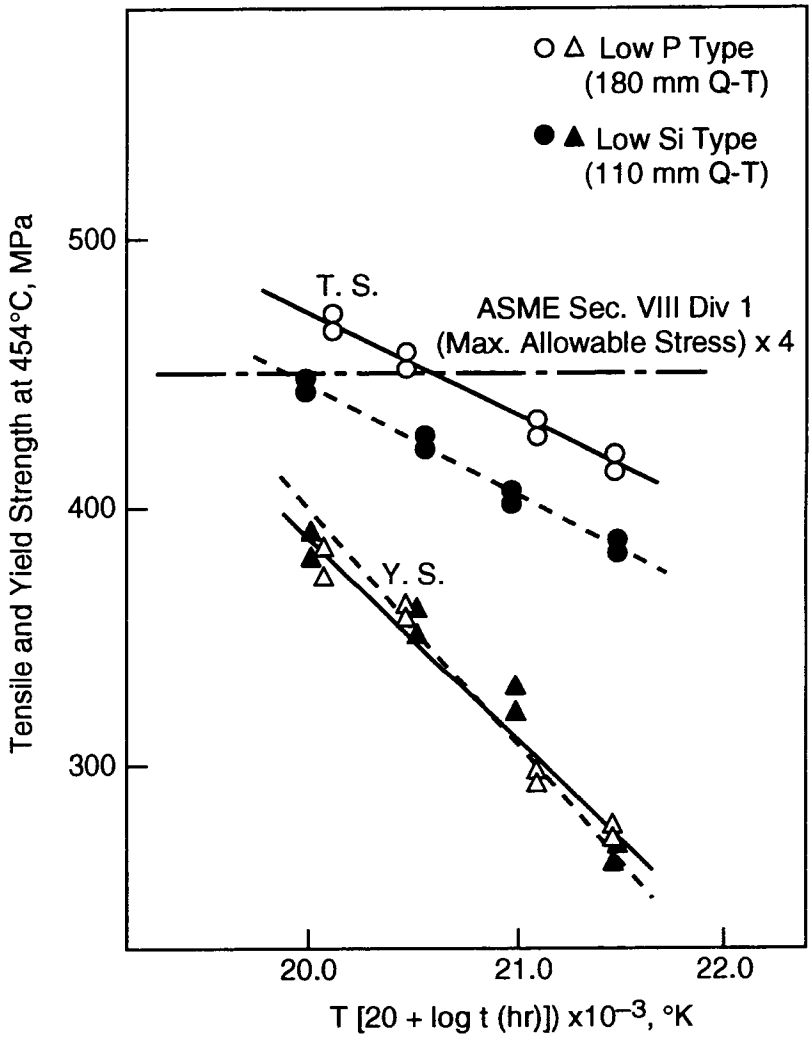

Figure 2-17. Comparison of high temperature tensile properties between low P and low-Si-type 2.25Cr-1Mo steel (Q-T: quenched and tempered; T.S.: tensile strength; Y.S.: yield strength) (Kusuhara et al., 1980)

(Figure 2-22) and also by lowering of the required preheating temperature to prevent weld cracking (Figure 2-23). It is possible to decrease the preheating temperature by more than 75 °C for Al-B treated steels. The weld cracking susceptibility was evaluated on the basis of a factor designated as P_{CM} and expressed by the following equation:

$$P_{CM}\,(wt.\ \%) = C + Si/30 + Mn/20 + Cu/20 + Ni/60 + Cr/20 + Mo/15 + V/10 + 5B \qquad (2\text{-}2)$$

where the concentration of the alloying elements is expressed in weight percent.

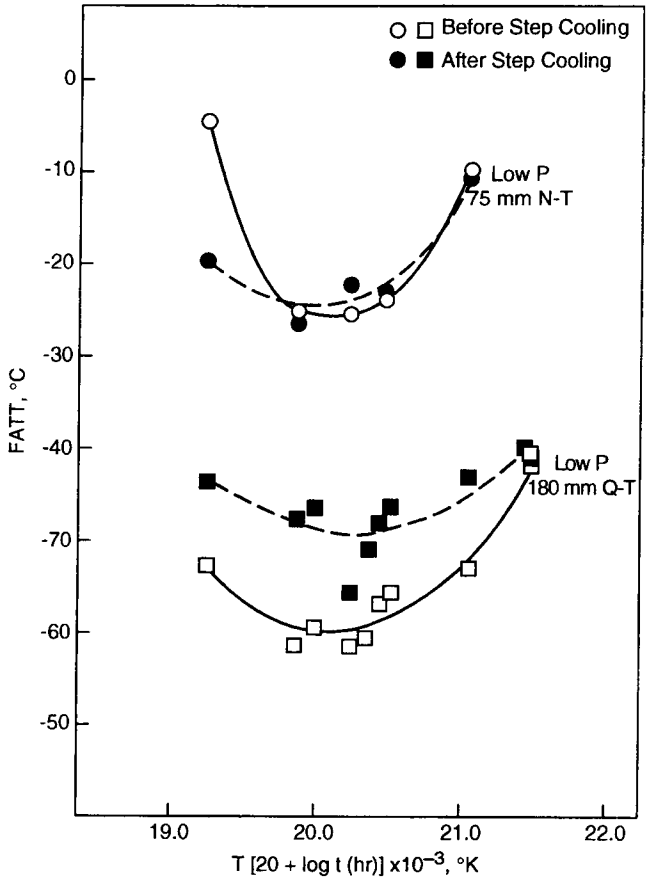

Figure 2-18. Charpy impact properties of 2.25Cr-1Mo steels before and after step cooling (N-T: normalized and tempered; Q-T: quenched and tempered (Kusuhara et al., 1980)

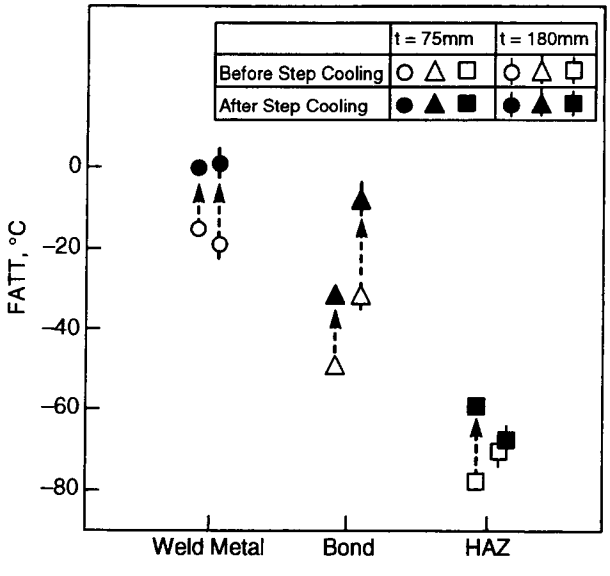

Figure 2-19. Charpy impact properties of weldment before and after step cooling (Kusuhara et al., 1980)

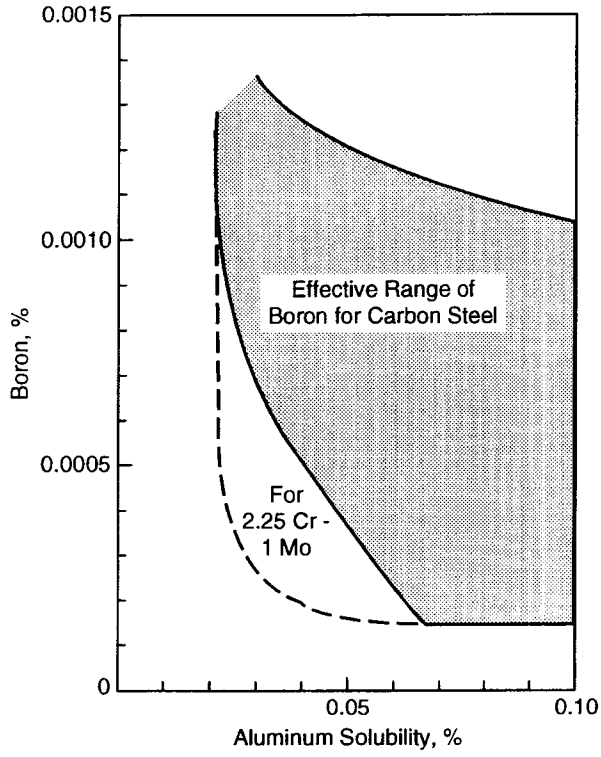

Figure 2-20. Effective range of soluble Al and B for hardenability for normalizing treatment (Nakanishi et al., 1984)

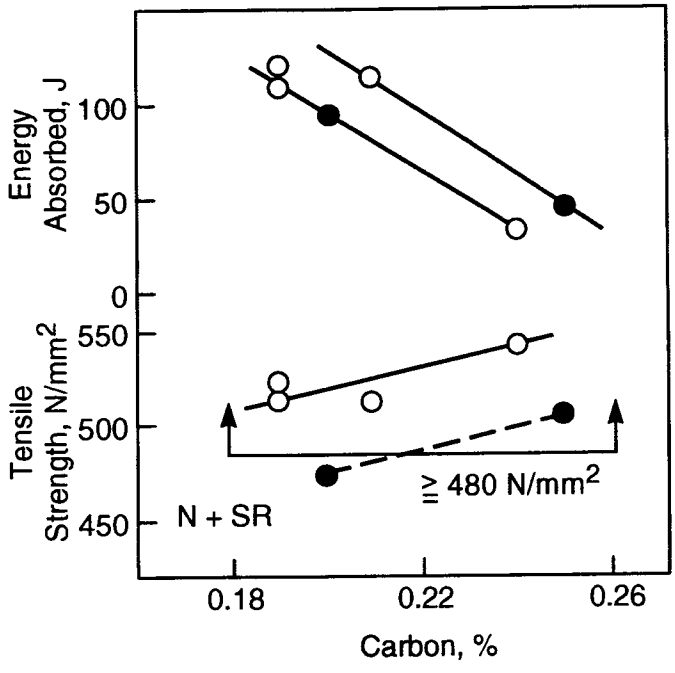

Figure 2-21. Effect of C and Al-B treatment on tensile strength and toughness of A515, Grade 70 steels. (○ = Al-B treated; ● = ordinary) (Nakanishi et al., 1984)

Table 2-8. Chemical composition of A515 Grade 70 and A516 Grade 70 (adapted from Nakanishi et al., 1984)

Steel		Element, wt. %								
		C	Si	Mn	Cu	Ni	Cr	Mo	Nb	B
A515 Grade 70	Al-B treated	0.20	0.25	1.00	—	0.15	0.15	0.15	—	0.0006
	Ordinary	0.29	0.25	1.00	0.15	0.20	0.15	0.12	—	—
A516 Grade 70	Al-B treated	0.15	0.25	1.10	—	—	0.30	0.15	0.02	0.0006
	Ordinary	0.21	0.25	1.10	0.30	0.30	—	—	0.02	—

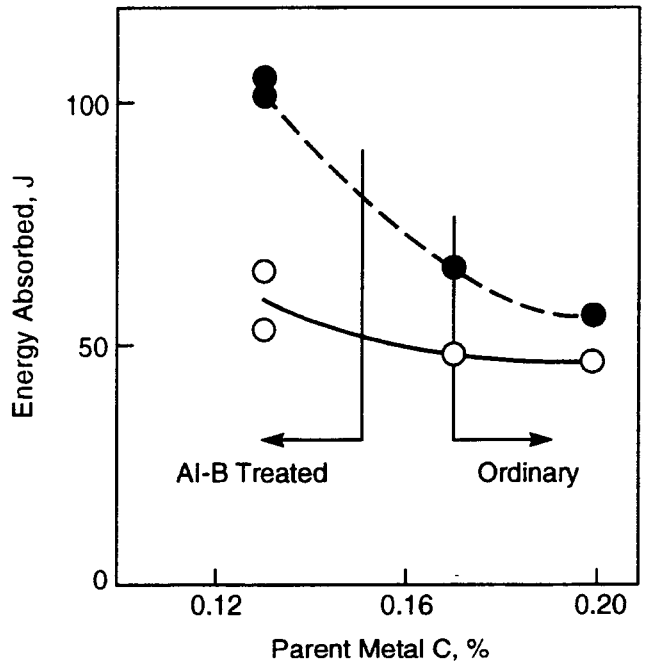

Figure 2-22. Toughness of welds in Al-B treated and ordinary A515, Grade 70 steel (Nakanishi et al., 1984)

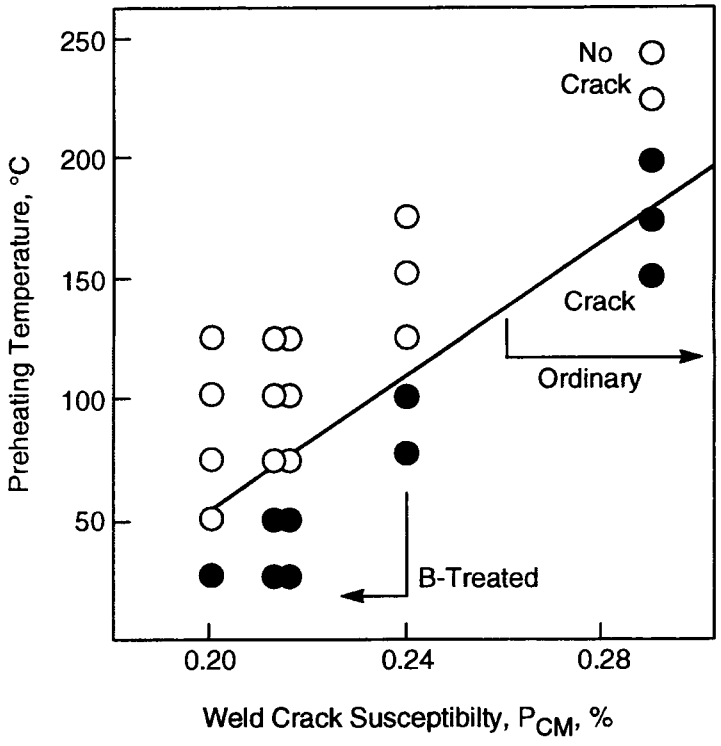

Figure 2-23. Weld cracking susceptibility of A515, Grade 70 steel in untreated and Al-B treated condition (Nakanishi et al., 1984)

3 PREDICTIVE APPROACHES RELATED TO THERMAL EMBRITTLEMENT

3.1 PHENOMENOLOGICAL AND MECHANISTIC OBSERVATIONS RELATED TO TEMPER EMBRITTLEMENT

McMahon (1968) and, more recently, Hickley and Bullock (1992), have summarized the most relevant observations regarding the phenomenological aspects of reversible temper embrittlement, many of which have been reviewed in Section 2, as follows:

(i) Embrittlement occurs within the temperature range of 350 to 575 °C and exhibits a C-shape curve temperature-time relationship within this range.

(ii) The degree and rate of embrittlement are profoundly affected by alloy content: (i) plain C steels (<0.5% Mn) do not embrittle; (ii) small amounts of Mo (<0.5%) and W delay embrittlement; (iii) Cr and Mn and to a lesser extent Ni enhance embrittlement; and (iv) a decrease in the C content reduces the degree of embrittlement, but a complete absence of C does not entirely prevent embrittlement.

(iii) Embrittlement occurs only in the presence of specific impurity elements that segregate to grain boundaries. These are Sb, P, Sn, and As in order of decreasing severity on a weight percent basis. Recently Bi, Se, Ge, and Te have been shown to produce temper embrittlement in Ni-Cr steels. Of the detrimental impurity elements found in steel, P has been shown to be the most predominant.

(iv) In low-alloy steels having ferrite plus carbide microstructures, embrittlement occurs by decohesion along prior austenite grain boundaries. Decohesion occurs in ferrite-ferrite and ferrite-carbide grain boundaries, but it is restricted almost entirely to those which lie along prior austenite grain boundaries.

(v) There is evidence that both impurity elements and alloying elements (such as Cr, Ni, and Mn) are concentrated on prior austenite grain boundaries in embrittled steel. However, the concentration of impurity elements are much higher, sometimes approaching 20 to 300 times their bulk concentrations.

(vi) If all other variables are being held constant, increases in prior austenite grain size results in increasing embrittlement.

(vii) Embrittlement is reversible. Severely embrittled material may be restored to its original condition by heating for short times above the embrittling temperature range.

(viii) Prolonged heating at temperatures above the embrittlement range results in a decrease in the embrittlement rate when subsequently heated in the embrittling range.

(ix) Embrittlement is strain rate dependent. Except at very low temperatures, an impact test such as the Charpy test is needed to observe the difference between embrittled and

de-embrittled material. There is some indication that embrittlement affects the flow strength of the material but does not affect the yield strength.

(x) For a given composition of the steel the shift in embrittlement is greater for the martensitic condition than for the bainitic and greater for the bainitic than for the pearlitic. The final embrittlement transition temperature is approximately the same for all conditions if they are all of about the same strength level. In other words, the different degrees of shift result from the different initial toughness levels of the three conditions.

(xi) Plastic deformation after embrittlement appears to lower the transition temperature whereas plastic deformation during an embrittlement treatment appears to delay the development of embrittlement. Strain up to 10 percent prior to isothermal aging accelerates the occurrence of embrittlement (van Zyl et al., 1994).

From all these observations, it can be concluded that chemical composition of the alloy, heat treatment and operating temperature play important roles in the development of temper embrittlement.

3.2 MODELING OF SEGREGATION AND TEMPER EMBRITTLEMENT

If a steel is held in the embrittling temperature range, segregation to prior austenite grain boundaries of impurity elements such as Sb, Sn, P, As, etc. will occur. This segregation, which is usually confined to one or two atomic layers and decays exponentially away from the grain boundaries, is in part due to reduction in lattice strain energy of the system. Impurity elements with the exception of As exhibit a marked difference in atomic radii with respect to Fe and by locating in distorted sites of the grain boundaries the effect of the mismatch can be minimized. The misfit strain energy in the lattice decreases in the order Sb > Sn > P, and it is reflected in their solubility in Fe in the same order.

Seah and Hondros (1973) showed that the theoretically calculated grain-boundary enrichment ratio is inversely proportional to the atomic solid solubility of the element in the parent lattice for a simple binary system, as illustrated in Figure 3-1 (Seah, 1983). Based on this relationship, the tendency for segregation should decrease in the order Sb > Sn > P. The chart on the right side of the same figure shows values obtained in steels in which the solubility is not known. It can be noted that the enrichment for impurities such as Sb, Sn, and P appears to be an order of magnitude higher in steels than in pure Fe.

Hondros (1965) also found that the driving force for segregation is lowering of the surface energy, as expressed in a simple manner by the Gibbs adsorption equation

$$X_b - X_c = -(X_c/kT)\,(d\gamma/dX_c) \qquad (3\text{-}1)$$

where X_b is the molar fraction of the impurity in the grain boundary, X_c is the molar fraction in the bulk, k is Boltzmann's constant, T is the absolute temperature, and $d\gamma/dX_c$ is the reduction in the grain-boundary surface energy due to segregation. This equation states that any solute which lowers γ tends to be segregated at equilibrium. This tendency increases as the temperature decreases and $d\gamma/dX_c$ increases. An element such as P has large values of $d\gamma/dX_c$, whereas Ni has a much lower value.

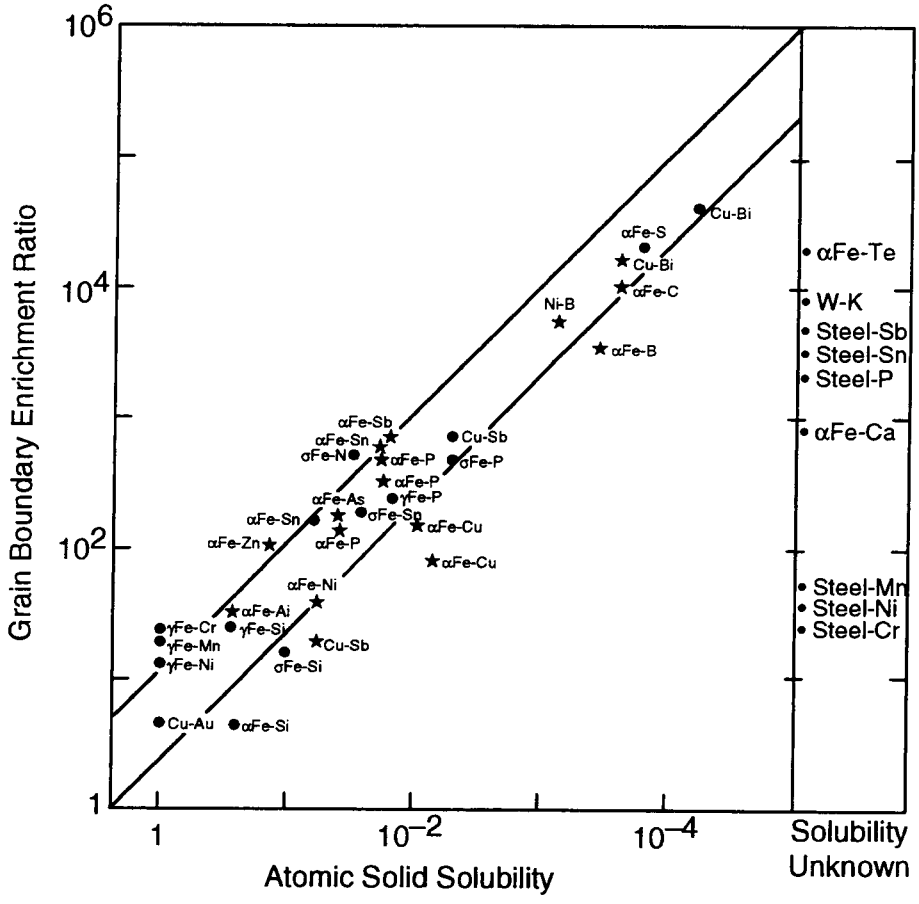

Figure 3-1. Predictive plot for the grain boundary enrichment ratio as a function of atomic solid solubility (Seah, 1983)

In the earliest theory developed for segregation to grain boundaries in binary systems, McLean (1957) proposed a model in which the solute atoms populate grain boundary and lattice sites with an energy difference, ΔG_b, the Gibbs free energy of segregation. Using simple statistical thermodynamics, McLean postulated that system energy was minimized for a fractional monolayer coverage of segregant, X_b, at the grain boundary, leading to the expression

$$X_b/\left(X_b^0 - X_b\right) = \left[X_c/(1 - X_c)\right] \exp\left(-\Delta G_b/RT\right) \tag{3-2}$$

where X_b^0 is the fractional coverage at saturation, and R is the gas constant.

Equation (3-2) was modified by Seah and Hondros (1973) by introducing $\Delta G_b'$, estimated by using a gas adsorption isotherm, and the atomic solid solubility, X_c^0, to obtain the following expression

$$X_b/\left(X_b^0 - X_b\right) = \left[X_c/X_c^0\right] \exp\left(-\Delta G_b'/RT\right) \tag{3-3}$$

Equation (3-3) in the dilute limit, if X_b^0 is one monolayer, can be expressed as

$$\beta_b = X_b/X_c = \left[1/X_c^0\right] \exp\left(-\Delta G_b'/RT\right) \tag{3-4}$$

where β_b is the grain boundary enrichment ratio plotted in Figure 3-1.

For ternary and more complicated systems the problem of site competition and cosegregation appears. It is assumed that no interaction exists between segregated atoms in simple models. If interaction exists, an interaction energy, ψ, can be postulated leading to a modification of the exponential factor in Eq. (3-2) (Seah, 1983). The new equation can be expressed as

$$X_b/\left(X_b^0 - X_b\right) = \left[X_c/\left(1 - X_c\right)\right] \exp\left\{\left[-\Delta G_b - Z\psi\left(X_b/X_b^0\right)\right]/RT\right\} \tag{3-5}$$

When the segregants are attracted, ψ is negative, and if they are repealed, ψ is positive. In the case of ψ equal to zero (no interaction), Eq. (3-5) is reduced to Eq. (3-2).

The most accepted model to explain cosegregation was developed by Guttmann (1975). This model is based in regular solid-solution theory and assumes that the driving force for segregation is an attractive interaction between the cosegregating solutes. In this case,

$$\frac{X_{bi}}{X_{bi}^0} = \frac{X_{ci}\exp\left(-\Delta G_{bi}/RT\right)}{1+\sum_{i=1}^{2} X_{ci}\left[\exp\left(-\Delta G_{bi}/RT\right)-1\right]} \tag{3-6}$$

where X_{b1} and X_{b2} are the molar fractional monolayers segregated by the impurity and alloying elements of bulk contents X_{c1} and X_{c2}, respectively. In addition,

$$\Delta G_{b1} = \Delta G_{b1}^0 + \alpha_{12}' X_{b2} \tag{3-7}$$

$$\Delta G_{b2} = \Delta G_{b2}^0 + \alpha_{12}' X_{b1} \tag{3-8}$$

where ΔG_{b1}^0 and ΔG_{b2}^0 are the free energy of segregation of the impurity and alloying elements separately in the matrix. The interaction coefficient, defined as

$$\alpha_{12}' = \alpha_{12} - \alpha_{10} - \alpha_{20} \tag{3-9}$$

represents the difference in the attractive interactions between the two solutes and their independent interactions with the solvent. If α_{12}' is negative, segregation of the alloying element enhances segregation of the impurity. As discussed by Seah (1983) the general effect of the interaction can be seen in Figure 3-1. Alloying elements with a negative value of α_{12}' cause the impurity element solubility to fall. Simultaneously, as predicted by Eqs. (3-6) and (3-7) the segregation level rises. Thus, the addition of an alloying element causes the point for the original binary system in Figure 3-1 to move diagonally upwards but to stay within the general correlation. If the interaction is too strong as, for example, in MnS

(α_{12} = 410.1 kJ/g at), stable compounds will precipitate in the interior of the grains, and if it is too weak, there will be insufficient driving force for segregation (Guttmann, 1975).

The thermodynamics of the cosegregation of P and alloying elements in iron and steels has been discussed by Guttmann et al. (1982), concluding that Ni, Cr, and Mo do not segregate *per se* in Fe and that the segregation of these elements is driven by that of P through a strong interactive attraction at the boundaries. Yu and McMahon (1980b) have applied the Guttmann's theory to provide a semiquantitative explanation of the enhanced segregation of P by Mn and Si in 2.25Cr-1Mo steel. However, Briant and Banerji (1983) have critically evaluated modeling the thermodynamics of grain boundary segregation, emphasizing the limitations of this type of approach. They indicate that it is hard to obtain an accurate estimation of the amount of grain boundary segregation in fracture surfaces, due to roughness, variations in the angle of the boundary, and additional experimental difficulties in the application of AES. An additional factor is the variation of grain boundary coverage from boundary to boundary that makes it difficult to accurately calculate the free energy of segregation. Regarding the Guttmann approach, the most important criticism of Briant and Banerji is that the model has little predictive capability because there is no reliable choice for the values of α.

In many practical situations where segregation is important, the segregant atoms often have insufficient time to reach equilibrium, particularly at relatively low temperatures. Therefore, the kinetics of segregation require consideration. The basic equation to describe the kinetics of segregation was first developed by McLean (1957). Solute atoms are assumed to segregate to a grain boundary from two infinite half crystals of uniform solute content. Diffusion in the crystals is described by Fick's laws and the ratio of the solute in the grain boundary to that in the adjacent atom layer of the bulk is given by the enrichment ratio defined in Eq. (3-4). The kinetics of the segregation are expressed by

$$\begin{aligned}&\left[X_b(t) - X_b(0)\right]/\left[X_b(\infty) - X_b(0)\right] \\ &= 1 - \exp\left(4Dt/\beta_b^2 f^2\right) erfc\left(4Dt/\beta_b^2 f^2\right)^{1/2}\end{aligned} \tag{3-10}$$

where $X_b(t)$ and $X_b(\infty)$ are the grain boundary content at time t and at equilibrium, respectively, and D is the diffusion coefficient at the temperature. The factor $f=a^3b^{-2}$ is related to the atom sizes of the solute and matrix elements, b and a, respectively.

For shorter times, Eq. (3-9) approximates to the following equation

$$\begin{aligned}&\left[X_b(t) - X_b(0)\right]/\left[X_b(\infty) - X_b(0)\right] \\ &= \left(2b^2/\beta_b 3\right)\left[4Dt/\pi\right]^{1/2}\end{aligned} \tag{3-11}$$

The main assumption made by McLean is that the grain boundary is very thin compared to the size of the grain and that the boundary can be treated as a separate phase. It should be noted that the equilibrium concentration should be known to predict the segregation kinetics. In practice, β_b is only constant for dilute systems with low segregation levels. As segregation proceeds, β_b falls as a result of saturation (Seah, 1983).

In more complex problems of kinetics of segregation in ternary systems, the McLean approach incorporating the Guttmann theory has been used to define the grain boundary concentration (Guttmann and McLean, 1979; Seah, 1983). However, predictions using Eq. (3-9) for a particular segregant, such as P in a Ni-Cr steel, exhibit good agreement with experimental results as noted by Briant and Banerji (1983). Recently, alternative mechanistic interpretations and models have been suggested. Militzer and Wieting (1989) questioned whether the segregation kinetics of P in steels is governed by bulk diffusion and suggested that the growth of a P-rich phase by grain boundary diffusion is the rate determining process.

As discussed above, there are clear evidences that the segregation of certain impurity elements to grain boundaries leads to grain boundary decohesion. Only in recent years, quantum mechanics theoretical calculations have been made to study changes in chemical bonding at the grain boundaries produced by impurity atoms that lead to decohesion (Briant and Banerji, 1983; Wu et al., 1994). Important advances have been made in this field, but a review of work in this area is out of the scope of this report.

3.3 APPLICATION OF MODELING TO LONG-TERM THERMAL AGING

As noted in Section 2.2.2.3, Druce et al. (1986) found a linear dependence between embrittlement and the degree of P segregation in A533B steel (Figure 2-10) suggesting that embrittlement in this steel is essentially controlled by P segregation. By applying McLean's equilibrium segregation theory, they were able to assess and predict grain boundary P segregation as a function of bulk P content, aging time, and temperature. Druce et al. (1986) found that ΔG_b can be expressed by the following equation

$$\Delta G_b\ (J/mol) = -63{,}000 + 21.0\ T(^\circ K) \tag{3-12}$$

by rearranging Eq. (3-2) in terms of ΔG_b and measuring the P/Fe PHR by using AES within the range of temperatures of 450 to 550 °C over which equilibrium was rapidly established.

The kinetics of segregation was modeled by using Eq. (3-10), assuming a simple linear dependence between grain boundary and bulk concentration of P that was found to be valid up to 0.2 grain boundary coverage. The diffusion coefficient of P in the matrix was evaluated by a compilation of high temperature diffusion data for iron and various steels as shown in Figure 3-2, from which the following expression was derived

$$D\ (cm^2/s) = 0.25\ \exp[-200\ (kJ/mol)/RT] \tag{3-13}$$

The predicted grain boundary coverage associated with each treatment was determined and compared with the experimental measurements obtained by AES, as depicted in Figure 3-3.

The modeling results clearly indicate that the equilibrium level of P segregation decreases and the rate of segregation increases as the temperature is increased, in agreement with the experimental results shown in Figure 2-9. Finally, the predicted grain boundary segregation kinetics combined with the embrittling potency of P as represented in Figure 2-10, allowed Druce et al. (1986) to predict the kinetics of embrittlement. The validity of the approach was confirmed by comparing for all the aging temperatures and times the predicted and observed shifts in the DBTT.

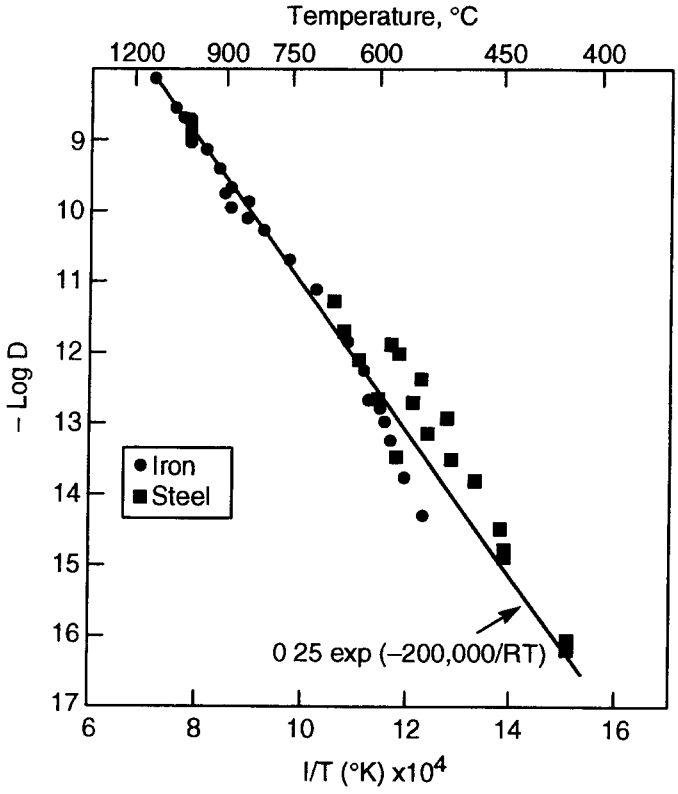

Figure 3-2. Compilation of phosphorus diffusion coefficients in iron and steels (Druce et al., 1986)

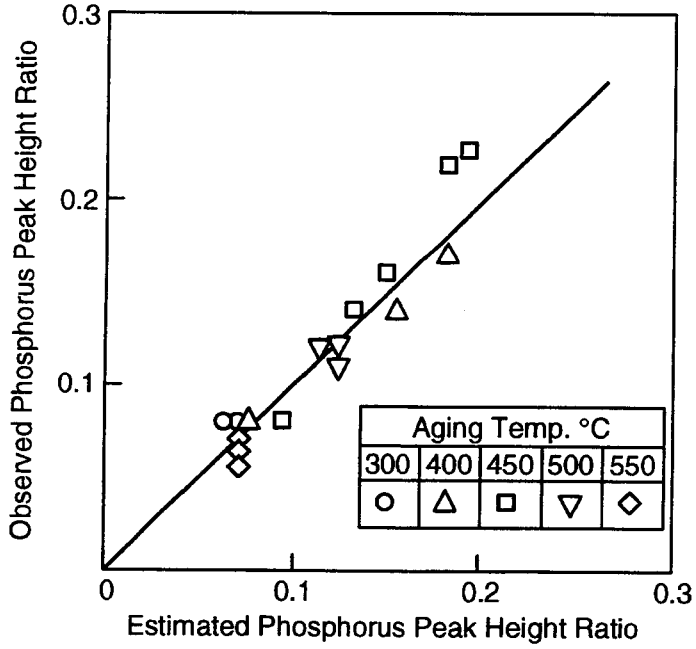

Figure 3-3. Comparison of the observed phosphorus segregation in A533B simulated coarse-grained heat affected zone with that estimated from McLean's model for equilibrium segregation (Druce et al., 1986)

It can be concluded, from the detailed analysis of this study, that a predictive approach based essentially on the detrimental role of P segregation could be appropriate as an initial attempt to assess the long-term effects of thermal aging on mechanical properties at temperatures below 350 °C.

3.4 PREDICTIVE EQUATIONS FOR COMPOSITION DEPENDENCE

Much of the research on temper embrittlement has been concentrated on the influence of various alloying and impurity elements on the susceptibility of the steels to embrittlement. A commonly used parameter to correlate temper embrittlement with chemical composition for 2.25Cr-1Mo steels is expressed as the J factor (Watanabe et al., 1974) as follows:

$$J = (Mn + Si)(P + Sn) \times 10^4 \tag{3-14}$$

This expression, in which all concentrations are in wt percent, indicates that the effects of the alloying elements Mn and Si are additive, as well as the effects of the impurity elements P and Sn. It should be noted that Sb is not included in the equation although it is the most potent embrittler of steels because it is seldom found in boundaries of commercial steels (Briant and Banerji, 1983). Application of this simple, empirical equation to commercial grade 2.25Cr-1Mo steel has provided successful correlation of the ΔFATT with the J factor using data obtained on different product forms, grain sizes, and heat treatment conditions. Figures 3-4 and 3-5 show the correlation between ΔFATT and the J factor for two classes of data: (i) step-cooling embrittlement and (ii) long-term isothermal embrittling, respectively (Viswanathan and Jaffe, 1982), based mostly on the extensive study conducted by Shaw (1982). The long-term isothermal embrittling studies include data for periods ranging from 20,000 to 60,000 hr at temperatures in the range of 343 to 510 °C (Viswanathan and Jaffe, 1982).

A comparison of the data in the two figures shows that the slope of isothermal data bands is roughly 1.5 times greater than that of the step-cooling embrittlement studies data. By knowing the service requirements in terms of the shift in FATT that is acceptable (i.e., ΔFATT over the service life), it is possible to use the ΔFATT-J factor correlation bands to estimate the acceptable value of the J factor. This information can be then used to control the level of the four principal embrittling elements (i.e., Mn, Si, Sn, and P) to limit the shift in FATT to an acceptable limit over the service life. Using this approach, Viswanathan and Jaffe (1982) have predicted the chemical composition requirements of the four embrittling elements in 2.25Cr-1Mo steels for the 30-yr life of a pressure vessel.

Bruscato (1970) have used a different empirical expression to asses the temper embrittlement susceptibility of 2.25Cr-1Mo shielded metal-arc weld deposits. The embrittlement factor was defined in terms of the embrittling impurities in weight percent as

$$EF = (10\ P + 5\ Sb + 4\ Sn + As)/100 \tag{3-15}$$

and used to correlate the effect of their content with the Mn+Si content of the welds. Bruscato concluded that for a given value of these alloying elements the EF should be reduced to decrease the susceptibility to embrittlement. However, Eq. (3-15) provides even less predictive information than Eq. (3-14) since the Mn and Si contents are not included and Bruscato (1970) recognized that P and Sn contribute to more than 90 percent of the value of EF in all the tested welds.

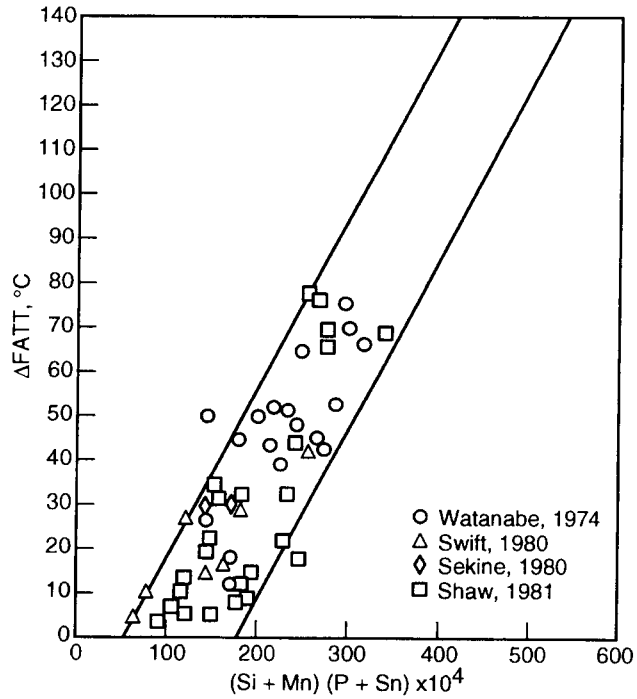

Figure 3-4. Correlation between J factor and ΔFATT results from step-cooling embrittlement studies (Viswanathan and Jaffe, 1982)

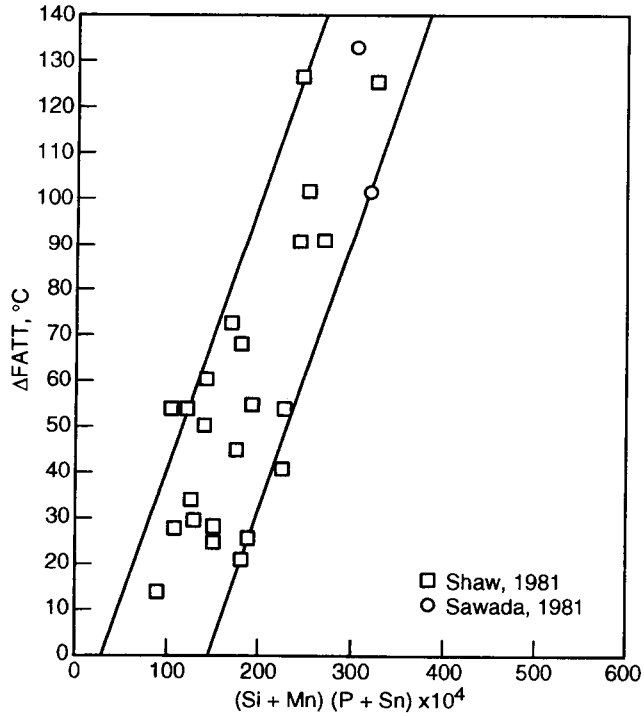

Figure 3-5. Correlation between J factor and ΔFATT results from long-time isothermal embrittlement studies (Viswanathan and Jaffe, 1982)

The literature also provides empirical equations for other types of steels. In a study of vacuum C deoxidized Ni-Cr-Mo-V rotor steels isothermally embrittled at 400 °C for 8,800 hr conducted by an ASTM task force, ΔFATT was correlated to the Mo concentration and impurity elements (all expressed in weight percent) by the following equation (Newhouse et al., 1972):

$$\Delta FATT(°C) = 7{,}524\ P + 7{,}194\ Sn + 1{,}166\ As - 52\ Mo - 450{,}000\ (PxSn) \quad (3\text{-}16)$$

This equation implies that impurity elements, such as P, Sn, and As, increase embrittlement, whereas Mo mitigates the deleterious effect of the impurities. The equation also includes a term accounting for a P-Sn interaction which decreases embrittlement.

The advantage of equations such as Eq. 3-14 and 3-16 is that the degree of embrittlement can be correlated to the bulk composition of the steel. However, one of the main limitation is that they are only valid for the specific class of steel on which the data is based. An additional limitation is the lack of consideration of metallurgical parameters such as grain size that are important factors in determining susceptibility to embrittlement.

McMahon and coworkers developed detailed correlations for 3.5Ni-1.7Cr steels doped with P, Sn, and Si (Takayama et al., 1980). Equations were generated in which the degree of embrittlement was correlated with the grain boundary concentration of each of the three dopants, the prior austenite grain size, and the hardness level. These equations were latter combined and extended to the case of a Ni-Cr-Mo-V steel containing 0.02 percent Si, 0.32 percent Mn, 0.019 percent P and 0.021 percent Sn. After forging, the steel was heat treated to produce a bainitic microstructure. Austenitizing and tempering treatments were adjusted to achieve hardness of 20 and 30 HRC and grain sizes corresponding to ASTM numbers 3 and 7. For an isothermal embrittlement at 480 °C for 6,000 hr, the following equation was obtained as reported by Viswanathan and Bruemmer (1985):

$$\Delta FATT = 4.8\ P + 24.5\ Sn + 13.75\ (7 - GS) + 2\ (HRC - 20) + 0.33\ (HRC - 20)\ (P + Sn) + 0.036\ (7 - GS)\ (HRC - 20)\ (P + Sn) \quad (3\text{-}17)$$

where ΔFATT is in °C, the concentrations of P and Sn are the Auger PHRs with respect to Fe, HRC is the Rockwell C hardness, and GS is the ASTM grain size number.

Although the approach described above seems to be useful for predictive purposes because metallurgical variables such as strength and grain size are considered, it requires sampling the material following accelerated embrittlement treatments or from components in service to measure by AES the grain boundary impurity concentrations on the fractured Charpy specimens. In addition, as discussed by Viswanathan and Bruemmer (1985), the approach was found to be inapplicable to Cr-Mo-V alloys since significant lower shifts in FATT were obtained after 6,000 hr of isothermal aging at 520 °C. In this case, P was the single segregant to grain boundaries even in Sn-doped steels.

For temperatures lower than 400 °C where embrittlement of 2.25Cr-1Mo steel is due solely to equilibrium P segregation, Hudson et al. (1988) proposed a very simple approach for predicting the behavior. By establishing as acceptance criterion a Charpy impact level of 25 J at 25 °C and calculating that this value corresponds to an AES P/Fe PHR of about 0.5, it is possible to estimate the acceptable bulk P levels as a function of the operating temperature. Figure 3-6 shows an example of this calculation for 2.25Cr-1Mo steel in which isothermal exposure for 25 yr of operation is required (Hudson et al., 1988). A similar approach can be used, assuming a critical value of the impact energy, to determine the expected lifetime for 2.25Cr-1Mo steel with a given P content after isothermal exposure. However, it should be modified to account for nonisothermal exposure over a range of temperatures as is the case for the WP under repository conditions.

3.5 CORRELATIONS BETWEEN TOUGHNESS PARAMETERS

The evaluation of component integrity or the prediction of a component life requires knowledge of the material properties, the defect distribution and the applied and/or residual stresses. Final failure is usually determined by degradation of mechanical properties such as strength and toughness. Strength represents the resistance to material flow and, hence, failure modes associated with large plastic deformations which generally are not common at moderate temperatures. Toughness represents the ability of a material to absorb energy without fracturing. At a given level of applied or residual stress, fracture toughness expressed by K_{Ic}, determines the largest size of a crack, preexisting from the fabrication stage or initiated in service, that can be tolerated, without catastrophic brittle fracture. As discussed in Section 2, a large fraction of toughness data available in the literature has been generated using the CVN impact test.

The CVN test has been used widely because it requires small metal samples, and it is simple and inexpensive to perform. It is commonly used as a screening test for evaluating notch toughness changes brought about by microstructural and microchemical modifications during fabrication of a component or in service, particularly in systems operating under harsh environmental conditions in terms of temperature, irradiation, hydrogen generation, etc. In many structural steel applications, the CVN test is used in procurement and quality assurance for assessing different heats of the same type of steel. Although there is a trend in the codes and specifications being developed for nuclear pressure vessels to use fracture mechanics principles in order to specify material toughness requirements, the general approach used in 10 CFR Part 50 Appendix G to insure an adequate margin of safety is based on CVN data. The minimum acceptable level for the USE in beltline material of reactor pressure vessels should be 50 ft·lb (68 J) throughout service life. If USE decreases below 50 ft·lb (68 J), the operation may continue if alternative methods can be used to demonstrate equivalent margins of safety. For protection against transients involving a pressurized thermal shock, a criterion based on the nil-ductility transition temperature (NDTT) is used. Thus, numerous empirical correlations have been developed to estimate K_{Ic} values from Charpy test results.

Some of the more common correlations for steels are listed in Table 3-1 with appropriate comments and data sources. It should be noted that most of these correlations are dimensionally incompatible, ignore differences between the two types of toughness measurements, and are valid only for limited types of materials and ranges of data. The correlations listed in Table 3-1 have been proposed and used for estimating K_{Ic} from standard Charpy test data for steels over two different temperature ranges in the CVN impact energy versus temperature curve. These ranges are the upper-shelf region and the transition-temperature region.

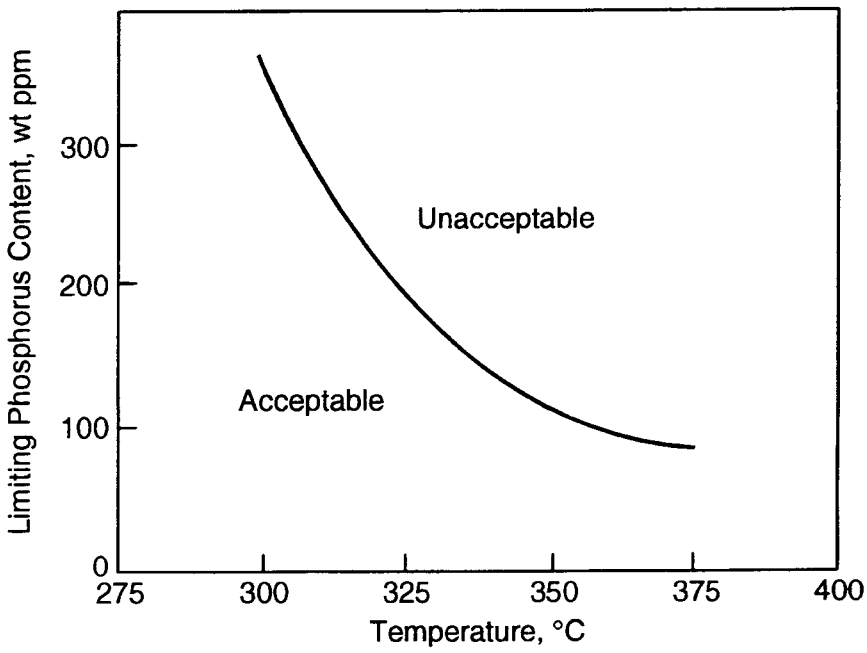

Figure 3-6. An acceptance criterion for 2.25Cr-1Mo steel based on a minimum Charpy impact energy of 25 J at 25 °C for 25 yr operating life, derived from an equilibrium model of phosphorus segregation (Hudson et al., 1988)

3.5.1 K_{Ic}-CVN Correlations in the Upper-Shelf Region

Three empirical correlations have been developed and applied in the upper-shelf temperature range where the Charpy impact energy of the steel has reached the maximum, as listed in Table 3-1. Rolfe and Novak (1970) established a correlation between K_{Ic} and upper-shelf CVN test data on the basis of the results of eleven steels having yield strengths in the range 110 to 246 ksi (759 to 1,696 MPa). The K_{Ic} values for these steels ranged from 87 to 246 ksi $\cdot$in.$^{1/2}$ (96 to 270 MPa $\cdot$m$^{1/2}$), and the CVN impact values ranged from 16 to 89 ft $\cdot$lb (22 to 121 J). The correlation proposed by Ault et al. (1971) is based on high-strength, low-toughness steels with yield strengths from 234 to 287 ksi (1,615 to 1,980 MPa), K_{Ic} values from 34 to 70 ksi $\cdot$in.$^{1/2}$ (37 to 77 MPa $\cdot$m$^{1/2}$), and CVN impact values from 11 to 21 ft-lb (15 to 29 J). The Rolfe and Novak correlation is one of the more widely used correlations for K_{Ic} and has been substantiated by additional tests by other investigators.

Iwadate et al. (1985) proposed a modified Rolfe-Novak correlation between the upper-shelf fracture toughness and the CVN impact energy at the corresponding temperature. The Iwadate correlation for a variety of low-alloy pressure-vessel and turbine steels in the upper-shelf temperature range is shown in Figure 3-7 and given also in Table 3-1. Results plotted in this figure indicate that the correlation is satisfactory for a wide range of steels.

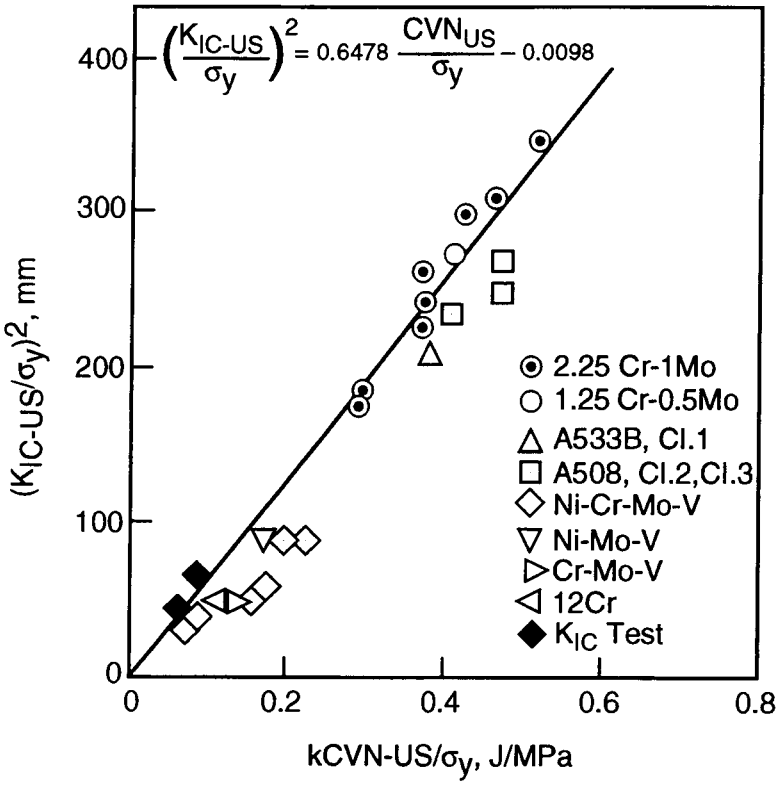

Figure 3-7. Correlation between K_{Ic} and CVN results in the upper-shelf region (Iwadate et al., 1985). σ_y is the yield strength of the material (US: upper shelf).

3.5.2 K_{Ic}-CVN Correlations in the Transition-Temperature Region

Several methods and correlations have been proposed and used for estimating K_{Ic} from standard Charpy test data for steels in the transition-temperature range. On the basis of various investigations, Barsom and Rolfe (1970), Sailors and Corten (1972), and Marandet and Sanz (1977) suggested relationships between K_{Ic} and CVN test results with different values of the constant of proportionality, as listed in Table 3-1. The constant of proportionality incorporates the effects of specimen size as well as notch acuity. Thus, it is possible to correlate K_{Ic} data and CVN energy absorption results by changing the value of the constant of proportionality. Figure 3-8 shows a good correlation between K_{Ic} and CVN results for both slow-bend and dynamic loading CVN tests. The constant of proportionality was determined to be 5 (Rolfe and Barsom, 1977).

Another method of predicting the entire K_{Ic} versus temperature curve from CVN and tensile data has been suggested by Begley and Logsdon (1971). At the upper-shelf temperature, they estimated K_{Ic} using the Rolfe-Novak correlation indicated as Ia in Table 3-1. At the lower-shelf temperature, K_{Ic} is estimated as $0.45\sigma_y$. At the 50 percent FATT, K_{Ic} is taken to be the average of the upper and lower-shelf values. The agreement between estimated and measured K_{Ic} values was found to be very good.

Table 3-1. Common K_{Ic}-CVN correlations for steels

Correlation	Comment	Reference
I. Upper-Shelf Region		
a. $(K_{Ic}/\sigma_y)^2 = 5(CVN/\sigma_y - 0.05)$	σ_y = 759 to 1696 MPa K_{Ic}(ksi·in.$^{1/2}$), CVN(ft·lb), σ_y(ksi)	Rolfe and Novak (1970)
b. $(K_{Ic}/\sigma_y)^2 = 1.37(CVN/\sigma_y) - 0.045$	High strength, low toughness steels K_{Ic}(ksi·in.$^{1/2}$), CVN(ft·lb), σ_y(ksi)	Ault et al. (1971)
c. $(K_{Ic}/\sigma_y)^2 = 0.6478(CVN/\sigma_y - 0.0098)$	Pressure-vessel steels K_{Ic}(MPa·m$^{1/2}$), CVN(J), σ_y(MPa)	Iwadate et al. (1985) Iwadate et al. (1977)
II. Transition-Temperature Region		
a. $K_{Ic}^2/E = 5(CVN)$ $K_{Ic}^2/E = 2(CVN)^{3/2}$	σ_y = 269 to 1696 MPa K_{Ic}(psi·in$^{1/2}$), CVN(ft·lb), E(psi)	Barsom (1975) Barsom and Rolfe (1970)
b. $K_{Ic}^2/E = 8(CVN)$	CVN = 7 to 70 J K_{Ic}(psi·in$^{1/2}$), CVN(ft·lb), E(psi)	Sailors and Corten (1972)
c. $K_{Ic} = 19(CVN)^{1/2}$	Medium-strength steels K_{Ic}(MPa·m$^{1/2}$), CVN(J)	Marandet and Sanz (1977)
d. K_{Ic} at FATT = $0.5(K_{Ic\text{-}US} + 0.45\sigma_y)$	$K_{Ic\text{-}US}$ from correlation Ia K_{Ic} & $K_{Ic\text{-}US}$(ksi·in.$^{1/2}$), σ_y(ksi)	Begley and Logsdon (1971)
e. $K_{Ic}/K_{Ic\text{-}US} = 0.0807 + 1.962$ exp[0.0287(T-FATT)]	For −40 °C>(T-FATT)	Iwadate et al. (1985) Iwadate et al. (1977)
$K_{Ic}/K_{Ic\text{-}US} = 0.623 + 0.406$ exp[-0.00286(T-FATT)]	For 350 °C>(T-FATT)>-40 °C K_{Ic} & $K_{Ic\text{-}US}$(MPa·m$^{1/2}$)	

σ_y: yield strength US: upper shelf

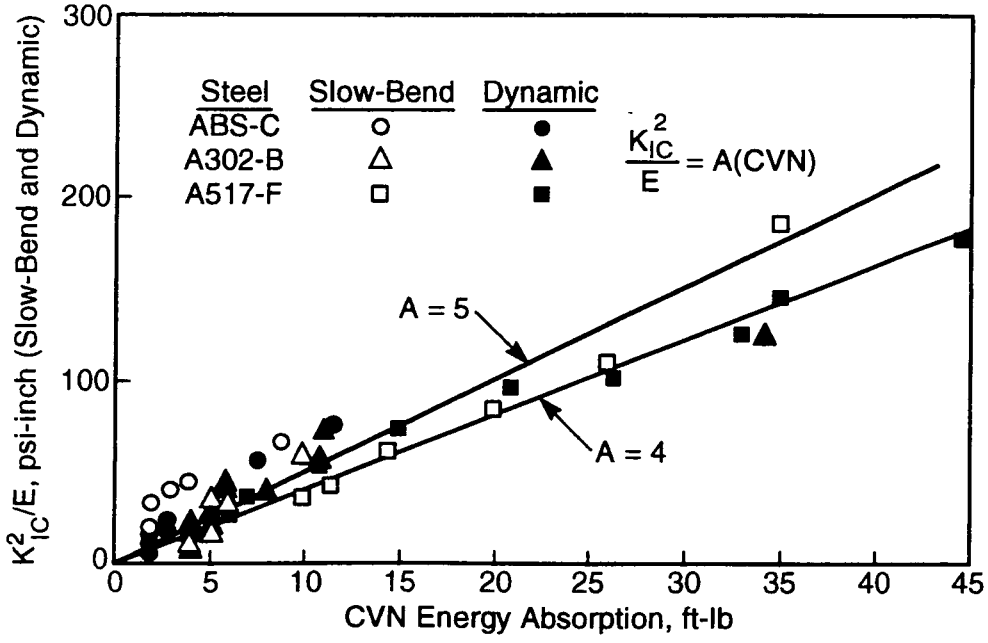

Figure 3-8. Correlation between K_{Ic} and CVN results in the transition-temperature region (Barsom and Rolfe, 1970)

Iwadate et al. (1985) have developed a correlation between excess temperature and the value of K_{Ic} at any temperature normalized with respect to the upper-shelf temperature. The excess temperature is defined as the test temperature minus FATT. The 99 percent confidence limit curve yields the equations shown in Table 3-1 as correlation IIe. Using these correlations, K_{Ic} can be estimated at any temperature.

3.6 ASSESSMENT OF THERMAL STABILITY

Susceptibility of low-alloy steels to temper embrittlement leads to fracture toughness degradation and decreases the tolerable flaw size for a given service condition, thus detrimentally affecting component life and structural integrity. The concept of life assessment and the methodologies applied to this evaluation have recently been reviewed by Viswanathan (1989). Measurements of subcritical crack growth rate and experimental data on the degree of temper embrittlement and toughness degradation after long-term exposure have been generated and analyzed in order to be used in remaining life prediction models for reactor pressure vessels (Iwadate et al., 1985) and turbine rotors (Swaminathan et al., 1991). Application of these life assessment techniques can be extended to the assessment of the thermal stability and mechanical properties of WP containers.

An appropriate procedure for assessing thermal stability and degradation of mechanical properties of the WP materials is proposed in Figure 3-9, and the major steps are discussed in detail below.

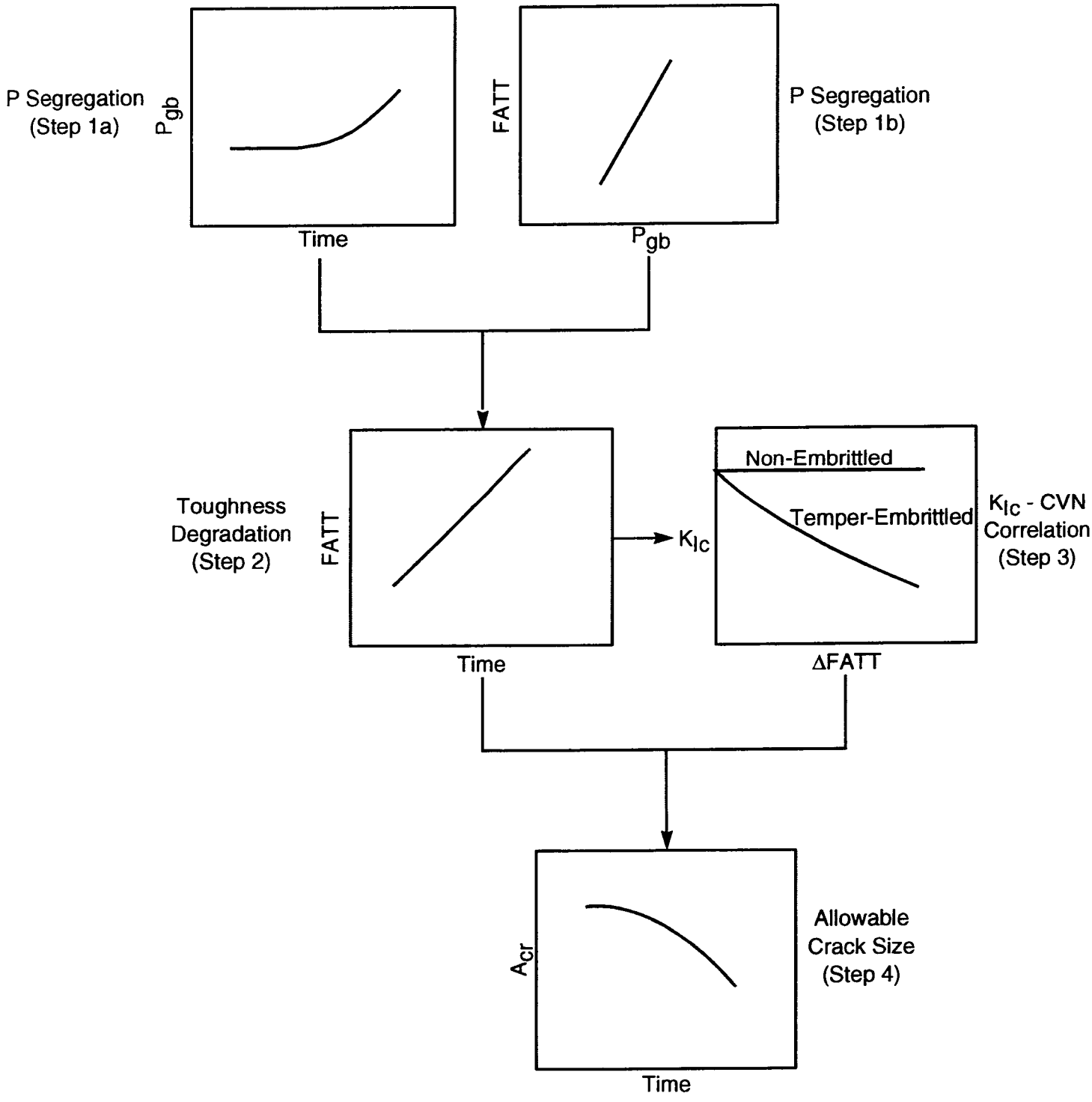

Figure 3-9. Procedure for assessing thermal stability and toughness properties of container materials

Step 1. The level of grain boundary P segregation can be predicted using acceptable models.

As discussed in Sections 2 and 3.1, P segregation to grain boundary has been found to be the dominant process governing temper embrittlement of thermally aged low-alloy steels at temperatures below 400 °C. By modeling the kinetics of segregation of P assuming that it is controlled by diffusion in the alloy matrix, it will be possible to provide a predictive methodology for estimating the degree of embrittlement and the time required for embrittlement. As discussed in Section 3.3, McLean's equilibrium segregation theory can be applied to assess and predict grain boundary P segregation as a function of bulk P content, aging time and temperature for Mn-Mo-Ni pressure vessel steels (Druce et al. 1986; Vatter et al., 1993). This model can be used for making acceptable calculations, extending its application to the candidate steels for disposal overpack.

In order to apply the model in a predictive manner, it is necessary to know the Gibbs free energy for the segregation of P and its diffusion coefficient at the temperature of aging. Extreme care must be exercised in the extrapolation as the model is very sensitive to the value of the diffusion coefficient which is dependent on temperature and on the composition and microstructure of the steel.

Step 1b. The toughness degradation of the steel is estimated using the relationship between P segregation and the degree of embrittlement as measured by the FATT or other equivalent parameter.

Temper embrittlement manifests itself as a shift of the impact transition curve to high temperatures, expressed as an increase of the FATT for the steel. The amount of shift (ΔFATT) has been found to be linearly related to the level of P segregation to the grain boundaries for pressure vessel steels. From the predicted grain boundary segregation the variation in FATT can be estimated using simplified assumptions. These estimates can then be compared with results of bounding calculations performed by using the predictive equations discussed in Section 4.1.

Step 2. The previous steps are combined to estimate the variation of toughness, ΔFATT, with time.

Step 3. The evolution of the fracture toughness K_{Ic} with time is calculated using an appropriate K_{Ic}-CVN correlations.

The increase in FATT with aging time should be accompanied by a reduction of K_{Ic} in the transition-temperature region. By selecting an appropriate K_{Ic}-CVN correlation from those listed in Table 3-1 (i.e., correlation IIe), it is possible to calculate the evolution of K_{Ic} with time over the range of temperatures expected during the slow cooling of the WPs.

Step 4. The change in the critical crack size a_{cr} as K_{Ic} changes with time can be calculated using principles of fracture mechanics

The consequence of fracture toughness degradation is that the tolerable crack size for a given stress level is reduced. The fracture criterion based on fracture mechanics can be expressed in the generalized form $K_{Ic} = Y\sigma(a_{cr})^{1/2}$, where Y is a flaw shape parameter which depends on the crack geometry and load distribution. The interaction of material properties, such as the fracture toughness, with the design stress (σ) and crack size (a) controls the fracture conditions in a component. The critical crack size may decrease during service as a result of the decrease in fracture toughness of the materials

and lead to premature failure of components. Calculations based on bounding values of residual stresses or sudden loads associated to seismic events should provide the stress level and, hence, the size of a tolerable crack. This flaw size can then be compared to detection limits by inspection techniques and monitored during the period before permanent closure.

It should be mentioned that a successful thermal stability assessment requires sufficient information for the specific material conditions to fully define both the segregation model parameters and the embrittlement potencies. Therefore, to validate the proposed procedure for the thermal stability assessment of the WP containers all of the pertinent material property data necessary to perform the thermal stability assessment should be generated for specific candidate container materials. A common pressure vessel steel, 2.25Cr-1Mo steel (ASTM A387 Grade 22), is recommended as a model container material for the initial demonstration of this procedure for the assessment of thermal stability and degradation of toughness properties.

4 SUMMARY, CONCLUSIONS, AND RECOMMENDATIONS

If a high thermal loading strategy is adopted to maintain a substantial volume of rock surrounding the WPs dry for a long period of time with the purpose of delaying the occurrence of aqueous corrosion, the outer disposal overpack can be exposed to elevated temperatures for hundreds of years. The precise evolution of the WP temperature with time depends on many factors related to the design of the repository and the EBS (i.e., AML, thermal properties of the backfill), including the operational approach adopted for the preclosure period (i.e., ventilation scheme, backfilling time). As illustrated in Figure 1-1, temperatures above 200 °C may prevail over several hundred years. No engineering experience exists on the stability of metallic materials for such extended periods at these elevated temperatures. The recent review of the consequences of thermal aging of nuclear reactor steam generator shells for operating times up to 30 to 40 yr (Nanstad et al., 1995), is a clear indication of this concern. Although the range of temperatures in the case of the repository is lower than the typical operating temperatures of nuclear power reactors (about 300 °C), the time of performance required at these lower temperatures is at least an order of magnitude longer. On the basis of the studies reviewed in the previous sections, it appears that the thermal embrittlement of C-Mn and Cr-Mo steels promoted by long-term exposure to the conditions prevailing in the repository is a plausible process that deserves further consideration and detailed analysis.

Taking into consideration the temperature and time constraints discussed above, it follows that the critical factors determining the possibility of thermal embrittlement are the metallurgical properties of the material selected for the outer disposal overpack and the effect of the fabrication processes on these properties. The main factors determining the metallurgical properties are the chemical composition of the steel and the sequence of heat treatments used to provide the required strength.

4.1 C-Mn STEELS

From the information reviewed in Section 2, it can be concluded that C-Mn steels, such as A516 Grade 55, are less susceptible to temper embrittlement than A387 Grade 22 (2.25Cr-1Mo) low-alloy steel. Although limited information is available for C steels as compared to low-alloy steels, it is widely accepted that Mn is a promoter of the segregation of P to grain boundaries (McMahon, 1968; Briant and Banerji, 1983) and steels containing more than 0.5 percent Mn may become susceptible to embrittlement depending upon the P content. McMahon (1968) concluded that Mn is roughly twice as strong as Cr as an enhancer of the P effect. Very large DBTT shifts have been reported for 1.5 Mn steels containing P from 0.01 to 0.04 percent (McMahon, 1968). Unfortunately, there have been no studies to predict quantitatively the degree of susceptibility that can be attained by A516 Grade 55 or similar C-Mn steels and the variability that can be expected from different heats.

No studies on the effect of other metallurgical variables such as grain size have been reported, undoubtedly because C-Mn steels are much less susceptible to embrittlement than low-alloy steels. As noted in Section 2.3.2 a decrease in the C content, combined with the addition of Al and B, leads to a substantial improvement in the toughness of A516 Grade 70 steel. However, the complexity of the microstructures developed in welds, as discussed in Section 2.2.6.3, deserves careful consideration. Apparently, the increase in Mn content has a beneficial effect in welds by promoting the formation of acicular ferrite.

4.2 LOW-ALLOY STEELS

On the other hand, as reviewed in Section 2.2, A533B steel, one of the Mn-Mo-Ni steels used in PWR pressure vessels, is susceptible to embrittlement in a condition simulating the microstructure of the HAZ after isothermal aging for 833 d at temperatures ranging from 400 to 550 °C (Druce et al., 1986). The embrittlement was directly related to the equilibrium segregation of P to the grain boundaries. Whereas Druce et al. (1986) did not observe embrittlement over the same aging time at 300 °C, we have conducted preliminary calculations, as shown in Figure 4-1, which indicate that significant P enrichment can be attained at lower temperatures but longer times. The work by Druce and coworkers (Druce et al., 1986, Hudson et al., 1988; and Vatter et al., 1993) clearly reveals that the microstructure more susceptible to embrittlement by thermal aging is the coarse-grained HAZ as compared to the other microstructures usually encountered in pressure vessels including fine-grained base material, fine-grained HAZ, and weld metal. Vatter et al. (1993) concluded that the weld metal, like the base material, has a lower susceptibility to thermal embrittlement.

The assessment of Vatter et al. (1988) and Nanstad et al. (1995) of service data for A302B steel, both base material and weld metal, aged for times up to 1,088 d (approximately 3 yr) at about 300 °C, revealed practically no shift in DBTT, but another pressure vessel steel (similar to A508 steel) exhibited an increase of about 25 °C after 12 yr of operation. Vatter et al. (1988) emphasizes that there is a lack of long-term aging data (>50,000 hr) at temperatures around 300 °C to establish useful correlations. Nanstad et al. (1995) concluded that the potential for thermal embrittlement of some of the currently used pressure vessel steels for times up to 30 to 40 yr cannot be dismissed on the basis of the data available. It should be noted that this conclusion refers to locations and/or conditions lacking the additional effect of high-energy neutron fluence, and, hence, it takes into consideration only thermal effects.

As reviewed in Section 2, the temper embrittlement of A387 Grade 22 (2.25Cr-1Mo) low-alloy steel has been extensively studied. It is clearly established that careful control of the P content reduces significantly the potential for embrittlement, as discussed in Section 2.3.1. Although this steel is more prone to thermal embrittlement than C-Mn steels, there is a more extensive database that can be used to assess potential problems, particularly in weldments.

4.3 PREDICTING THERMAL EMBRITTLEMENT

The work of Hudson et al. (1988) has shown that at temperatures below 450 °C, where the degree of thermal embrittlement is due solely to equilibrium P segregation to grain boundaries, it is possible to calculate the bulk P levels required to produce specific embrittlement effects. However, the main uncertainty in using this approach is related to the extrapolation of the diffusion coefficient of P in the bainite matrix from high temperatures to the temperatures prevailing in the repository. At high temperatures, the original bainite structure is transformed to a ferrite-carbide microstructure, as discussed in Section 2.2.2.2. Druce et al. (1986) have shown that P has the same diffusion coefficient in Fe and in a number of steels, but a more detailed assessment of the information available is necessary in order to conclude that the effects of steel composition and microstructure are negligible. Another source of uncertainty is related to the estimation of the free amount of P in the matrix available for segregation. This amount may not be necessarily equal to the bulk content of P as determined by chemical analysis.

Since P segregation appears to exhibit equilibrium characteristics in several cases, Guttmann's ternary regular solution model can provide an adequate framework for analyzing the case of C-Mn steels,

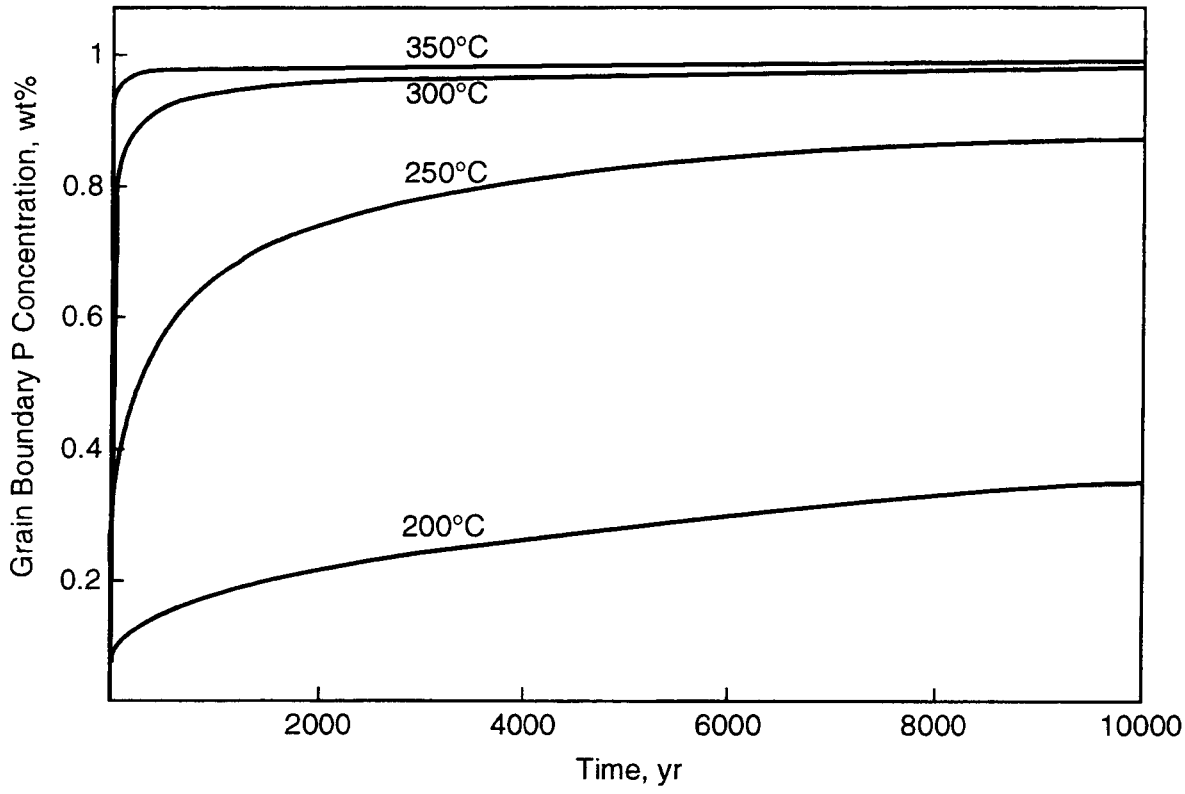

Figure 4-1. Predicted kinetics of phosphorus segregation to grain boundaries of a pressure vessel steel at various temperatures assuming parameters used by Druce et al. (1986)

such as A516 Grade 55, in terms of variation of compositions and the interaction of P and Mn in governing segregation and embrittlement. It should be noted, however, that nonequilibrium processes can also occur, often simultaneously. McLean's model can be used for predicting the segregation and embrittlement kinetics as applied by Druce and coworkers (Druce et al., 1986; Hudson et al., 1988; Vatter et al., 1993) to pressure vessel steels, but additional data on segregation free energies and diffusivities of P in steels should be compiled and evaluated to assess the validity of the parameters included in the equations provided by these authors. The predictive equations for temper embrittlement, reviewed in Section 3.4, can be used to predict the possibility of thermal embrittlement. However, these equations were empirically developed for the specific case of low-alloy steels. In this sense, they can be applied to A387 Grade 22 to define the range of compositions that can be less prone to thermal effects. As noted above, the approach developed by Hudson et al. (1988) can be used to define the maximum acceptable amount of P.

Whereas the degree of embrittlement has been correlated with the grain boundary P content for Ni-Cr-Mo-V rotor steel (Viswanathan and Bruemmer, 1985) and Ni-Mo pressure vessel steel (Vatter et al., 1993), no correlation was found in the literature for C-Mn steels. Unfortunately, the data for the pressure vessel steel cannot be compared directly with that for the rotor steel because the degrees of embrittlement, although linearly related to the P/Fe PHR in both cases, were measured through ΔDBTT and ΔFATT, respectively.

The effect of thermal aging on the parameters used for assessing thermal embrittlement (i.e., ΔDBTT and ΔFATT) can be determined, and the variation of fracture toughness, given by K_{Ic}, can be calculated as a function of time following the procedure described in Section 3.6. Using fracture mechanics concepts, the critical crack size a_{cr} can then be calculated as a function of time for a given stress level.

The calculation of tensile stress level can be made by considering the load that can be imposed on the WP as a consequence of seismic events or other forms of sudden loading. Finite difference methods or other approaches should be used to calculate the residual stresses on the outer disposal overpack once the detailed design and other aspects of the fabrication scheme are better defined.

From the review and analysis of the information available, the following recommendations are made for future work.

- Develop a complete assessment of the potential for thermal embrittlement of an outer disposal overpack made of A387 Grade 22 steel using the data available in the literature and following the approach described in Section 3.6.

- On the basis of such assessment, identify the critical aspects that require further study. The aspect that should be better defined is the use of fracture mechanics concepts to establish the failure criterion. Analysis of alternative approaches based on fracture stress concepts should be explored.

- Apply the Guttmann theory to the case of C-Mn steels such as A516 Grade 55 to explore the potential for P segregation to grain boundaries on a thermodynamics basis. Use the McLean's model to calculate the concentration at grain boundaries after a detailed review of certain critical modeling parameters, such as the diffusion coefficients for P in steels.

- Define an experimental program if it appears justified by the lack of information on microstructural and mechanical factors that may contribute to the risk of thermal embrittlement of the overpack.

The results of these activities would provide NRC with a better understanding of the potential for thermal embrittlement of overpack materials due to long-term aging. These studies are needed to support sensitivity analyses, and to address uncertainties in models (i.e., applicability of Guttmann and McLean theory to C-Mn steels), parameters (i.e., coefficient diffusion of P in steels), and data (i.e., correlations between ΔDBTT and K_{Ic}). A more complete evaluation of the embrittlement of steel overpacks under repository conditions will provide staff with the knowledge base needed to assess the adequacy of the DOE treatment of this potential failure mode.

5 REFERENCES

American Society for Testing and Materials. 1995a. A516-90. Standard specification for pressure vessel plates, carbon steels for moderate- and lower-temperature service. *Annual Book of ASTM Standards*. Philadelphia, PA: American Society for Testing and Materials: Vol. 01.04: 248–250.

American Society for Testing and Materials. 1995b. A387-92. Standard specification for pressure vessel plates, alloy steel, chromium-molybdenum. *Annual Book of ASTM Standards*. Philadelphia, PA: American Society for Testing and Materials: Vol. 01.04: 210–212.

American Society for Testing and Materials. 1995c. A302-93. Standard specification for pressure vessel plates, alloy steel, manganese-molybdenum and manganese-molybdenum-nickel. *Annual Book of ASTM Standards*. Philadelphia, PA: American Society for Testing and Materials: Vol. 01.04: 154–155.

American Society for Testing and Materials. 1995d. A508-94. Standard specification for quenched and tempered vacuum-treated carbon and alloy steel forgings for pressure vessels. *Annual Book of ASTM Standards*. Philadelphia, PA: American Society for Testing and Materials: Vol. 01.05: 293–298.

American Society for Testing and Materials. 1995e. A515-92. Standard specification for pressure vessel plates, carbon steel, for intermediate- and higher-temperature service. *Annual Book of ASTM Standards*. Philadelphia, PA: American Society for Testing and Materials: Vol. 01.04: 246–247.

American Society for Testing and Materials. 1995f. A533-93. Standard specification for pressure vessel plates, alloy steel, quenched and tempered, manganese-molybdenum and manganese-molybdenum-nickel. *Annual Book of ASTM Standards*. Philadelphia, PA: American Society for Testing and Materials: Vol. 01.04: 256–257.

Ault, R.T., G.M. Wald, and R.B. Bertola. 1971. *Development of an Improved Ultra High Strength Steel for Forged Aircraft Components*. AFML TR 7127. Wright-Patterson Air Force Base, OH: Air Force Materials Laboratory.

Bandyopadhyay, N., C.L. Briant, and E.L. Hall. 1985. Effect of microstructural changes on the caustic stress corrosion cracking resistance of a NiCrMoV rotor steel. *Metallurgical Transactions* 16A: 1,333–1,344.

Barsom, J.M., and S.T. Rolfe. 1970. Correlations between K_{Ic} and Charpy V-notch test results in the transition temperature range. *Impact Testing of Materials*. ASTM-STP 466. Philadelphia, PA: American Society for Testing and Materials: 281–302.

Barsom, J.M. 1975. The development of AASHTO fracture toughness requirements for bridge steels. *Engineering Fracture Mechanics* 7: 605–618.

Begley, J.A., and W.A. Logsdon. 1971. *Correlation of Fracture Toughness and Charpy Properties for Rotor Steels*. WRL 71-1E7-MSLRF-P1. Pittsburgh, PA: Westinghouse Research Laboratory.

Bodnar, R.L., and R.F. Cappellini. 1982. *Bethlehem Steel Corporation Summary of Progress on RP 2060-2: High Purity Steels for Utility Components (RP 2060-2)*. Presented at the EPRI Steering Committee Meeting, Washington, DC, December 6, 1982.

Briant, C.L. 1988. Metallurgical applications of Auger electron spectroscopy. *Treatise on Materials Science and Technology. Volume 30: Auger Electron Spectroscopy*. C.L. Briant and R.P. Messuer, eds. New York, NY: Academic Press: 111–163.

Briant, C.L., and S.K. Banerji. 1978. Intergranular failure in steel: The boundary composition. Review No. 232. *International Metals Review* 4: 164–198.

Briant, C.L., and S.K. Banerji. 1983. Intergranular fracture in ferrous alloys in nonaggressive environments. *Treatise on Materials Science and Technology. Volume 25: Embrittlement of Engineering Alloys*. C.L. Briant and S.K. Banerji, eds. New York, NY: Academic Press: 21–58.

Bruscato, R. 1970. Temper embrittlement and creep embrittlement of 2¼ Cr-1Mo shielded metal-arc weld deposits. *Welding Research Supplement* 49: 148s–156s.

Chandel, R.S., R.F. Orr, J.A. Gianetto, J.T. McGrath, and R.F. Knight. 1985. The mechanical properties of 2.25Cr-1Mo weld metals deposited by SAW-NG process. *Journal of Materials for Energy Systems* 7(2): 137–146.

Doering, T.W. 1993. Robust waste package concept (multibarrier). *High Level Radioactive Waste Management*. La Grange Park, IL: American Nuclear Society: 1: 551–557.

Druce, S.G., G. Gage, and G. Jordan. 1986. Effect of ageing on properties of pressure vessel steels. *Acta Metallurgica* 34: 641–652.

Dumoulin, Ph., M. Guttmann, M. Foucault, M. Palmier, M. Wayman, and M. Biscondi. 1980. Role of molybdenum in phosphorus—induced temper embrittlement. *Metal Science* 14: 1–15.

Ewalds, H.L., and R.J.H. Wanhill. 1985. *Fracture Mechanics*. London, U.K.: Edward Arnold and Delft, The Netherlands: Delftse U.M.

Fukakura, J., M. Asano, M. Kikuchi, and M. Ishikawa. 1993. Effect of thermal aging on fracture toughness of RPV steel. *Nuclear Engineering and Design* 144: 423–429.

Grosse-Woerdemann, J., and S. Dittrich. 1982. Prevention of temper embrittlement in 2 1/4Cr-1Mo weld metal. *Metal Progress* 122(2): 43–49.

Guttmann, M. 1975. Equilibrium segregation in a ternary solution: A model for temper embrittlement. *Surface Science* 53: 213–227.

Guttmann, M., and D. McLean. 1979. Grain boundary segregation in multicomponent systems. *Interfacial Segregation*. W.C. Johnson and J.M. Blakely, eds. Metals Park, OH: ASM International: 261–350.

Hickley, J.J., and J.H. Bulloch. 1992. The role of reverse temper embrittlement on some low and high temperature crack extension processes in low carbon, low alloy steels: A review. *International Journal on Pressure Vessels and Piping* 49: 339–386.

Hondros, E.D. 1965. The influence of phosphorus in dilute solid solution on the absolute surface and grain boundary energies of iron. *Proceedings of the Royal Society of London* A286: 479–498.

Hudson, J.A., S.G. Druce, G. Gage, and M. Wall. 1988. Thermal ageing effects in structural steels. *Theoretical and Applied Fracture Mechanics* 10: 123–133.

Iwadate, T., T. Karushi, and J. Watanabe. 1977. Prediction of fracture toughness K_{Ic} of 2 1/4 Cr-1 Mo pressure vessel steel from Charpy V notch test results. *Flaw Growth and Fracture*. ASTM-STP 631. Philadelphia, PA: American Society for Testing and Materials: 493–506.

Iwadate, T., J. Watanabe, and Y. Tanaka. 1985. Prediction of the remaining life of high temperature/pressure reactors made of Cr-Mo steels. *Transactions of the ASME, Journal of Pressure Vessel Technology* 107: 230–238.

Jaffe, L.D., and D. Buffum. 1949. Temper brittleness of plain carbon steels. *Transactions of the American Institute of Mining and Metallurgical Engineers* 180: 513–518.

Joshi, A., and D.F. Stein. 1972. Temper embrittlement of low-alloy steels. *Temper Embrittlement of Alloy Steels*. ASTM STP 499. Philadelphia, PA: American Society for Testing and Materials: 59–89.

Khadkikar, P.S., and P.F. Wieser. 1986. Temper embrittlement in low alloy steels. IIM Review No. 26. *Transactions of the Indian Institute of Metals* 39(5): 510–527.

Kikutake, T., K. Yamanaka, H. Nakao, and K. Ito. 1983. Properties of ASTM A387-22 (2¼Cr-1Mo) steel plates produced by BOP. *Nippon Steel Technical Report*. No. 22 (December): 35–45.

Kusuhara, Y., T. Sekine, T. Enami, and H. Ooi. 1980. BOF-LRF refined ultralow phosphorus 2.25Cr-1Mo steel plate of low temper embrittlement susceptibility. *Proceedings of the Fourth International Conference on Pressure Vessel Technology*. London, England: Institute of Mechanical Engineers.

Lei, T.C., C.H. Tang, and M. Su. 1983. Effect of molybdenum on temper brittleness and internal friction behavior of medium carbon alloy steels. *Metal Science* 17: 249–255.

Low, J.R., Jr., D.F. Stein, A.M. Turkalo, and R.P. Laforce. 1968. Alloy and impurity effects on temper brittleness of steel. *Transactions of the Metallurgical Society of AIME* 242: 14–24.

Low, J.R., Jr. 1978. Embrittlement of steels. *Metals Handbook. Vol. 1, 9th Edition. Properties and Selection: Irons and Steels*. Metals Park, OH: American Society for Metals: 683–688.

Lonsdale, D., and P.E.J. Flewitt. 1978. The role of grain size on the ductile-brittle transition of a 2.25 pct Cr-1 pct Mo steel. *Metallurgical Transactions* 9A: 1,619–1,623.

Manteufel, R.D. 1996. Effects of ventilation and backfill on an underground nuclear waste repository. *International Journal of Heat and Mass Transfer*. Accepted for publication.

Marandet, B., and G. Sanz. 1977. Evaluation of the toughness of thick medium-strength steels by using linear elastic fracture mechanics and correlations between K_{Ic} and Charpy V-notch. *Flaw Growth and Fracture*. ASTM-STP 631. Philadelphia, PA: American Society for Testing and Materials: 72–95.

McCright, R.D. 1995. *Updated Candidate List for Engineered Barrier Materials*. UCRL-ID-119442. Livermore, CA. Lawrence Livermore National Laboratory.

McGrath, J.T., R.S. Chandel, R.F. Orr, and J.A. Gianetto. 1989. A review of factors affecting the integrity of weldments in heavy wall reactor vessels. *Canadian Metallurgical Quarterly* 28(1): 75–83.

McLean, D. 1957. *Grain Boundaries in Metals*. London, U.K.: Oxford University Press.

McMahon, C.J., Jr. 1968. Temper brittleness—An interpretive review. *Temper Embrittlement in Steel*. ASTM STP 407. Philadelphia, PA: American Society for Testing and Materials: 127–167.

Militzer, M., and J. Wieting. 1989. Segregation mechanisms of temper embrittlement. *Acta Metallurgica* 37: 2,585–2,593.

Murza, J.C., and C.J. McMahon, Jr. 1980. The effects of composition and microstructure on temper embrittlement in 2 1/4Cr-1Mo steel. *Journal of Engineering Materials and Technology: Transactions of the ASME* 102: 369–375.

Nakanishi, M., S. Watanabe, and J. Furusawa. 1984. On the improvement of ductility and toughness in welded joints of Al-B treated thick plates for pressure vessels. Paper No. 42. *International Conference on the Effects of Residual, Impurity, and Microalloying Elements on Weldability and Weld Properties*. Cambridge, U.K.: The Welding Institute.

Nanstad, R.K., D.J. Alexander, W.R. Corwin, E.D. Eason, G.R. Odette, R.E. Stoller, and J.A Wang. 1995. *Preliminary Review of Data Regarding Chemical Composition and Thermal Embrittlement of Reactor Vessel Steels*. ORNL/NRC/LTR-95/1. Oak Ridge, TN: Oak Ridge National Laboratory.

Newhouse, D.L., et al. 1972. Temper embrittlement study of nickel-chromium-molybdenum-vanadium rotor steels, I: Effects of residual elements. *Temper Embrittlement of Alloy Steels*. STP 499. Philadelphia, PA: American Society for Testing and Materials: 3–36.

Ohtani, H., and C.J. McMahon, Jr. 1975. Modes of fracture in temper embrittled steels. *Acta Metallurgica* 23: 377–386.

Rellick, J.R., and C.J. McMahon, Jr. 1974. Intergranular embrittlement of iron-carbon alloys by impurities. *Metallurgical Transactions* 5: 2,439–2,450.

Rolfe, S.T., and S.R. Novak. 1970. Slow-bend K_{Ic} testing of medium-strength high-toughness steels. *Review of Developments in Plane-Strain Fracture Toughness Testing*. ASTM-STP 463. Philadelphia, PA: American Society for Testing and Materials: 124–159.

Rolfe, S.T., and J.M. Barmson. 1977. *Fracture and Fatigue Control in Structures. Applications of Fracture Mechanics*. Englewoods Cliffs, NJ: Prentice Hall.

Sailors, R.H., and H.T. Corten. 1972. Relationship between material fracture toughness using fracture mechanics and transition temperature. *Fracture Toughness, Proceedings of the 1971 National Symposium on Fracture Mechanics*. ASTM-STP 514. Philadelphia, PA: American Society for Testing and Materials: 164–191.

Sato, S., S. Matsui, T. Enami, and T. Tobe. 1982. Strength and temper embrittlement of heavy-section 2 1/4Cr-1Mo steel. *Application of 2 1/4Cr-1Mo Steel for Thick Wall Pressure Vessels*. ASTM STP 755. Philadelphia, PA: American Society for Testing and Materials: 363–382.

Seah, M.P. 1983. AES in metallurgy. *Practical Surface Analysis by Auger and X-ray Photoelectron Spectroscopy*. D. Briggs and M.P. Seah, eds. New York, NY: J. Wiley & Sons: 247–282.

Seah, M.P., and E.D. Hondros. 1973. Grain boundary segregation. *Proceedings of the Royal Society of London* A335: 191–212.

Shaw, B.J. 1982. *Characterization Study of Temper Embrittlement of Chromium-Molybdenum Steels*. API Publication 959. Washington, DC: American Petroleum Institute.

Sridhar, N., G.A. Cragnolino, D.S. Dunn, and H.K. Manaktala. 1994. *Review of Degradation Modes of Alternate Container Designs and Materials*. CNWRA 95-010. San Antonio, TX: Center for Nuclear Waste Regulatory Analyses.

Takayama, S., T. Ogura, S-C. Fu, and C.J. McMahon, Jr. 1980. The calculation of transition temperature changes in steels due to temper embrittlement. *Metallurgical Transactions* 11A: 1,513–1,530.

Tavassoli, A.A., A. Bougault, and A. Bisson. 1984. The effect of residual elements on the temper embrittlement susceptibility of large A508, Class 3, vessel forgings. Paper No. 43. *International Conference on the Effects of Residual, Impurity, and Microalloying Elements on Weldability and Weld Properties*. Cambridge, U.K.: The Welding Institute.

TRW Environmental Safety Systems, Inc. 1994. *Initial Summary Report for Repository/Waste Package Advanced Conceptual Design*. CRWMS M&O Document DOC No. B00000000-01717-5705-00015. Rev. 00. Las Vegas, NV: TRW Environmental Safety Systems, Inc.

TRW Environmental Safety Systems, Inc. 1995a. *Strategy for Waste Containment and Isolation for the Yucca Mountain Site. Preliminary YMSCO Review Draft*. Las Vegas, NV: TRW Environmental Safety Systems, Inc.

TRW Environmental Safety Systems, Inc. 1995b. *Total System Performance Assessment—1995: An Evaluation of the Potential Yucca Mountain Repository*. CRWMS M&O Document DOC No. B00000000-01717-2200-00136. Rev. 01. Las Vegas, NV: TRW Environmental Safety Systems, Inc.

Ucisik, A.H., C.J. McMahon, Jr., and H.C. Feng. 1978. The influence of intercritical heat treatment on the temper embrittlement susceptibility of P-doped Ni-Cr steel. *Metallurgical Transactions* 9A: 321–329.

Van Zyl, F.H., J.P. Strydon, P.P. Smit, and R. Emmerich. 1994. The high temperature ageing of a low-alloy steel in the presence or absence of strain. *International Journal of Pressure Vessels and Piping* 59: 91–105.

Vander Voort, G.F. 1990. Embrittlement of steels. *Metals Handbook, Vol. 1, 10th edition, Properties and Selection: Irons, Steels, and High-Performance Alloys*. Materials Park, Ohio: ASM International: 689–736.

Vatter, I.A., C.A. Hippsley, and S.G. Druce. 1993. Review of thermal ageing data and its application to operating reactor pressure vessels. *International Journal of Pressure Vessels and Piping* 54: 31–48.

Vinson, D.W., W.M. Nutt, and D.B. Bullen. 1995. *Survey of the Degradation Modes of Candidate Materials for High-Level Radioactive Waste Disposal Containers. Iron-Base Corrosion-Allowance Materials*. UCRL-CR-120464. Livermore, CA: Lawrence Livermore National Laboratory.

Viswanathan, R. 1989. *Damage Mechanisms and Life Assessment of High-Temperature Components*. Metals Park, OH. ASM International.

Viswanathan, R., and S.M. Bruemmer. 1985. In-service degradation of toughness of steam turbine rotors. *Transactions of the ASME. Journal of Engineering Materials and Technology* 107: 316–324.

Viswanathan, R., and R.I. Jaffe. 1982. 2¼Cr-1Mo steels for coal conversion pressure vessels. *Transactions of the ASME. Journal of Engineering Materials and Technology* 104: 220–226.

Viswanathan, R., and A. Joshi. 1975. Effect of microstructure on the temper embrittlement of Cr-Mo-V steels. *Metallurgical Transactions* 6A: 2,289–2,297.

Wada, T., and G.T. Eldis. 1982. Transformation characteristics of 2 1/4 Cr-1Mo steel. *Application of 2 1/4 Cr-1 Mo Steel for Thick Wall Pressure Vessels*. ASTM STP 755. Philadelphia, PA: American Society for Testing and Materials: 343–362.

Wada, T., and W.C. Hagel. 1976. Effect of trace elements, molybdenum, and intercritical heat treatment on temper embrittlement of 2-1/4Cr-1Mo steel. *Metallurgical Transactions* 7A: 1,419–1,426.

Wada, M., K. Hosoi, and O. Nishikawa. 1982a. Atom probe analysis of 2.25Cr-1Mo steel. *Acta Metallurgica* 30: 1,013–1,018.

Wada, M., S. Fukase, and O. Nishikawa. 1982b. Role of carbides in the grain boundary segregation of phosphorus in a 2.25Cr-1Mo steel. *Scripta Metallurgica* 16: 1,373–1,378.

Watanabe, J., Y. Shindo, Y. Murakami, T. Adachi, S. Ajiki, and K. Miyano. 1974. Temper embrittlement of 2¼Cr-1Mo pressure vessel steel. *29th Petroleum Mechanical Engineering Conference*. New York, NY: American Society of Mechanical Engineers.

Yu, J., and C.J. McMahon, Jr. 1980a. The effect of composition and carbide precipitation on temper embrittlement of 2.25Cr-1Mo steel: Part I. Effect of P and Sn. *Metallurgical Transactions* 11A: 277–289.

Yu, J., and C.J. McMahon, Jr. 1980b. The effect of composition and carbide precipitation on temper embrittlement of 2.25Cr-1Mo steel: Part II. Effect of Mn and Si. *Metallurgical Transactions* 11A: 291–300.

APPENDIX

Table A-1. Chemical composition specified for low-carbon/low-alloy steels included in this report (extracted from American Society for Testing and Materials, 1995a, c, d, e, f)

Steel	Element, wt. %								
	C	Mn	Si	Cr	Mo	Ni	V	S	P
A302 Grade B (UNS K12022)	0.25 max [a]	1.07–1.62 [b]	0.13–0.45 [b]	—	0.41–0.64 [b]	—	—	0.035 max	0.035 max
A508 Grade 3 Class 1* (UNS K12042)	0.25 max	1.20–1.50	0.15–0.40	0.25 max	0.45–0.60	0.40–1.00	0.05 max	0.025 max	0.025 max
A515 Grade 70 (UNS K03101)	0.35 max [a]	1.30 max [b]	0.13–0.45 [b]	—	—	—	—	0.035 max	0.035 max
A516 Grade 70 (UNS K02700)	0.31 max [c]	0.79–1.30 [b]	0.13–0.45 [b]	—	—	—	—	0.035 max	0.035 max
A533 Type B (UNS K12539)	0.25 max	1.07–1.65 [b]	0.13–0.45 [b]	—	0.41–0.64 [b]	0.37–0.73 [b]	—	0.035 max	0.035 max

[a] — Over 50 mm thick
[b] — Product analysis
[c] — Over 100 mm thick
* — New ASTM designation for A508 Class 3

Table A-2. Mechanical properties specified for low-carbon/low-alloy steels included in this report (extracted from American Society for Testing and Materials, 1995a, c, d, e, f)

Steel	Tensile Strength (MPa)	Yield Strength, min (0.2% Offset) (MPa)	Elongation in 50 mm, min (%)	Reduction in Area, min (%)
A302 Grade B (UNS K12022)	550–690	345	18	—
A508 Grade 3 Class 1* (UNS K12042)	550–725	345	18	38
A515 Grade 70 (UNS K03101)	485–620	260	21	—
A516 Grade 70 (UNS K02700)	485–620	260	21	—
A533 Type B Class 2 (UNS K12539)	620–795	485	16	—
* New ASTM designation for A508 Class 3				